Cold atoms in contact with an environment

Masterarbeit in Physik
von
Alexander Schäbe

angefertigt am
Helmholtz-Institut für Strahlen- und Kernphysik

vorgelegt der

Mathematisch-Naturwissenschaftlichen Fakultät
der
Rheinischen Friedrich-Wilhelms-Universität Bonn

September 2015

1. Gutachter(in): Prof. Dr. Corinna Kollath
2. Gutachter(in): Prof. Dr. Johann Kroha

Contents

1 Introduction **1**

2 Bose-Einstein condensation **3**
2.1 Static properties . . . 3
2.1.1 Ideal Bose gas . . . 3
2.1.2 The Gross-Pitaevskii equation . . . 6
2.1.2.1 Stationary Gross-Pitaevskii equation . . . 6
2.1.2.2 Time-dependent Gross-Pitaevskii equation . . . 8
2.1.3 Thomas-Fermi approximation . . . 9
2.2 Hydrodynamics and excitation modes . . . 9
2.3 Gross-Pitaevskii equation for two species . . . 11

3 Concept of open quantum systems **13**
3.1 Open quantum systems . . . 13
3.2 Lindblad equation . . . 14
3.3 Quantum Zeno effect . . . 15
3.4 Gross-Pitaevskii equation with dissipation . . . 16
3.4.1 Single species system with dissipation . . . 16
3.4.2 Condensate mixture with dissipation . . . 17
3.5 Dimensionless equation . . . 17

4 Numerical methods **19**
4.1 Split step method . . . 19
4.2 Imaginary time evolution . . . 20
4.3 Solving the GPE . . . 22
4.3.1 Different interactions . . . 22
4.3.2 Real time evolution . . . 23

5 Convergence & Consistency **27**
5.1 Consistency . . . 27
5.2 Convergence . . . 29
5.2.1 Convergence in space . . . 29
5.2.2 Convergence in time . . . 30

6 Static properties of a two-component gas in 1D **31**
6.1 State separation . . . 31
6.2 State diagram . . . 33
6.3 Ground state approximations . . . 34

7 Dynamical properties of a two-component gas in 1D **39**
7.1 Breathing mode . . . 39
7.2 Atom loss dynamics for no state separation . . . 40
7.2.1 Atom loss for different γ . . . 40

7.2.2 Evolution of the densities . . . 41
7.2.3 Approximation for the decay curves . . . 42
7.2.4 Hydrodynamic approach to a two-level system with dissipation . . . 45
7.3 Atom loss dynamics for state separation ($\kappa_{11} = \kappa_{22} \lesssim \kappa_{12}^c$) . . . 46
7.3.1 Atom loss for different γ . . . 46
7.3.2 Evolution of the densities . . . 47
7.3.3 Approximation for the decay curves . . . 48
7.3.4 Hydrodynamic approach to a two-level system with dissipation . . . 51
7.3.5 Quantum Zeno effect . . . 53
7.4 Atom loss dynamics for state separation ($\kappa_{12} = \kappa_{11} >> \kappa_{22}$) . . . 54
7.4.1 Atom loss for different γ . . . 54
7.4.2 Evolution of the densities . . . 54
7.4.3 Hydrodynamic approach to a two-level system with dissipation . . . 56
7.5 Decay for different $\kappa_{11} = \kappa_{22}$ . . . 57
7.6 Decay for different $\kappa_{11} = \kappa_{12}$ and $\kappa_{22} = 0$ . . . 58

8 Static properties of a two-component gas in 2D **61**
8.1 State separation . . . 61
8.2 State diagram . . . 62
8.3 Ground state approximations . . . 63

9 Dynamical properties of a two-component gas in 2D **67**
9.1 Breathing mode . . . 67
9.2 Atom loss dynamics for no state separation . . . 67
9.2.1 Atom loss for different γ . . . 67
9.2.2 Evolution of the density . . . 67
9.2.3 Approximation for the decay curves . . . 68
9.2.4 Hydrodynamic approach to a two-component system with dissipation 73
9.2.5 Asymmetric trapping potential . . . 74
9.3 Atom loss dynamics for state separation ($\kappa_{11} = \kappa_{22} \leq \kappa_{12}^c$) . . . 75
9.3.1 Atom loss for different γ . . . 75
9.3.2 Evolution of the density . . . 76
9.3.3 Approximation for the decay curves . . . 77
9.3.4 Hydrodynamic approach to a two-component system with dissipation 80
9.3.5 Asymmetric trapping potential . . . 81
9.4 Atom loss dynamics for state separation ($\kappa_{12} = \kappa_{11} >> \kappa_{22}$) . . . 83
9.4.1 Atom loss for different γ . . . 83
9.4.2 Evolution of the density . . . 83
9.4.3 Hydrodynamic approach to a two-component system with dissipation 84

10 Conclusion **87**

Bibliography **89**

List of Figures **91**

Appendix **95**
1 Gross-Pitaevskii equation with dissipation . . . 95
1.1 One-body loss . . . 95
1.2 Condensate mixture with two-body loss . . . 96

2 Conversion to units according to [16] 97
3 Useful formulas 98

CHAPTER 1

Introduction

There is an increasing interest in the physics of cold atoms due to the experimental access of producing temperatures of the order of nK. This allowed in the 90s to create a Bose-Einstein condensate (BEC) [1] [2]. This effect was predicted by Einstein based on the work of Bose nearly 70 years before its experimental realization. The absence of a mechanism similar to the Pauli principle for fermions allows bosons to occupy the lowest energy state macroscopically and form a condensate. In order to create a condensate in experiment, new techniques like laser cooling were used to slow down the particles. To lower the temperature further, the atoms were confined to a magnetic trap.
It is also possible to create mixtures of condensates. An example for this is a Bose-Einstein condensate with two different internal states, e.g. hyperfine states. This was already achieved with ^{87}Rb atoms in [3]. Some of the atoms of this condensate were in the state $|F = 2, m_f = 2\rangle$ and the other atoms were in the state $|F = 1, m_f = -1\rangle$. Also the interaction between two atoms can be changed in many cases using Feshbach resonances which uses the tuning of the scattering length by an external magnetic field. This gives the opportunity to investigate the effects of the interspecies and intraspecies interaction. Applying a mean field model to a condensate leads to the Gross-Pitaevskii equation (GPE). Its model for a one component gas can be also used to describe this kind of condensates and will provide the basis for theoretical description in this thesis.
Due to the internal structure of the atoms in such a condensate, inelastic scattering processes between both hyperfine states can occur. The energy difference between these two energy levels is converted to kinetic energy and this can lead to two-body losses. This causes the change of the density depending on the scattering rate [4] which generates an instable system. Due to these losses, the system is not isolated and requires the model of open quantum systems. For situations like this, the Lindblad equation provides a valid description. Therefore, it has to be combined with the description for the interacting two component Bose-Einstein condensate which is confined to a trap.
The results of this thesis will concentrate on the consequences of two particle losses caused by inelastic scattering and the effects related to this instability. In this work, we will study how the stability is influenced by the parameters of the system such as interactions or geometry of the trapping potential. Further, the dynamics will be investigated as the system evolves in time.
The thesis is organized as follows. In chapter 2 the term 'condensate' is explained. Since we are interested in a description close to experiments, we will take the interaction and the confinement to a trapping potential into account. This includes also the dynamics of a condensate. In chapter 3, we will provide the concept of systems with dissipation. Since it is complicated to solve a two level system with dissipation analytically, chapter 4 defines the numerical methods we use to solve the GPE. In chapter 5 , the methods are verified and compared to already known results. In chapter 6, the static properties of a BEC consisting of

two components in 1D are discussed and then in chapter 7, we probe the dynamic properties of a two level BEC with losses. Different approximations are considered in order to provide an analytic description at small times.
After that, these considerations for a such an instable system are extended to two dimensions. The results for the static case and the dynamics can be found in chapter 8 and 9 correspondingly. Chapter 10 will conclude and summarize the results.

CHAPTER 2

Bose-Einstein condensation

One of the most famous properties of bosons is the macroscopic occupation of the ground state at low temperatures. This process is called Bose-Einstein condensation and this chapter will discuss its theoretical description.
In part 2.1, several methods are discussed in order to describe the formation of a condensate. The first section 2.1.1 concentrates on bosons in a box at low temperatures and neglects the interaction among the particles. Section 2.1.2 introduces the Gross-Pitaevskii equation (GPE) which allows us to take a potential and the interaction into account. Then, the related dynamics will be discussed in chapter 2.2.
The considerations will follow [5], [6] and [7].

2.1 Static properties

2.1.1 Ideal Bose gas

The Hamiltonian for a free particle of mass m is given by

$$\hat{H} = \frac{\hat{p}^2}{2m}, \tag{2.1}$$

where $\hat{p}$ is the momentum operator. The mean occupation number for Bosons reads

$$n(\epsilon_p) = \frac{1}{e^{\beta(\epsilon_p - \mu)} - 1} \quad . \tag{2.2}$$

μ is the chemical potential and is a quantity how the energy of a system is affected by a change of the particle number. Further, β is defined as $\beta = (k_B T)^{-1}$ with the temperature T and the Boltzmann constant k_B. $\epsilon_{\vec{p}}$ is the energy of a free particle and given by $\epsilon_{\vec{p}} = \frac{\vec{p}^2}{2m} \geq 0$. Note that formula 2.2 is only valid for the case $\mu < \epsilon_{\vec{p}}$ for all $\vec{p}$. Since $\vec{p} = 0$ is a possible value and occurs at low temperatures, it follows $\mu < 0$. Only positive values for mean occupation number and temperature are physical and consequently, one can see from equation 2.2 that $e^{\beta\mu} \leq 1$.
Let us introduce the fugacity $z = e^{\beta\mu}$. Due to its structure, $n(\epsilon_p)$ diverges for $z \to 1$ for $T = 0$. This corresponds to the macroscopic occupation of the ground state, which is the effect of Bose-Einstein condensation. As one can see, the low temperature behavior of fermions differs strongly from that of bosons, since the Pauli principle limits the occupation number for each state.
To obtain the total particle number of the condensate, we sum over all momenta and

get

$$N = \sum_p n(\epsilon_p) = \sum_p \frac{1}{\frac{1}{z}e^{\beta\epsilon_p} - 1}. \tag{2.3}$$

Assuming the Bose gas being confined in a box, the values of the momenta are known to be $\vec{p} = \frac{2\pi\hbar\vec{n}}{L}$ which can be obtained from the boundary condition of the particle wave function $\Psi(x) = \Psi(x + L)$ in a one-dimensional box where L is the length of the box and $\vec{n}$ a vector of integer numbers. For very large volumes ($L \to \infty$), the discrete momentum spectrum turns in to a continuous one. This allows us later to rewrite the sum to an integral.
Now, some new quantities like the thermal wavelength $\lambda = \frac{h}{\sqrt{2\pi m k_B T}}$, $v = \frac{V}{N}$ and the Bose-function

$$g_\nu(z) = \frac{1}{\Gamma(\nu)} \int_0^\infty dx \frac{x^{\nu-1}}{\frac{1}{z}e^x - 1}. \tag{2.4}$$

are introduced. The entire particle number consists of the particle number N_0 in the $\vec{p} = 0$ state and the number N_e in the excited states.

$$N = \sum_p n(\epsilon_p) = N_0 + N_e \tag{2.5}$$

$$= \frac{1}{\frac{1}{z} - 1} + \sum_{p \neq 0} \frac{1}{\frac{1}{z}e^{\beta\epsilon_p} - 1} \tag{2.6}$$

The second part of equation 2.5 can be rewritten as an integral

$$N_e = \frac{V}{(2\pi\hbar)^3} \int d^3p \; n(\epsilon_p) \tag{2.7}$$

which is given by

$$N_e = \frac{V}{(2\pi\hbar)^3} \; 4\pi \int_0^\infty d|p| \; |p|^2 \; n(\epsilon_{|p|}). \tag{2.8}$$

in spherical coordinates. This form shows that the $|p| = 0$ state does not contribute to the integral and hence, it has been taken out of the sum in equation 2.6. Using the integral from formula 2.4, the following expression is derived:

$$N_e = \frac{V}{\lambda^3} g_{3/2}(z) \tag{2.9}$$

For very low temperatures, $\vec{p} \to 0$ and $z \to 1$. $g_{3/2}(z)$ is a monotonically increasing function and $g_{3/2}(1) \approx 2.612$ is the largest value for $0 < z \leq 1$. Due to this, the number of particles in the excited states is limited and the system starts then with the formation of a condensate. It is also possible to express that limit in form of a temperature:

$$T = \frac{2\pi\hbar^2}{m k_B (g_{3/2}(1) v)^{2/3}} \coloneqq T_c, \tag{2.10}$$

where $v = \frac{V}{N}$ and T_c is called the critical temperature. Using the obtained definitions, the number of atoms in the excited states is

$$N_e = N \frac{v}{\lambda^3} g_{3/2}(z) \tag{2.11}$$

$$= N \left(\frac{T}{T_c}\right)^{3/2} \frac{g_{3/2}(z)}{g_{3/2}(1)}. \tag{2.12}$$

in terms of the critical temperature.
Further, the condensate fraction $\frac{N_0}{N}$ can be calculated. Since for $T < T_c$ the number of particles in the excited states is still limited, the fugacity is still $z \approx 1$. Using formulas 2.6 and 2.12:

$$\frac{N_0}{N} = \frac{N - N_e}{N} \tag{2.13}$$

$$\approx 1 - \left(\frac{T}{T_c}\right)^{3/2} \tag{2.14}$$

For $T > T_c$, most of the atoms are in the excited state and no macroscopic fraction in the ground state, so one can conclude:

$$\frac{N_0}{N} = \begin{cases} 1 - \left(\frac{T}{T_c}\right)^{3/2} & \text{for } T < T_c \\ 0 & \text{for } T > T_c \end{cases} \tag{2.15}$$

This behavior of $\frac{N_0}{N}$ is shown in figure 2.1.

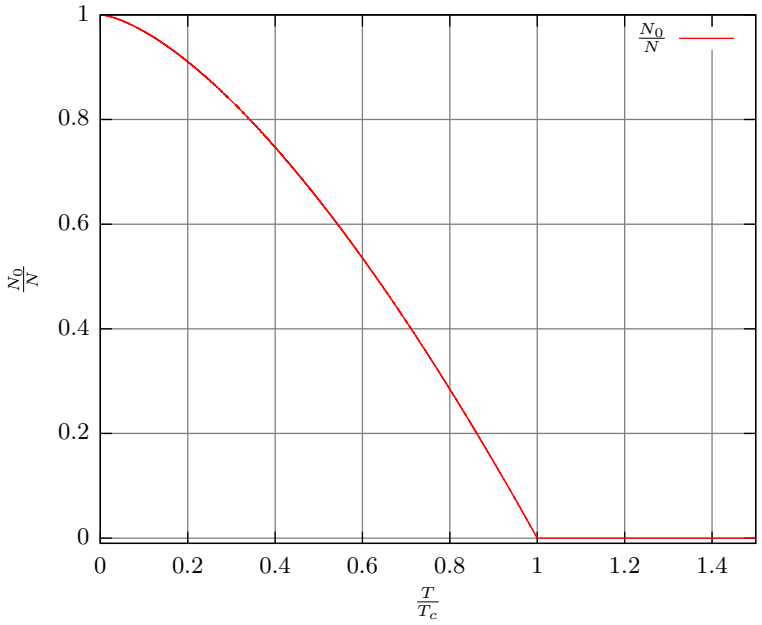

Figure 2.1: Plot of the condensate fraction $\frac{N_0}{N}$ depending on $\frac{T}{T_c}$. The curve shows the $1 - \left(\frac{T}{T_c}\right)^{3/2}$ behavior below T_c while for $T > T_c$ no macroscopic fraction is in the ground state.

2.1.2 The Gross-Pitaevskii equation

2.1.2.1 Stationary Gross-Pitaevskii equation

In experiments, a BEC is spatially confined to a potential $V(\vec{r})$ which is a known and solvable problem similar to the situation in the previous section. If now all N particles in the condensate interact, the Hamilton operator has to be modified by a term like $V(\vec{r}_i - \vec{r}_j)$ where $\vec{r}_i - \vec{r}_j$ is the distance between two interacting particles. Due to that, it is challenging to obtain a solution for a Hamiltonian of the form

$$H = \sum_{i=1}^{N} \left[\frac{\vec{p_i}^2}{2m} + V_{ext}(\vec{r}_i) \right] + \sum_{i<j} V(\vec{r}_i - \vec{r}_j). \tag{2.16}$$

One of the requirements for the following considerations is that the condensate is said to be a dilute gas leading to $\bar{n}a^3 \ll 1$ where $\bar{n}$ is the average density and a the scattering length. This means that the scattering volume is much smaller than the volume for each particle. It allows us to consider only low energy s-wave scattering and gives for the corresponding interaction potential

$$V(\vec{r}_i - \vec{r}_j) = U_0 \ \delta(\vec{r}_i - \vec{r}_j), \tag{2.17}$$

with

$$U_0 = \frac{4\pi\hbar^2 a}{m}. \tag{2.18}$$

The parameter a is the s-wave scattering length and the relevant parameter for the interaction at low energies. The sign of the interaction is responsible whether it is attractive $U_0 < 0$ or repulsive $U_0 > 0$. To solve this Hamiltonian in equation 2.16, the ansatz would be the most general wave function containing the spatial dependency for each particle of that condensate.

$$\Psi = \Psi(\vec{r}_1, \vec{r}_2, \ldots, \vec{r}_N) \tag{2.19}$$

It is very complicated to obtain that wave function by solving the Schrödinger equation. For a BEC, a mean field approach of the following form is used:

$$\Psi(\vec{r}_1, \vec{r}_2, \ldots \vec{r}_N) = \prod_{i=1}^{N} \Phi(\vec{r}_i), \tag{2.20}$$

where $\Phi(\vec{r}_i)$ are the single particle wave functions. This ansatz for the wave function neglects correlations between the particles but they are taken into account by the interaction in formula 2.17. Further, it assumes that all N particles with $N \gg 1$ are in the same state which is a reasonable assumption for a condensate at $T = 0$.
Since the ground state is the state with the lowest energy, minimizing the energy with the new ansatz in equation 2.20 and the N particle Hamiltonian should provide the solution for the wave function of the BEC.
The energy is the expectation value of the Hamiltonian and thus, we start with:

$$E = \int \ldots \int \Psi^*(\vec{r}_1, \vec{r}_2, \ldots, \vec{r}_N) \ H \ \Psi(\vec{r}_1, \vec{r}_2, \ldots, \vec{r}_N) \ d\vec{r}_1 \ldots d\vec{r}_N \tag{2.21}$$

Using equations 2.20, 2.16 and the normalization condition for the single particle wave function which is given by

$$\int d\vec{r}\ \Phi^*(\vec{r})\ \Phi(\vec{r}) = 1 \tag{2.22}$$

yields to

$$E = N \cdot \int d\vec{r} \left[\frac{\hbar^2}{2m} |\nabla\Phi(\vec{r})|^2 + V(\vec{r})|\Phi(\vec{r})|^2 + \frac{N-1}{2} U_0 |\Phi(\vec{r})|^4 \right]. \tag{2.23}$$

The form of the interaction term requires more explanation. The interaction energy reads

$$E_{int} = U_0 \prod_{j,i=1}^{N} \sum_{k<l} \int \dots \int \Phi^*(\vec{r}_j)\delta(\vec{r}_k - \vec{r}_l)\Phi(\vec{r}_i) d\vec{r}_1 \dots d\vec{r}_N. \tag{2.24}$$

Only terms of the form

$$E_{int} \propto \int \int \Phi^*(\vec{r}_i)\Phi^*(\vec{r}_j)\delta(\vec{r}_j - \vec{r}_i)\Phi(\vec{r}_i)\Phi(\vec{r}_j) d\vec{r}_i d\vec{r}_j \tag{2.25}$$

will contribute to the interaction energy part. All single particle wave functions with indices $\neq k, l$ give a factor of 1 due to normalization. Only the sum with $k < l$ is left where the limit for l is N. This corresponds to building up pairs among N bosons what gives the prefactor of $\binom{N}{2}$. The evaluation of the δ function leads to:

$$E_{int} = U_0 \frac{N(N-1)}{2} \int \int \Phi^*(\vec{r}_j)\Phi^*(\vec{r}_i)\delta(\vec{r}_j - \vec{r}_i)\Phi(\vec{r}_i)\Phi(\vec{r}_j) d\vec{r}_i d\vec{r}_j \tag{2.26}$$

$$= U_0 \frac{N(N-1)}{2} \int |\Phi(\vec{r}_i)|^4 d\vec{r}_i \tag{2.27}$$

Using

$$\Psi(\vec{r}) = \sqrt{N}\Phi(\vec{r}) \tag{2.28}$$

and the fact, that $N - 1 \approx N$ for large N, equation 2.23 turns into

$$E(\Phi(\vec{r})) \approx \int d\vec{r} \left[\frac{\hbar^2}{2m} |\nabla\Psi(\vec{r})|^2 + V(\vec{r})|\Psi(\vec{r})|^2 + \frac{U_0}{2} |\Psi(\vec{r})|^4 \right] \tag{2.29}$$

All products of wave functions for $i \neq j$ vanish due to normalization. Using integration by parts, the kinetic term of equation 2.29 can be rewritten as:

$$E_{kin} = -N \cdot \int \frac{\hbar^2}{2m} \Psi^*(\vec{r}) \nabla^2 \Psi(\vec{r})\ d\vec{r} \tag{2.30}$$

Since we need to fulfill the condition of constant particle number, we use the method of Lagrange multipliers to minimize the energy. The condition of constant particle number reads:

$$\int d\vec{r}\ |\Psi(\vec{r})|^2 = N = const. \tag{2.31}$$

This leads to:

$$\delta E - \mu \delta N = 0, \tag{2.32}$$

where μ is the Lagrange multiplier.
To minimize that expression, one varies equation 2.32 with respect to Ψ^*:

$$\left(\frac{\delta E}{\delta \Psi^*} - \mu \frac{\delta N}{\delta \Psi^*}\right) \delta\Psi^* = \int d\vec{r} \Big[-\frac{\hbar^2}{2m} (\delta\Psi^*) \nabla^2 \Psi + V(\delta\Psi^*)\Psi \tag{2.33}$$

$$+ U_0 (\delta\Psi^*)\Psi|\Psi|^2 - \mu(\delta\Psi^*)\Psi\Big] \tag{2.34}$$

To get the expression with the minimal value, the following equation arises.

$$\mu\Psi(\vec{r}) = -\frac{\hbar^2}{2m}\nabla^2\Psi(\vec{r}) + V(\vec{r})\Psi(\vec{r}) + U_0|\Psi(\vec{r})|^2\Psi(\vec{r}) \tag{2.35}$$

This is the static Gross-Pitaevskii equation (GPE). To obtain the one particle equation, we insert 2.28 into equation 2.35. It has a nonlinear interaction term which makes it difficult to solve and it resembles a Schrödinger equation but its eigenvalue is the chemical potential and not the energy per particle. The chemical potential is the change of energy of the system if the particle number of the system is changed. Since the particles interact, the change of energy is not the energy of one particle, but the entire system is influenced.

2.1.2.2 Time-dependent Gross-Pitaevskii equation

To obtain the dynamics of a system containing N bosons, the time dependence is important. The variational principle is used for this. According to [8], the action is defined as:

$$S = \int_{t_1}^{t_2} \int \mathcal{L}(\Psi(\vec{r},t), \partial_{r_i}\Psi(\vec{r},t), \partial_t\Psi(\vec{r},t))\; d\vec{r}\; dt \tag{2.36}$$

The corresponding Lagrange density is given by

$$\mathcal{L}(\Psi(\vec{r},t), \partial_{r_i}\Psi(\vec{r},t), \partial_t\Psi(\vec{r},t)) = i\frac{\hbar}{2}\left(\Psi\partial_t\Psi^* - \Psi^*\partial_t\Psi\right) + \frac{\hbar^2}{2m}|\vec{\nabla}\Psi|^2$$

$$+ V(\vec{r})|\Psi|^2 + \frac{2\pi a\hbar^2}{m}|\Psi|^4 \tag{2.37}$$

In order to minimize the action, one has to vary the Lagrangian with respect to the field Ψ^* and its derivatives $\partial_t\Psi^*$ and $\partial_{r_i}\Psi^*$. For a minimal action, one obtains:

$$0 = \sum_{i=1,2,3} \partial_{r_i} \frac{\partial\mathcal{L}}{\partial(\partial_{r_i}\Psi^*)} + \partial_t \frac{\partial\mathcal{L}}{\partial(\partial_t\Psi^*)} - \frac{\partial\mathcal{L}}{\partial\Psi^*} \tag{2.38}$$

This leads to

$$i\hbar\frac{\partial\Psi(\vec{r},t)}{\partial t} = -\frac{\hbar^2}{2m}\nabla^2\Psi(\vec{r},t) + V(\vec{r})\Psi(\vec{r},t) + \frac{4\pi a\hbar^2}{m}|\Psi(\vec{r},t)|^2\Psi(\vec{r},t) \tag{2.39}$$

This is the time-dependent Gross-Pitaevskii equation. If the solution of the GPE for the static case is known, one can obtain the solution for the time-dependent case by

$$\Psi(\vec{r},t) = e^{-i\frac{\mu t}{\hbar}}\Psi(\vec{r}). \tag{2.40}$$

Equation 2.39 is relevant for the dynamics of the condensate.

2.1.3 Thomas-Fermi approximation

We will now consider the case of a large particle number N. In that case, the density profile of a condensate becomes quite smooth, especially at the center of the trap. Hence, the derivative of the wave function contributes at this region not as significant as the potential and the interaction term of equation 2.35. Neglecting the kinetic term in the GPE, this equation can be solved for $n(\vec{r})$ and gives:

$$n(\vec{r}) = \frac{\mu - V(\vec{r})}{U_0} \tag{2.41}$$

This is known as the Thomas-Fermi approximation. If now a 3-dimensional harmonic oscillator potential of the form

$$V(\vec{r}) = \frac{1}{2}m\left(\omega_x^2x^2 + \omega_y^2y^2 + \omega_z^2z^2\right) \tag{2.42}$$

is assumed and no limitation is used, equation 2.41 can provide negative values for the density which are unphysical. To avoid this, the solution of $n(\vec{r}) = 0$ has to be determined in order to obtain the bound of the Thomas-Fermi profile. The solution for this is the Thomas-Fermi radius $R_{TF,i}$:

$$R_{TF,i}^2 = \frac{2\mu}{m\omega_i^2}, \tag{2.43}$$

with $i = x, y, z$. For $|r_i| > R_{TF,i}$, one has to set $n(\vec{r}) = 0$ since a negative density is unphysical. Figure 2.2 shows the direct comparison of the Thomas-Fermi approximation and a numerical solution of the Gross-Pitaevskii equation for the 1D case. The other dimensions have been integrated out. For the center of the trap, it describes the overall shape of the condensate quite good but it looses its accuracy at the edges because the kinetic energy term diverges there and cannot be neglected. Only this region gives a contribution to the kinetic part GPE for a large number of particles.

2.2 Hydrodynamics and excitation modes

In order to study the low lying excitation modes of a Bose gas, we will use a hydrodynamic approach assuming that $Na/a_s \gg 1$ which means that the interactions are large compared to the kinetic energy. Starting from the ground state of a BEC in a harmonic trap, these modes can be excited by a sudden change or a temporary switch off of the trapping potential. This will cause a pulsation of the condensate with a certain frequency which depends on the interaction strength. We will start with a general theoretical treatment.
In order to calculate the oscillation frequency of the Bose gas, one starts with the time-dependent GPE 2.39. Since the wave function of the condensate is a complex number, a

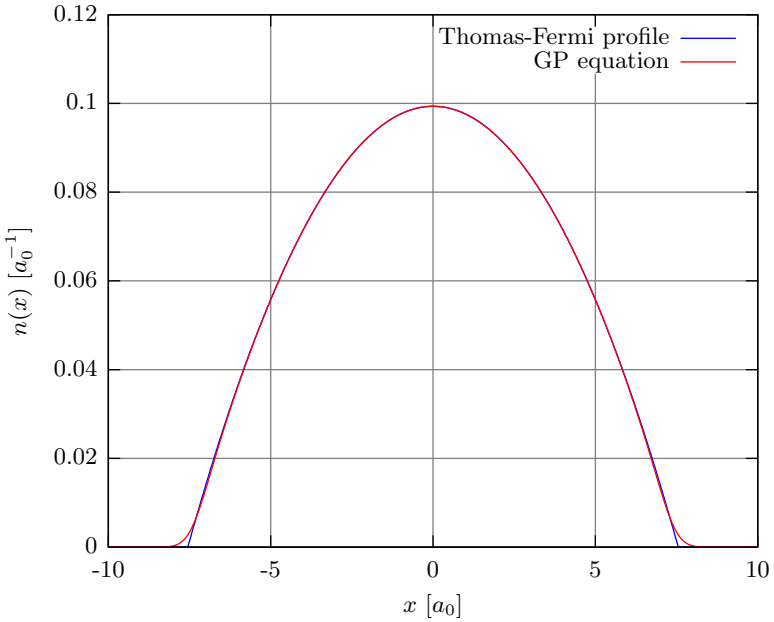

Figure 2.2: Thomas-Fermi approximation for an example of $N = 2 \cdot 10^4$ trapped ^{87}Rb atoms and a trapping frequency of $\omega = 2\pi \cdot 200\,\mathrm{Hz}$ and a scattering length of $a = 5.45\,\mathrm{nm}$ for the 1D case. a_0 is the oscillator length and defined as $a_0 = \sqrt{\frac{\hbar}{m\omega}}$. The approximation of the density profile with the parabola in equation 2.41 is a good approximation but the difference between that approximation and the solution of the Gross-Pitaevskii equation at the edges is quite large. For $|x_i| > R_{TF,i}$, this approximation becomes unphysical.

general ansatz has the form

$$\Psi(\vec{r},t) = \sqrt{n(\vec{r},t)} exp\left(iS(\vec{r},t)\right) \tag{2.44}$$

where $S(\vec{r},t)$ is the phase of the complex number and $\sqrt{n(\vec{r},t)}$ denotes the amplitude. The amplitude is chosen to fulfill the condition $\Psi^*(\vec{r},t)\Psi(\vec{r},t) = n(\vec{r},t)$. Inserting this definition of the wave function and separating the imaginary and real part, one obtains the following two equations:

$$m\frac{\partial}{\partial t}\vec{v} + \vec{\nabla}\left(V + U_0 n - \frac{\hbar^2}{2m\sqrt{n}}\nabla^2\sqrt{n} + \frac{mv^2}{2}\right) = 0 \tag{2.45}$$

$$\frac{\partial n}{\partial t} + \vec{\nabla}\cdot(\vec{v}n) = 0 \tag{2.46}$$

where the velocity field $\vec{v}(\vec{r},t) = \frac{\hbar}{m}\vec{\nabla}S(\vec{r},t)$ was introduced. Since this excitation mode is a deviation of the density from the equilibrium state, the ansatz for the density is given by

$$n(\vec{r},t) = n_0(\vec{r}) + \delta n(\vec{r},t) \tag{2.47}$$

where $n_0(\vec{r})$ is the equilibrium density and $\delta n(\vec{r},t)$ a small perturbation. The small perturbation evolves in time like $\delta n(\vec{r},t) \propto e^{-i\omega_0 t}$. ω_0 is the oscillating frequency of the condensate. This ansatz is used in order to solve the coupled equations 2.45 and 2.46. From this, a dispersion relation between the frequencies of the condensate and the trapping potential is

found. A detailed calculation for the 1D case is not shown here and can be found e.g. in [9]. The ratios of both frequencies are $\omega_0^2 = 4\omega^2$ for the Tonks-Girardeau regime and $\omega_0^2 = 3\omega^2$ for the 1D mean-field regime ($U_0 = 0$ and $U_0 = \infty$). In 2D, it was found in [10] to be $\omega_0^2 = 4\omega^2$.

2.3 Gross-Pitaevskii equation for two species

As mentioned in the introduction, we want to describe a condensate mixture of the same kind of atoms but with different internal states.
In order to do that, we assume a mixture of two different condensates with different particle numbers, N_1 and N_2. Not only the interaction among the particles of one kind (intraspecies interaction) contributes to the total Hamiltonian, but also the interaction between the different particle species has to be taken into account (interspecies interaction).
The ansatz for the wave function is very similar to the case of just one type of atoms.

$$\Psi(\vec{r}_1, \dots \vec{r}_{N_1}, \vec{q}_1 \dots \vec{q}_{N_2}) = \prod_{i=1}^{N_1} \Phi_1(\vec{r}_i) \prod_{i=1}^{N_2} \Phi_2(\vec{q}_i) \tag{2.48}$$

$\Phi_1(\vec{r}_i)$ and $\Phi_2(\vec{q}_i)$ denote the single particle wave functions for each species. Further, one can insert this expression into the corresponding Hamiltonian and obtain an expression for the energy.

$$\begin{aligned} E \approx \int d\vec{r} \Bigg[& N_1 \frac{\hbar^2}{2m_1} |\nabla \Phi_1|^2 + N_1 V_1(\vec{r}) |\Phi_1(\vec{r})|^2 + \frac{1}{2} U_{11} N_1^2 |\Phi_1(\vec{r})|^4 + N_2 \frac{\hbar^2}{2m_2} |\nabla \Phi_2|^2 \\ & + N_2 V_2(\vec{r}) |\Phi_2(\vec{r})|^2 + \frac{1}{2} U_{22} N_2^2 |\Phi_2(\vec{r})|^4 + U_{12} N_1 N_2 |\Phi_1(\vec{r})|^2 |\Phi_2(\vec{r})|^2 \Bigg] \end{aligned} \tag{2.49}$$

Here, the approximation $N_1 - 1 \approx N_1$ and $N_2 - 1 \approx N_2$ was used again. U_{11} and U_{22} are the intraspecies interactions, U_{12} is the interspecies interaction. The general form of these interactions are given by

$$U_{ij} = \frac{2\pi\hbar^2 a_{ij}}{m_{ij}} \quad (i, j = 1, 2) \tag{2.50}$$

where $m_{ij} = \frac{m_i m_j}{m_i + m_j}$ is the reduced mass and a_{ij} is the scattering length for the species i and j where $a_{12} = a_{21}$. This leads to $U_{12} = U_{21}$ what we will use throughout the following chapters.
Since there are N_1 particles which can interact with N_2 of the other kind, one obtains the prefactor $N_1 N_2$ for the interspecies interaction term. The same substitution of the form of 2.28 for the single species case gives:

$$\Psi_1(\vec{r}) = \frac{1}{\sqrt{N_1}} \Phi_1(\vec{r}) \tag{2.51}$$

$$\Psi_2(\vec{r}) = \frac{1}{\sqrt{N_2}} \Phi_2(\vec{r}) \tag{2.52}$$

To minimize the energy, the condition of constant particle number is required. But now the energy has to be varied for each particle number.

$$\delta E - \mu_1 \delta N_1 - \mu_2 \delta N_2 = 0 \tag{2.53}$$

Thus, one obtains for each particle species an equation which is coupled by the additional interspecies interaction term to the other species:

$$\mu_1 \Psi_1(\vec{r}) = \left(-\frac{\hbar^2}{2m_1}\nabla^2 + V_1(\vec{r}) + U_{11}|\Psi_1(\vec{r})|^2 + U_{12}|\Psi_2(\vec{r})|^2 \right) \Psi_1(\vec{r}) \tag{2.54}$$

$$\mu_2 \Psi_2(\vec{r}) = \left(-\frac{\hbar^2}{2m_2}\nabla^2 + V_2(\vec{r}) + U_{22}|\Psi_2(\vec{r})|^2 + U_{12}|\Psi_1(\vec{r})|^2 \right) \Psi_2(\vec{r}) \tag{2.55}$$

We will see that the interspecies interaction term becomes highly relevant for the ground state. For the dynamics of such a system, we use the time-dependent equations:

$$i\hbar\partial_t \Psi_1(\vec{r},t) = \left(-\frac{\hbar^2}{2m_1}\nabla^2 + V_1(\vec{r}) + U_{11}|\Psi_1(\vec{r},t)|^2 + U_{12}|\Psi_2(\vec{r},t)|^2 \right) \Psi_1(\vec{r},t) \tag{2.56}$$

$$i\hbar\partial_t \Psi_2(\vec{r},t) = \left(-\frac{\hbar^2}{2m_2}\nabla^2 + V_2(\vec{r}) + U_{22}|\Psi_2(\vec{r},t)|^2 + U_{12}|\Psi_1(\vec{r},t)|^2 \right) \Psi_2(\vec{r},t) \tag{2.57}$$

Their derivation is analogous to the case of a one component BEC discussed in section 2.1.2.2.

CHAPTER 3

Concept of open quantum systems

Due to the complexity which arises when a system is coupled to an environment, new methods are required. This section will introduce these and will explain the necessary modifications of GPE in order to consider a dissipative BEC consisting of two components. All information for this section are mainly taken from [11].

3.1 Open quantum systems

The properties of a system S are described by the density operator which is given by

$$\rho_S = \sum_i p_i \left|\Psi_i\right\rangle \left\langle\Psi_i\right| \tag{3.1}$$

The density operator gives information about which states $|\Psi_i\rangle$ are occupied with a certain probability p_i. Let S now be an open quantum system. Such system is described by the figure 3.1 shown below. The aim is to obtain how only the system S is evolves in time by

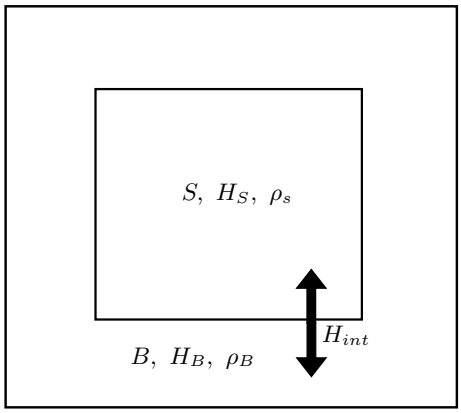

Figure 3.1: Sketch for the physical situation of an open quantum system. The system S described by the Hamiltonian H_S interacts with the environment B with H_B via H_{int}. The density operators ρ_S and ρ_B are the best quantities to get information over all possible states in the corresponding systems.

the interaction with the environment B. The most general ansatz for solving such a physical situation is to introduce a new Hilbert space of the form $\mathcal{H} = \mathcal{H}_S \otimes \mathcal{H}_B$. The Hamiltonian of the entire system is the combination of all Hamilton operators which are involved in order to describe this system.

$$H(t) = H_S \otimes \mathbb{1}_B + \mathbb{1}_S \otimes H_B + H_{int}(t) \tag{3.2}$$

Solving such a Hamiltonian requires a very precise knowledge about the environment which can have an infinite number of degrees of freedom. The exact expression for the evolution in time of the system S would read

$$\frac{d\rho_S(t)}{dt} = -\frac{i}{\hbar} \cdot tr_B \left[H(t), \rho(t)\right], \tag{3.3}$$

where $tr_B \left[\dots\right]$ means the sum over all degrees of freedom of the system B and $H(t)$ and $\rho(t)$ are the Hamilton operator and the density operator of the entire system. How to approximate such an expression will be described in the following section.

3.2 Lindblad equation

Instead of solving the equation for an entire system, it is much simpler to concentrate only on the system S itself because its evolution in time is what one is interested in. This idea is used in order to simplify the calculation and the exact expression in equation 3.3.
For that, it is necessary to introduce two new concepts.

- Dynamical map
  The time expansion of the density operator of a system S is given by

  $$\rho_S(t) = tr_B \left(U(t,0)[\rho_S(0) \otimes \rho_B]U^\dagger(t,0)\right), \tag{3.4}$$

  with the time evolution operator $U(t,0) = exp(-iHt)$. Introducing a dynamical map means that we define a linear operator V(t) which maps the density operator $\rho(0)$ to the same Hilbert space at a different time t.

  $$\rho_S(t) = V(t)\rho_S(0) \tag{3.5}$$

- Quantum Markov processes
  Assuming that the future state depends only on the present state and not on any in the past is the property of a Markovian processes. This can be expressed by the semigroup property.

  $$V(t_1)V(t_2) = V(t_1 + t_2), \qquad t_1,\ t_2 \geq 0 \tag{3.6}$$

  The dynamical map is the condition to write the time evolution of an open quantum system in that way.

Using these two concepts, a representation for $V(t)$ is required. Introducing the generators $\mathcal{L}$ of the semigroup, one obtains with the exponential representation of $V(t)$:

$$V(t) = exp\left(\mathcal{L}t\right) \tag{3.7}$$

Since $\rho_S(t) = V(t)\rho_S(0)$, the time derivative gives:

$$\frac{d}{dt}\rho_S(t) = \mathcal{L}\rho_S(t) \tag{3.8}$$

This is the form of the differential equation we want to get. A possible representation of $\mathcal{L}$ is given in the Lindblad equation. It reads:

$$\mathcal{L}\rho_S = \frac{d\rho_S}{dt} = -\frac{i}{\hbar}[H, \rho_S] + \sum_{k=1}^{N^2-1} \gamma_k \left(A_k \rho_S {A_k}^\dagger - \frac{1}{2} {A_k}^\dagger A_k \rho_S - \frac{1}{2} \rho_S {A_k}^\dagger A_k \right), \tag{3.9}$$

where A_k and $A_k^\dagger$ are the Lindblad operators which describe how the system is coupled to the environment. The parameter γ_k gives the strength of this coupling. The Lindblad equation gives the time derivative of the density operator ρ_S of an open quantum system.

3.3 Quantum Zeno effect

One effect which can be observed when the Lindblad equation is solved is the Quantum Zeno effect.
Every observable A can be decomposed into the eigenstates and the corresponding eigenvalues of that observable.

$$A = \sum_n a_n \left|\Psi_n\right\rangle \left\langle\Psi_n\right| \tag{3.10}$$

Let now ϑ be a time interval after which a measurement of a system is performed. For $\vartheta \to 0$, the measurement becomes continuous.
The Schrödinger equation of a time-dependent state reads:

$$i\hbar \frac{\partial}{\partial t} \left|\Psi(t)\right\rangle = \hat{H} \left|\Psi(t)\right\rangle \tag{3.11}$$

That gives us the time expansion of a time-dependent state.

$$\left|\Psi(t)\right\rangle = e^{-i\frac{\hat{H}t}{\hbar}} \left|\Psi_n\right\rangle \tag{3.12}$$

$$= \left(1 - i\frac{\hat{H}t}{\hbar} - \frac{1}{2}\frac{\hat{H}^2 t^2}{\hbar^2} + \dots\right) \left|\Psi_n\right\rangle \tag{3.13}$$

The probability density for the transition from the initial state to the state after the time interval ϑ is given by:

$$w_{nn}(\vartheta) = \left|\left\langle\Psi_n|\Psi(\vartheta)\right\rangle\right|^2 \tag{3.14}$$

With the time expansion given above, one obtains:

$$w_{nn}(\vartheta) = \left| 1 - i\frac{\vartheta}{\hbar} \left\langle\Psi_n\right| \hat{H} \left|\Psi_n\right\rangle - \frac{1}{2}\frac{\vartheta^2}{\hbar^2} \left\langle\Psi_n\right| \hat{H}^2 \left|\Psi_n\right\rangle + \mathcal{O}(\vartheta^3) \right|^2 \tag{3.15}$$

$$= 1 - \frac{\vartheta^2}{\hbar^2} \underbrace{\left(\left\langle\Psi_n\right| \hat{H}^2 \left|\Psi_n\right\rangle - \left(\left\langle\Psi_n\right| \hat{H} \left|\Psi_n\right\rangle\right)^2 \right)}_{(\Delta E_n)^2} + \mathcal{O}(\vartheta^3) \tag{3.16}$$

After a time $\tau = k\vartheta$:

$$w_{nn}(\tau) \approx \left[1 - (\Delta E_n)^2 \frac{\vartheta^2}{\hbar^2}\right]^k \tag{3.17}$$

For a large number of measurements in that certain time interval τ, the length of the interval for the time measurement $\vartheta \to 0$ yields to $w_{nn}(\tau) \to 1$ after some algebra.
The consequence is that a system can be completely frozen just by applying a continuous measurement which is the Quantum Zeno effect. The coupling to the environment is represented by the γ_k in equation 3.9 and for large values, the system which is described by the Lindblad equation should evolve slower compared to a smaller coupling.

3.4 Gross-Pitaevskii equation with dissipation

We want now to combine the Gross-Pitaevskii equation and the concept of an open quantum system. For this, the Lindblad equation is used. Once the atoms have left the condensate, they will never return. Thus, such system has no memory effects what is an important condition for the application of the Lindblad equation.

3.4.1 Single species system with dissipation

In terms of the bosonic field operators, the Hamiltonian we used to obtain the Gross-Pitaevskii equation is given by [12]:

$$\hat{H} = \int d\vec{r}\ \hat{\Psi}^\dagger(\vec{r}) \left(-\frac{\hbar^2}{2m}\nabla^2 + V_{ext}(\vec{r})\right) \hat{\Psi}(\vec{r}) + \frac{U_0}{2} \int d\vec{r}\ \hat{\Psi}^\dagger(\vec{r})\hat{\Psi}^\dagger(\vec{r})\hat{\Psi}(\vec{r})\hat{\Psi}(\vec{r}) \tag{3.18}$$

The field operators fulfill the following commutation relations:

$$[\hat{\Psi}(\vec{r}), \hat{\Psi}(\vec{r}')] = 0 \tag{3.19}$$

$$[\hat{\Psi}^\dagger(\vec{r}), \hat{\Psi}^\dagger(\vec{r}')] = 0 \tag{3.20}$$

$$[\hat{\Psi}(\vec{r}), \hat{\Psi}^\dagger(\vec{r}')] = \delta^3(\vec{r} - \vec{r}') \tag{3.21}$$

Considering n-body losses, the Lindblad operators A_k in equation 3.9 are given by $A_k = \left(\hat{\Psi}(\vec{r})\right)^n$ with $\hat{\Psi}(\vec{r}) = \sum_p \Psi_p(\vec{r})\ \hat{a}_p$ [13]. The field operator $\hat{\Psi}(\vec{r})$ annihilates a particle at position $\vec{r}$ in the state p. Concentrating first on single particle losses, we introduce the dissipator for this case:

$$\mathcal{D}(\hat{\rho}) = -\int d\vec{r}\ \gamma(\vec{r})(\hat{\Psi}^\dagger(\vec{r})\hat{\Psi}(\vec{r})\hat{\rho} + \hat{\rho}\hat{\Psi}^\dagger(\vec{r})\hat{\Psi}(\vec{r}) - 2\hat{\Psi}(\vec{r})\hat{\rho}\hat{\Psi}^\dagger(\vec{r})). \tag{3.22}$$

One obtains with that

$$i\hbar Tr\left[\dot{\hat{\rho}}\hat{\Psi}(\vec{r})\right] = i\hbar\langle\dot{\hat{\Psi}}(\vec{r})\rangle = Tr\left[\hat{\Psi}(\vec{r})([\hat{H}, \hat{\rho}] + i\hbar\hat{\mathcal{D}}(\hat{\rho}))\right], \tag{3.23}$$

where $\dot{\hat{\rho}}$ denotes the time derivative of the density operator. Using the commutation relations 3.19, 3.20 and 3.21 and the invariance of the trace under cyclic permutations, it

leads to

$$i\hbar\langle\dot{\hat{\Psi}}(\vec{r})\rangle = \left\langle\left[-\frac{\hbar^2}{2m}\nabla^2 + V_{ext}(\vec{r}) + U_0\hat{\Psi}^\dagger(\vec{r})\hat{\Psi}(\vec{r})\right]\hat{\Psi}(\vec{r})\right\rangle - i\hbar\gamma(\vec{r})\left\langle\hat{\Psi}(\vec{r})\right\rangle. \tag{3.24}$$

Assuming a large particle number, one can use the mean-field approximation which is given by $\hat{\Psi} \simeq \hat{\Psi}^\dagger \simeq \langle\hat{\Psi}\rangle = \Psi$ and therefore, equation 3.24 turns into the time-dependent Gross-Pitaevskii equation 2.39 with an additional term which takes the losses into account.

$$i\hbar\dot{\Psi}(\vec{r}) = \left[-\frac{\hbar^2}{2m}\nabla^2 + V_{ext}(\vec{r}) + U_0\hat{\Psi}^\dagger(\vec{r})\hat{\Psi}(\vec{r})\right]\hat{\Psi}(\vec{r}) - i\hbar\gamma(\vec{r})\hat{\Psi}(\vec{r}) \tag{3.25}$$

The complete calculation can be found in the appendix. The density of a condensate described by equation 3.25 becomes smaller since the $i\hbar\gamma$ term causes non-unitary time evolution and provides a damping term.

3.4.2 Condensate mixture with dissipation

As mentioned previously, we want to describe a condensate with two internal states. Due to the two-body losses by scattering, two particles of each species leave the system. The simultaneous destruction of two atoms of different species has to be taken into account by the Lindblad operator. Thus, it reads:

$$\hat{A}(\vec{r}) = \hat{\Psi}_1(\vec{r})\hat{\Psi}_2(\vec{r}) \tag{3.26}$$

$$\hat{A}^\dagger(\vec{r}) = \Psi_2^\dagger(\vec{r})\hat{\Psi}_1^\dagger(\vec{r}) \tag{3.27}$$

Using this operator, one can derive $\langle\dot{\hat{\Psi}}_1(\vec{r})\rangle$ and $\langle\dot{\hat{\Psi}}_2(\vec{r})\rangle$ (see appendix 1.2). Each state is represented by one GPE (see equations 2.56 and 2.57). Assuming $\frac{\gamma(\vec{r})}{2} = \gamma = const.$, the corresponding system of equations is:

$$i\hbar\frac{\partial\Psi_1(\vec{r})}{\partial t} = \left(-\frac{\hbar^2}{2m_1}\nabla^2 + V_1(\vec{r}) + U_{11}|\Psi_1(\vec{r})|^2 + (U_{12} - i\hbar\gamma)|\Psi_2(\vec{r})|^2\right)\Psi_1(\vec{r}) \tag{3.28}$$

$$i\hbar\frac{\partial\Psi_2(\vec{r})}{\partial t} = \left(-\frac{\hbar^2}{2m_2}\nabla^2 + V_2(\vec{r}) + U_{22}|\Psi_2(\vec{r})|^2 + (U_{12} - i\hbar\gamma)|\Psi_1(\vec{r})|^2\right)\Psi_2(\vec{r}) \tag{3.29}$$

Later, this system of coupled equation is solved for one dimension in order to obtain the evolution over time.

3.5 Dimensionless equation

In the previous chapter, we have obtained the equations 3.28 and 3.29 which we are going to study. For most of the following considerations, we rescale time and space by the trapping frequency and the characteristic length a_0 of the condensate. This makes it possible to work with parameters of a more convenient magnitude.

$$\tilde{t} = \omega t \quad \tilde{x} = \frac{x}{a_0} \tag{3.30}$$

Inserting this in the one particle GPE gives

$$i\hbar\omega\frac{\partial\Psi(\tilde{x},\tilde{t})}{\partial\tilde{t}} = \left(-\frac{\hbar^2}{2m}\frac{1}{a_0^2}\frac{\partial^2}{\partial\tilde{x}^2} + \frac{1}{2}m\omega^2\tilde{x}^2a_0^2 + \frac{U_0N}{a_0}|\Psi(\tilde{x},\tilde{t})|^2\right)\Psi(\tilde{x},\tilde{t}) \tag{3.31}$$

Dividing by $m\omega^2a_0^2$ and defining $\epsilon = \left(\frac{a_s}{a_0}\right)^2$ where $a_s = \sqrt{\frac{\hbar}{m\omega}}$ and $\kappa = \frac{U_0N}{m\omega^2a_0^3}$ gives:

$$i\epsilon\frac{\partial\Psi(\tilde{x},\tilde{t})}{\partial\tilde{t}} = \left(-\frac{1}{2}\epsilon^2\frac{\partial^2}{\partial\tilde{x}^2} + \frac{1}{2}\tilde{x}^2 + \kappa|\Psi(\tilde{x},\tilde{t})|^2\right)\Psi(\tilde{x},\tilde{t}) \tag{3.32}$$

Thus, κ is of order 1. In the following, we redefine $\tilde{x} \coloneqq x$ and $\tilde{t} \coloneqq t$.
For the two level condensate with dissipation, the dimensionless equations read:

$$i\epsilon\partial_t\Psi_1(x,t) = \left(-\frac{1}{2}\epsilon^2\partial_x^2 + \frac{1}{2}x^2 + \kappa_{11}|\Psi_1(x,t)|^2 + (\kappa_{12}-i\gamma)|\Psi_2(x,t)|^2\right)\Psi_1(x,t) \tag{3.33}$$

$$i\epsilon\partial_t\Psi_2(x,t) = \left(-\frac{1}{2}\epsilon^2\partial_x^2 + \frac{1}{2}x^2 + \kappa_{22}|\Psi_2(x,t)|^2 + (\kappa_{12}-i\gamma)|\Psi_1(x,t)|^2\right)\Psi_2(x,t) \tag{3.34}$$

ϵ can be set to 1 if the characteristic length is the oscillator length.
For the case of two dimensions, the rescaled Gross-Pitaevskii equations have the following form:

$$\begin{aligned} i\epsilon\partial_t\Psi_1(x,y,t) = \Bigg(&-\frac{1}{2}\epsilon^2(\partial_x^2+\partial_y^2) + \frac{1}{2}(x^2+\frac{\omega_y^2}{\omega_x^2}y^2) + \kappa_{11}|\Psi_1(x,y,t)|^2 \\ &+ (\kappa_{12}-i\gamma)|\Psi_2(x,y,t)|^2\Bigg)\Psi_1(x,y,t) \end{aligned} \tag{3.35}$$

$$\begin{aligned} i\epsilon\partial_t\Psi_2(x,y,t) = \Bigg(&-\frac{1}{2}\epsilon^2(\partial_x^2+\partial_y^2) + \frac{1}{2}(x^2+\frac{\omega_y^2}{\omega_x^2}y^2) + \kappa_{22}|\Psi_2(x,y,t)|^2 \\ &+ (\kappa_{12}-i\gamma)|\Psi_1(x,y,t)|^2\Bigg)\Psi_2(x,y,t) \end{aligned} \tag{3.36}$$

The time t is rescaled by the trapping frequency ω_x in x-direction and the coordinates x and y by the oscillator length in x-direction. Following the steps for the one-dimensional case, one obtains the dimensionless equations for two dimensions. All results are obtained by calculations with the dimensionless equations.

CHAPTER 4

Numerical methods

The nonlinear structure of the equation 2.39 makes an analytic treatment very complicated. Since the case of the condensate mixture with two-body losses described by 3.33 and 3.34 is even more difficult, a numerical method is required.
In this section, the methods to solve such equations will be discussed starting with a simple problem. Later, it is applied to different physical situations. For the examples in this chapter, only one-dimensional systems are considered. The methods will be later used for problems in two dimensions.

4.1 Split step method

In order to obtain the time evolution of a wave function, the split operator method is used [14]. The general form of the time evolution is given by:

$$\Psi(\vec{r}, t + \Delta t) = e^{-\frac{i}{\hbar}\hat{H}\Delta t}\Psi(\vec{r}, t) \tag{4.1}$$

with the time evolution operator

$$\hat{U}(t + \Delta t, t) = e^{-\frac{i}{\hbar}\hat{H}\Delta t}. \tag{4.2}$$

The Hamiltonian for the harmonic oscillator has the form

$$\hat{H} = \hat{T} + \hat{V} = \frac{\hat{p}^2}{2m} + \hat{V}(\vec{r}). \tag{4.3}$$

Using the series representation of the exponential function gives:

$$\begin{aligned} e^{-\lambda(\hat{T}+\hat{V})} &= 1 - \lambda(\hat{T} + \hat{V}) + \frac{\lambda^2}{2}(\hat{T} + \hat{V})^2 + \dots \\ &= 1 - \lambda(\hat{T} + \hat{V}) + \frac{\lambda^2}{2}(\hat{T}^2 + \hat{V}\hat{T} + \hat{T}\hat{V} + \hat{V}^2) - \mathcal{O}(\lambda^3) \end{aligned} \tag{4.4}$$

Considering the general form for the time evolution in formula 4.1, both $\hat{T}$ and $\hat{V}$ act on the wave function at the same time and one has to decide to work either in the position or in the momentum space. In order to avoid this and to use that $\hat{T}$ is diagonal in momentum space and $\hat{V}$ in position space, one uses the Trotter-Suzuki decomposition to approximate the exponential function with a product of three exponential functions. Each of them contains

only one operator of the Hamiltonian:

$$e^{-\lambda\hat{T}/2}e^{-\lambda\hat{V}}e^{-\lambda\hat{T}/2} \approx \left(1-\frac{\lambda\hat{T}}{2}+\frac{\lambda^2\hat{T}^2}{4}-\mathcal{O}(\lambda^3)\right)\left(1-\lambda\hat{V}+\frac{\lambda^2\hat{V}^2}{2}-\mathcal{O}(\lambda^3)\right) \cdot \left(1-\frac{\lambda\hat{T}}{2}+\frac{\lambda^2\hat{T}^2}{4}-\mathcal{O}(\lambda^3)\right) \tag{4.5}$$

$$= 1-\lambda(\hat{T}+\hat{V})+\frac{\lambda^2}{2}(\hat{T}^2+\hat{V}\hat{T}+\hat{T}\hat{V}+\hat{V}^2)-\mathcal{O}(\lambda^3) \tag{4.6}$$

Note, that the formulas 4.4 and 4.6 differ in the order $\mathcal{O}(\lambda^3)$. If one chooses λ to be small enough, the deviations between the expansions 4.4 and 4.6 and also with the exact exponential expression get smaller.
If that algorithm is used, one needs to check that the choice of λ is sufficiently small to keep the error of this approximation negligible. The time expansion for a time interval $T = n \cdot \Delta t$ reads:

$$\Psi(\vec{r},T) = \left(e^{-\frac{i}{\hbar}\hat{H}\Delta t}\right)^n \Psi(\vec{r},0) \tag{4.7}$$

$$\approx \left(e^{-\frac{i}{\hbar}\frac{\hat{T}}{2}\Delta t}e^{-\frac{i}{\hbar}\hat{V}\Delta t}e^{-\frac{i}{\hbar}\frac{\hat{T}}{2}\Delta t}\right)^n \Psi(\vec{r},0) \tag{4.8}$$

By using an FFT (Fast Fourier Transformation) algorithm to transform the wave function from momentum space to position space and vice versa, the time dependent wave function for the time interval $T = n \cdot \Delta t$ can be calculated.
In the case of the Gross-Pitaevskii equation, an interaction terms of the form $U_0|\Psi(x)|^2$ has to be added to the Hamiltonian. Since it depends only on $\vec{r}$, the equation 4.9 for the k-th time step reads

$$\Psi(\vec{r},k\Delta t) \approx \left(e^{-\frac{i}{\hbar}\frac{\hat{T}}{2}\Delta t}e^{-\frac{i}{\hbar}(\hat{V}+U|\Psi(\vec{r},(k-1)\Delta t)|^2)\Delta t}e^{-\frac{i}{\hbar}\frac{\hat{T}}{2}\Delta t}\right)\Psi(\vec{r},(k-1)\Delta t). \tag{4.9}$$

4.2 Imaginary time evolution

To obtain the ground state for a system like equations 3.33 and 3.34, the imaginary time propagation is used [15]. The representation of an arbitrary state in the basis of the eigenfunctions of the Hamiltonian is given by:

$$|\Psi\rangle = \sum_n c_n |\Phi_n\rangle, \tag{4.10}$$

where Ψ is an arbitrary state and Φ_n are the eigenfunctions. The time-dependent Schrödinger equation is

$$i\hbar\frac{d}{dt}|\Psi\rangle = \hat{H}|\Psi\rangle \tag{4.11}$$

Combining both equations gives:

$$i\hbar\sum_n \frac{dc_n}{dt}|\Phi_n\rangle = \sum_n c_n E_n |\Phi_n\rangle \tag{4.12}$$

$$\rightarrow c_n(t) = c_n(0)e^{-\frac{iE_n t}{\hbar}} \tag{4.13}$$

Thus:

$$|\Psi(t)\rangle = \sum_n e^{-\frac{iHt}{\hbar}} c_n |\Phi_n\rangle = \sum_n e^{-\frac{iE_n t}{\hbar}} c_n |\Phi_n\rangle = e^{-\frac{itE_0}{\hbar}} c_0 |\Phi_0\rangle + e^{-\frac{itE_1}{\hbar}} c_1 |\Phi_1\rangle + \dots \quad (4.14)$$

Calculating the energy:

$$E = \langle\Psi| H |\Psi\rangle = |c_0|^2 E_0 + |c_1|^2 E_1 + |c_2|^2 E_2 + \dots \quad (4.15)$$

The mixed terms vanish due to orthogonality ($\langle\Phi_i|\Phi_j\rangle = \delta_{ij}$).
For the imaginary time evolution, one uses the substitution $t = i\tau$. The states and energy become:

$$|\Psi(t)\rangle = \sum_n e^{-\frac{\tau H}{\hbar}} c_n |\Phi_n\rangle = \sum_n e^{-\frac{\tau E_n}{\hbar}} c_n |\Phi_n\rangle = e^{-\frac{\tau E_0}{\hbar}} c_0 |\Phi_0\rangle + e^{-\frac{\tau E_1}{\hbar}} c_1 |\Phi_1\rangle + \dots \quad (4.16)$$

The substitution causes an exponential decay of the energy. The high energies are exponentially suppressed and for large τ the ground state energy E_0 is left. Convergence requires that $E_0 > 0$, otherwise one has to introduce a shift of the energy spectrum. To implement

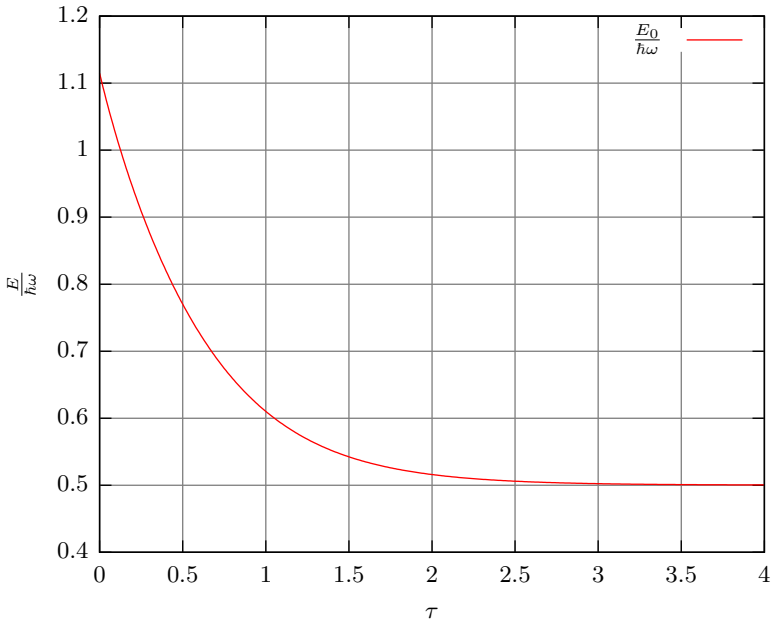

Figure 4.1: Imaginary time evolution for the harmonic oscillator. By solving the corresponding Hamiltonian analytically, one obtains the ground state energy of 0.5 $\hbar\omega$. This plot shows the convergence of the energy using the imaginary time evolution converging to the same value.

the time evolution in equation 4.16, the split step algorithm is used which was previously discussed.
The Gross-Pitaevskii equation for the non-interacting case is the Schrödinger equation for the harmonic oscillator. Its solution is known as

$$\Psi(x) = \left(\frac{m\omega}{\hbar\pi}\right)^{1/4} exp\left(-\frac{m\omega x^2}{2\hbar}\right) \quad (4.17)$$

and gives the opportunity to check the result obtained from the split-step method.
The corresponding Hamiltonian in 1D reads:

$$\hat{H}\Psi(x) = \left(-\frac{\hbar^2}{2m}\frac{\partial^2}{\partial x^2} + \frac{1}{2}m\omega^2 x^2\right)\Psi(x) \tag{4.18}$$

For convergence issues, the starting function is already a Gaussian function, but any function can be used. Using this method, the energy converges to a value of $E_0 \approx 0.5\,\hbar\omega$ what is shown in figure 4.1. The corresponding ground state can be found in figure 4.2. Since this time evolution is non-unitary, the norm decays as well. Thus, the wave function is normalized during every iteration. This algorithm is for all situations used throughout the entire thesis.

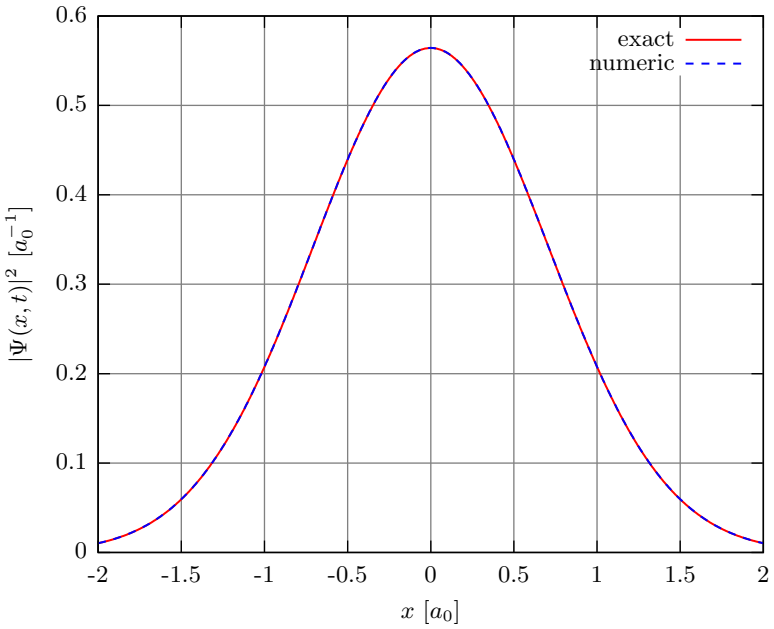

Figure 4.2: Ground state density for the harmonic oscillator. The exact and the numeric solution are plotted. Both curves are on top of each other. As expected, they are Gauss shaped functions with mean energy of 0.5 $\hbar\omega$.

4.3 Solving the GPE

In the following, we will apply the methods from the previous section in order to solve the GPE for several cases. In order to do this, the first program part calculates the ground state using the imaginary time evolution. The program is written in *Python*, since it provides an FFT algorithm. For the dynamics, the real time evolution is applied to the previously calculated ground state.

4.3.1 Different interactions

First, we consider the static case. According to equation 3.32, the dimensionless Gross-Pitaevskii equation for $\epsilon = 1$ in 1D is:

$$i\frac{\partial\Psi(x,t)}{\partial t} = \left(-\frac{1}{2}\frac{\partial^2}{\partial x^2} + \frac{1}{2}x^2 + \kappa|\Psi(x,t)|^2\right)\Psi(x,t) \tag{4.19}$$

With the ansatz $\Psi(x,t) = e^{-i\mu t}\Psi(x)$, one obtains the time-independent GPE

$$\mu\Psi(x) = \left(-\frac{1}{2}\frac{\partial^2}{\partial x^2} + \frac{1}{2}x^2 + \kappa|\Psi(x)|^2\right)\Psi(x) \tag{4.20}$$

With the previously discussed methods, one is able to calculate the ground state for different interactions κ. Since the interaction is repulsive, the density profiles become wider, the

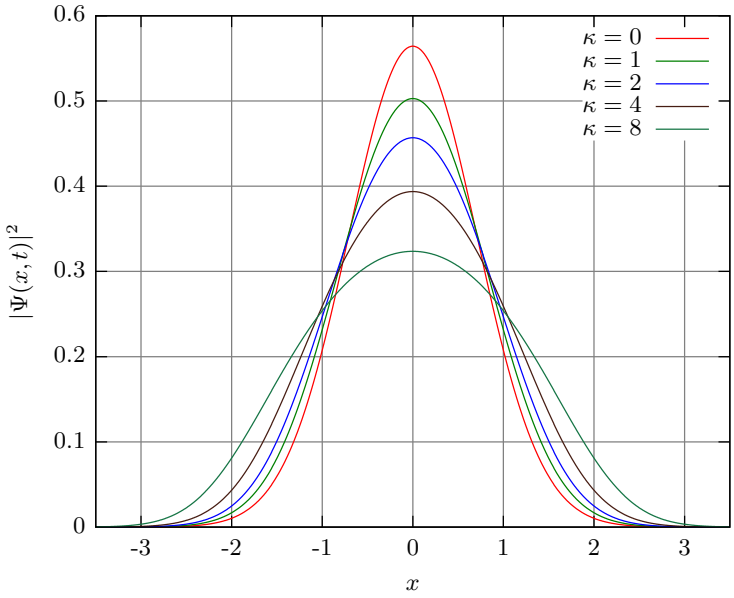

Figure 4.3: Ground state density for the Gross-Pitaevskii equation. As the repulsive interaction is increased, the density profiles get wider.

larger the interaction gets. The potential confines the atoms to a certain spatial region, but if the interaction is large enough, the gas lowers its energy by extending the density profile.

4.3.2 Real time evolution

For the real time evolution, we use the same decomposition as for the imaginary time evolution but the substitution $it \to \tau$ is not used. It is now possible to calculate how the density evolves in time.
In order to discuss the real time evolution, the breathing mode, which was already mentioned in section 2.2, will be studied.
To excite these modes, the frequency of a harmonic trap is altered. This causes an oscillation of the density which frequency depends on the interaction. Considering now the change of the trapping frequency by e.g. 10%, the change of κ and ϵ has to taken into account. Since $\epsilon \propto \frac{1}{\omega}$ and $\kappa \propto \frac{1}{\omega^2}$ the change gives:

$$\epsilon \to \frac{\epsilon}{1.1} \tag{4.21}$$

$$\kappa \to \frac{\kappa}{1.1^2} \tag{4.22}$$

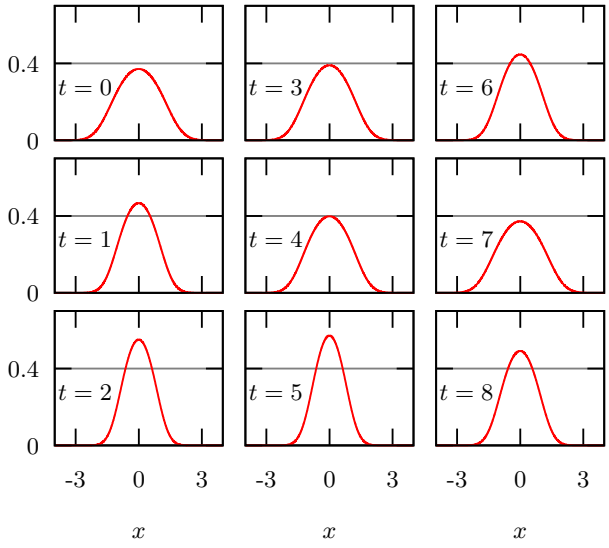

Figure 4.4: Behavior of the density over time after changing the trapping potential by 40% for no interaction. The width and the maximum of the density starts oscillating. The plot $t = 0$ shows the ground state. At $t = 1$, one can see that the width of the curve got already smaller and the height increased too and reaches its maximum for $t = 2$. From $t = 3$ to $t = 4$, the density expands again and repeats pulsating in the time interval 5 to 8.

To extract the frequency of the oscillating condensate, $n(x = 0, t)$ is plotted versus time. This oscillation can be described by a function of the form

$$f(t) = a \cdot sin\left(b\left(t - t_0\right)\right) \tag{4.23}$$

With a fit of this function to $n(x = 0, t)$, one is able to obtain how $\frac{\omega}{\omega_0}$ depends on κ, where ω is the frequency of the mode and ω_0 the frequency of the harmonic trap. The corresponding plot is shown in figure 4.5. The ratio $\frac{\omega}{\omega_0}$ is for small interaction as expected ≈ 2 but drops down with increasing κ to $\sqrt{3}$ which is in agreement with [10].

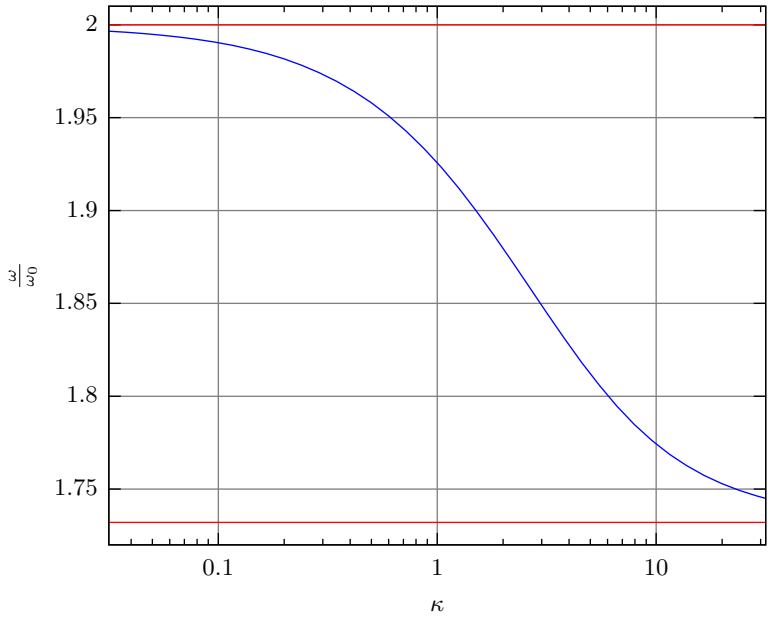

Figure 4.5: Breathing mode frequency versus the interaction for a change of 10% of the trapping frequency. One can see that for small interactions $\frac{\omega}{\omega_0} \approx 2$ and for large $\frac{\omega}{\omega_0} \approx \sqrt{3}$ (both red lines).

CHAPTER 5

Convergence & Consistency

By discretizing time and space, there is always an error compared to the analytical solution. Thus, it is always recommended to check for convergence. For these numerical methods which are used here, it means that changing the discretization steps should not affect the results considerably.
It was already mentioned in the previous chapter that the precision of the split-step method depends on the Δt. Minimizing this inaccuracy requires a small time step size and should be checked in order to investigate the convergence behavior.
First, the results from [16] are reproduced and then, the program is checked for the system according to equations 3.33 and 3.34 for convergence.

5.1 Consistency

In order to check the program, we try to reproduce some of the results from [16].
For that, we have to change the units of the original time-dependent Gross-Pitaevskii equation. We start with the form of equation 2.35 in absence of a potential, but with dissipation.

$$i\hbar\frac{\partial}{\partial t}\Psi = -\frac{\hbar^2}{2m}\frac{\partial^2}{\partial x^2}\Psi + U_0|\Psi|^2\Psi - i\hbar\gamma(x)\Psi \tag{5.1}$$

The transformation to the dimensionless equation for this special case can be found in the section 2 of the appendix , since the unit system of this paper is different from the rest of this thesis. The new GPE reads:

$$i\partial_{\tilde{t}}\tilde{\Psi} = -\partial_{\tilde{x}}^2\tilde{\Psi} + \tilde{U}|\tilde{\Psi}|^2\tilde{\Psi} - i\tilde{\gamma}(\tilde{x})\tilde{\Psi} \tag{5.2}$$

The form of $\tilde{\gamma}(\tilde{x})$ is given by

$$\tilde{\gamma}(\tilde{x}) = \tilde{\gamma_0}e^{-\frac{\tilde{x}^2}{2\tilde{\zeta}^2}} \tag{5.3}$$

The next step is now to reproduce the results of that paper.
Figure 5.1 shows the density at $\tilde{x} = 0$ for various values of ζ which represents the width of the Gaussian dissipation for $\tilde{\gamma_0} = 0.5$ starting with a constant background of $\tilde{\Psi} = \rho_0 = 0.4$ and an interaction $\tilde{U} = \sigma = 1$. The following plots are generated with the program and are shown below. The second plot gives the ratio of condensed atoms and initial atom number versus time for a different $\tilde{\gamma_0}$. Unfortunately, the value of $\tilde{\zeta}$ is not given in [16]. For the plot, a value of $\tilde{\zeta} = 1.2$ is used and it produces a plot which is quite similar to that one in the paper. That means that the program using the split step method produces the same results. It is a valid method to describe the physical situation.

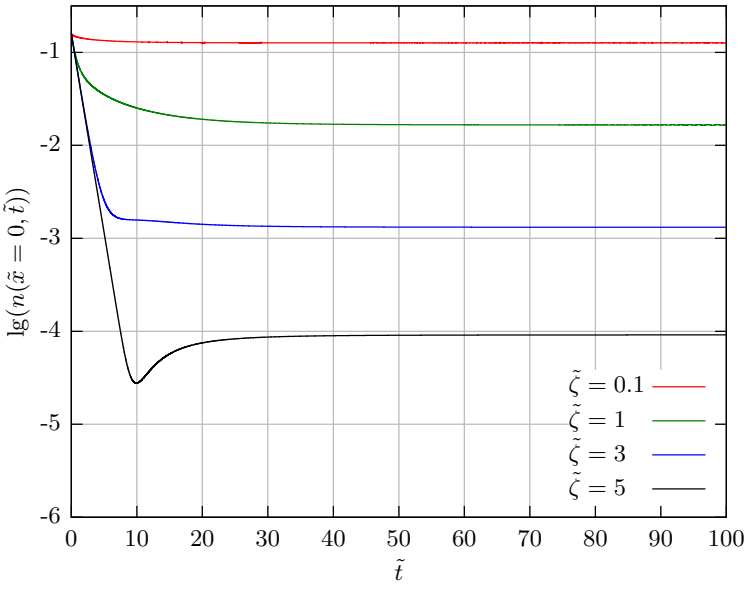

Figure 5.1: Reproduced plot from the paper. The figure shows the density in the center versus the time for different values of the width of the Gaussian dissipation. This plot is identical to the figure 1a from the paper.

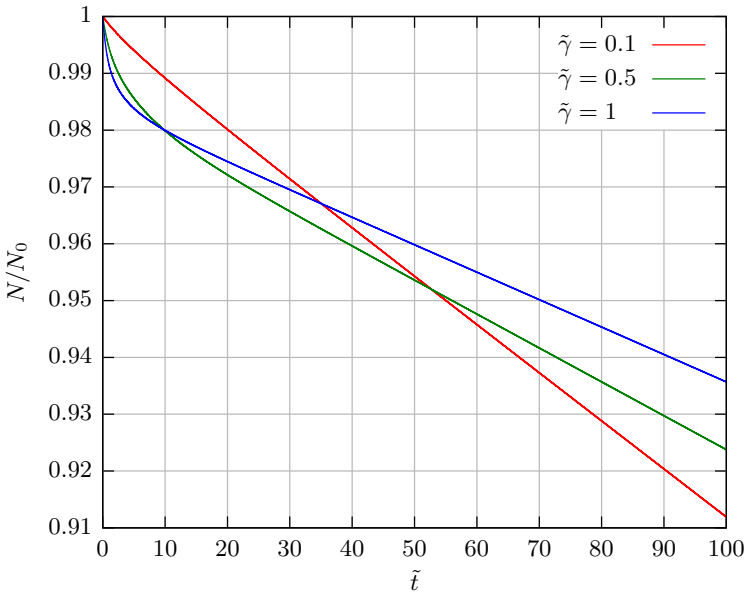

Figure 5.2: The second plot from the paper. Unfortunately, it was not possible to reproduce that plot completely since the exact value of $\tilde{\zeta}$ was not given. Assuming a value of $\tilde{\zeta} = 1.2$, it is very similar to figure 1b from the paper. For a large coupling, the loss is smaller for large times which corresponds to the Quantum-Zeno effect.

The figure 5.1 shows the Quantum Zeno effect. Since a larger value $\tilde{\gamma_0}$ represents a stronger coupling, it suggests that the loss of atoms should be also larger. The plot shows the opposite effect for large times. According to the paper, the larger dissipation causes a less efficient long term particle loss since there is not a sufficient amount of particles. For a

smaller dissipation parameter $\tilde{\gamma}_0$, there is no lack of particles which guarantees a continuous dissipation.

5.2 Convergence

Now, the convergence of the computing program for a system described by equations 3.33 and 3.34 is checked. The following considerations are also carried out for the two dimensional case given by the equations 3.35 and 3.36.

5.2.1 Convergence in space

In order to check, if there are any deviations one chooses more points in a interval. We consider the change of particle number for the two level system in an interval of $-5 < x < 5$ using 2400, 8000 and 20000 discretization steps, for different interactions. The y-axis is

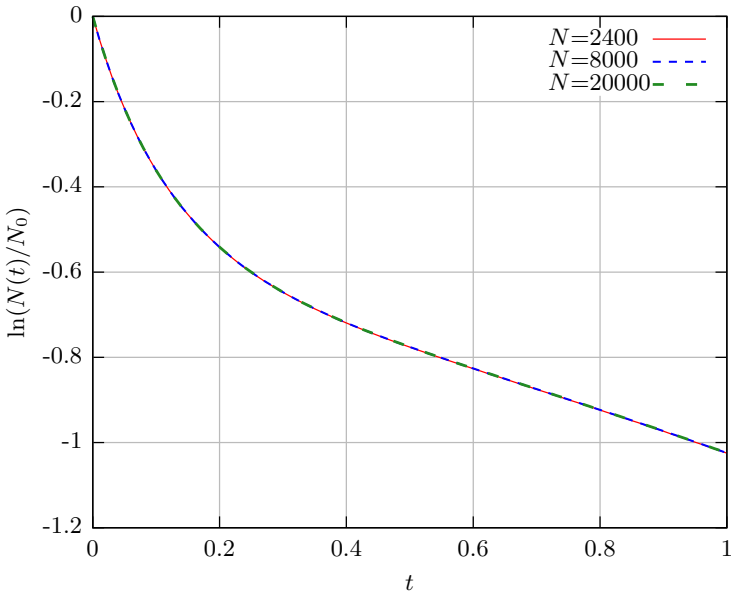

Figure 5.3: Plot for the program which solves equation 3.33 and 3.34 for a fixed interval for x of $[-5, 5]$, $\gamma = 10$, $\kappa_{11} = \kappa_{22} = 0$ and $\kappa_{12} = 2$. There is no apparent difference between the plots, so one can conclude that $N = 2400$ is sufficient. The form of the curve will be discussed later.

scaled logarithmically, the x-axis shows the time from 0 to 1. The differences between the curves are not visible on that scale. All lines are on top of each other which implies that the algorithm converges with respect to the space discretization. On a smaller scale, one sees a small deviation and the difference that between 20000 and 8000 points is smaller than between 2400 and 8000 points. This is an indication for convergence.
In two dimensions, the space is discretized in form of a grid. For a convergence check, the number of steps are $N_x = N_y = 100$, $N_x = N_y = 200$ and $N_x = N_y = 240$ where N_x and N_y are the number of steps per dimension. One observes also a convergence behavior similar to the one-dimensional case. Therefore, it is not discussed explicitly here. All following calculations in two dimensions are done with $N_x = N_y = 230$ steps.

5.2.2 Convergence in time

The convergence for the time parameter should also be checked for the same reasons as the convergence in space. Further, the program is much more sensitive in relation to the time step than in relation to the space step. This is a consequence to the Trotter-Suzuki decomposition, which was already discussed in section 4.1.
The figure 5.4 below shows the calculation for the time steps 10^{-2}, 10^{-3} and 10^{-4} for one dimension. The values for the interactions are $\kappa_{12} = 3$, $\kappa_{11} = \kappa_{22} = 0$ and $\gamma = 10$. For

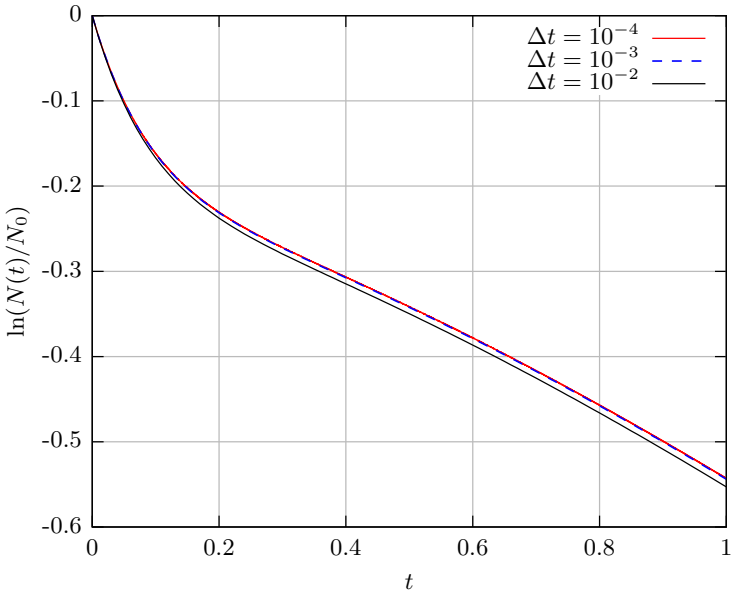

Figure 5.4: Plot in order to check the convergence of the program with respect to the time steps for $\kappa_{11} = \kappa_{22} = 0$, $\kappa_{12} = 3$ in 1D and the number of 2400 steps in space. The smaller Δt gets, the smaller the difference becomes between the decay curves for the different values of Δt.

these parameters, there is a relatively large deviation between $\Delta t = 10^{-2}$ and $\Delta t = 10^{-3}$. The difference between the curves with $\Delta t = 10^{-3}$ and $\Delta t = 10^{-4}$ is much smaller, so the program converges regarding the time steps. Since there is only a minor difference between $\Delta t = 10^{-4}$ and $\Delta t = 10^{-3}$, the latter is used for the following results in order to keep the computation time small.
For two dimensions, the convergence was checked for the same step size. Since the convergence with respect to Δt is related to the noncommutativity of the kinetic energy operator and the operators in position space, it exhibits the same properties. All following calculations are done with $\Delta t = 10^{-3}$ because the results are sufficiently precise and the computation time is rather small.

CHAPTER 6

Static properties of a two-component gas in 1D

In this chapter, the focus will be on the static properties of a two-component Bose gas. The shape of the ground states for different interactions according to the dimensionless form of equations 2.56 and 2.57 will be discussed, since the initial distribution is important for the dynamics studied in the following chapter.
The separation of both components was already studied in detail. Using Feshbach resonances, the scattering length between ^{85}Rb and ^{87}Rb was tuned and made it possible to observe the separation of both species [17]. Theoretical studies in [18] provide a method using the Thomas-Fermi approximation how the species separate and offer an insight into the shape and position of each component in the trap. Similar to this, ground state studies with a modified Gauss ansatz have been made in [19].

6.1 State separation

Due to the form of the equations 3.33 and 3.34, one expects a competition of the interspecies (κ_{12}) and intraspecies interaction (κ_{11} and κ_{22}). In the following section, we will derive which of them influences the form of the ground state the most.

- If $\kappa_{12}^c \lesssim \kappa_{11} = \kappa_{22}$, then κ_{11} and κ_{22} contribute more to the energy of the system than the interspecies interaction. κ_{12}^c denotes the critical interspecies interaction where state separation occurs. It is then energetically more favorable to place the atoms in the middle of the trap instead of at the edges. This is shown below in figure 6.1 for $\kappa_{11} = \kappa_{22} = 4$ and $\kappa_{12} = 3$. Since $\kappa_{12}^c \lesssim \kappa_{11} = \kappa_{22}$, both density profiles are on top of each other.

- Consider now the case for $\kappa_{11} = \kappa_{22} \lesssim \kappa_{12}^c$, e.g. $\kappa_{11} = \kappa_{22} = 3$ and $\kappa_{12} = 5$. The ground state for this setting is shown in figure 6.2. The system minimizes the energy by increasing the distance between the two components, since κ_{12} is larger than κ_{11}. Keeping both kinds of them at the same position would cost too much energy. For a much clearer separation, one needs to choose κ_{12} much larger than $\kappa_{11} = \kappa_{22}$ in order to decrease the overlap.
  Due to that choice of the interactions, the system looses its mirror symmetry what has an influence on the computation time for the ground state. It depends on the initial conditions for each of these wave functions. As already mentioned, a Gaussian function is assumed, but now one can add the position of the curve as an initial condition. If e.g $\Psi_1(x) = e^{-x^2}$ and $\Psi_2(x) = e^{-x^2}$ is assumed, the computation time for the case of state separation becomes quite large. The program needs some time to decide which curve is shifted to the right and which one to the left. This happens based on numerical

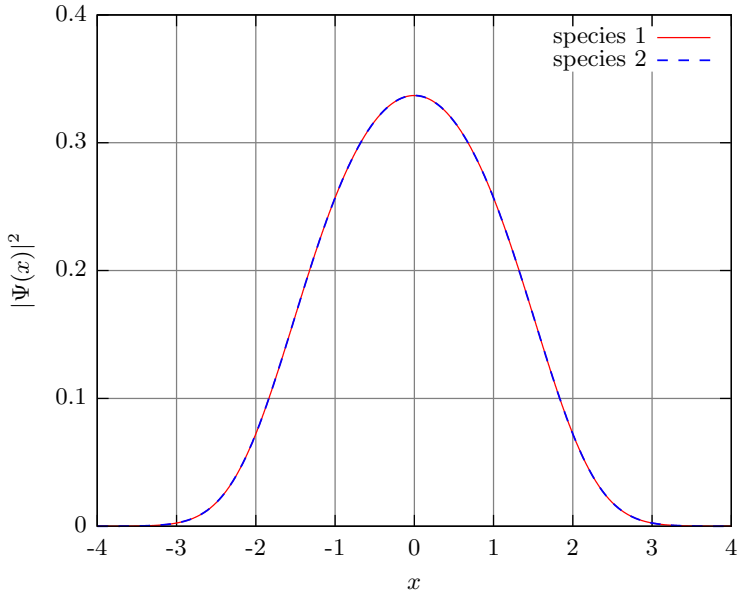

Figure 6.1: Ground state of a two level system for $\kappa_{11} = \kappa_{22} = 4$ and $\kappa_{12} = 3$. Since the interaction for each species is larger than the interaction between themselves, the atoms arrive at positions with as much distance as possible from the potential. Thus, both distributions have the same position and form.

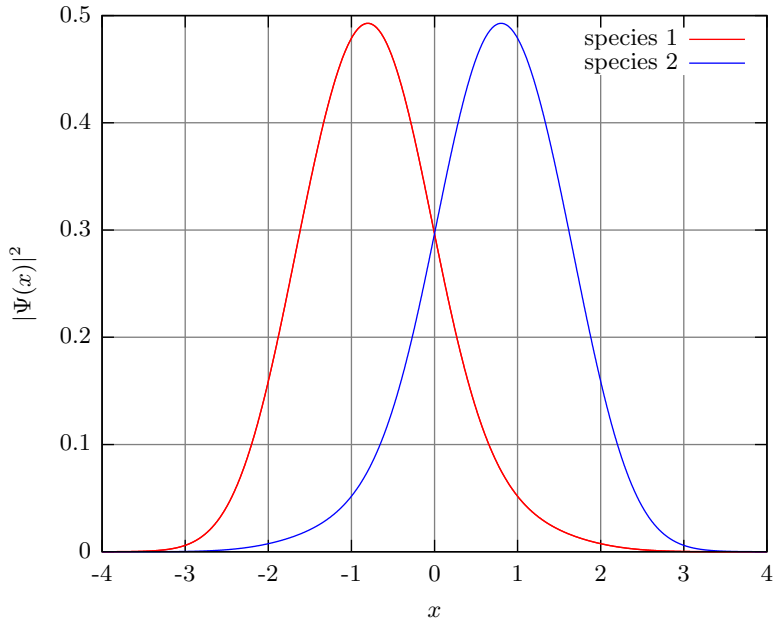

Figure 6.2: Ground state of a two level system for $\kappa_{11} = \kappa_{22} = 3$ and $\kappa_{12} = 5$. Both species have separated since $\kappa_{12}^c \gtrsim \kappa_{11} = \kappa_{22}$, but they overlap anyway. Any further increase of κ_{12} leads to a smaller coexisting region of both components.

fluctuations. To avoid this and keep the computation time small, the initial curves have the form $\Psi_1(x) = e^{-(x+b)^2}$ and $\Psi_2(x) = e^{-(x-b)^2}$ for the cases $\kappa_{11} = \kappa_{22} \lesssim \kappa_{12}^c$ where b is a shift along the x-axis. If $\kappa_{11} = \kappa_{22} \gtrsim \kappa_{12}^c$ and no state separation occurs, the densities are just shifted back to the middle during the ground state calculation,

i.e. $b = 0$. If κ_{12} is sufficiently large, the initial shift and the form of the density is adjusted.

- Considering the case, $\kappa_{11} = \kappa_{12} >> \kappa_{22}$. An example with $\kappa_{11} = 8$, $\kappa_{22} = 0$, $\kappa_{12} = 8$ is shown in figure 6.3. One component is concentrated in the center of the trap. The space near the edges of the potential is filled up with atoms of the other species. Although state separation occurs, the system keeps its mirror symmetry.
  Since the second species does not have any interaction with itself, the density is quite narrow due to the fact that its shape is not affected by κ_{22}. In contrast to that, the first component has to deal with the large interactions κ_{11} and κ_{12}. Since the middle of the trap is energetically favorable for the second species, the atoms of the first species is forced to align around the second one and the potential. Despite the state separation, there is no symmetry breaking since the symmetry of the system is still conserved.

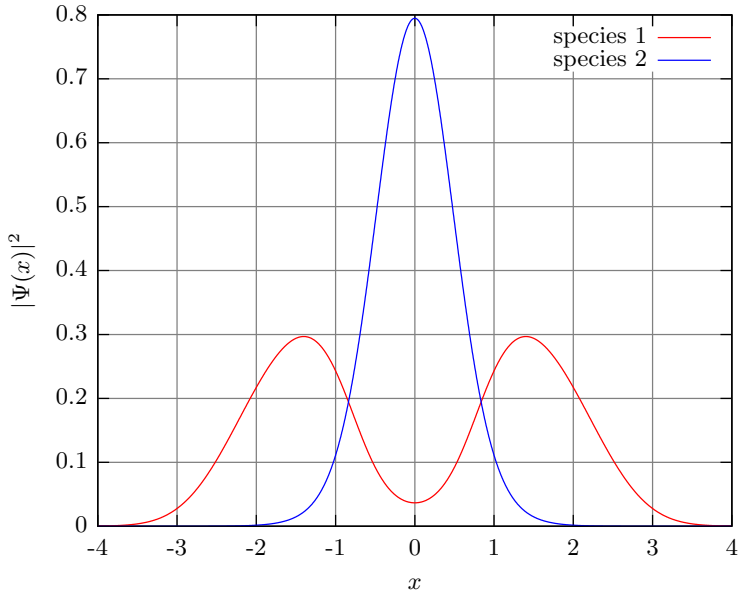

Figure 6.3: Ground state of a two level system for $\kappa_{11} = 8$, $\kappa_{22} = 0$ and $\kappa_{12} = 8$. Since one species has no interaction among its particles, it is concentrated in the middle of the trap. The other particles fill the space between the potential boundary and the other particle species.

6.2 State diagram

As already mentioned, the dissipation of the two-component condensate depends strongly on the overlap of both densities. Thus, it is interesting to know how the overlap is influenced by the interaction κ_{12}. To summarize the cases for different values of $\kappa_{11} = \kappa_{22}$ and κ_{12}, one can plot the strength of the state separation versus the interactions in form of a state diagram.
Setting $\kappa_{11} = \kappa_{22}$, one obtains the diagram which is shown in figure 6.4. The x-axis gives the strength of $\kappa_{11} = \kappa_{22}$ whereas the y-axis provides the value for κ_{12}. The color code stands for the peak position of one component and it gives the magnitude of the state separation. For the case $\kappa_{11} \gtrsim \kappa_{12}^c$, the repulsion between both species is not large enough to cause a

separation of both, since their own interaction provides a bigger part of the energy. Since the potential still confines the atoms spatially, it is energetically favorable to stay in the middle of the trap without any state separation. This corresponds to the yellow area of figure 6.4.
If $\kappa_{11} \lesssim \kappa_{12}^c$, the state with lowest energy is that with the state separation, due to its larger contribution to the energy of the system. The separation is the red part of figure 6.4. For the homogeneous case, one expects $\sqrt{\kappa_{11}\kappa_{22}} = \kappa_{11} = \kappa_{12}^c$. This is also observed in [19] for the same setup but for another method to obtain the ground state.
To point out the difference of the homogeneous case and the case of a trapped two-component gas, figure 6.4 shows a black line which divides the regions of state separation and no state separation for $\kappa_{12}^c = \kappa_{11}$. Due to the existence of a potential, a larger interspecies interaction is necessary in order to separate the different species. The value of κ_{12}^c for the trapped case comes close to that of the homogeneous case if the interactions get larger. Since the system looses its symmetry if the components separate, the diagram provides as well information about the symmetry breaking.

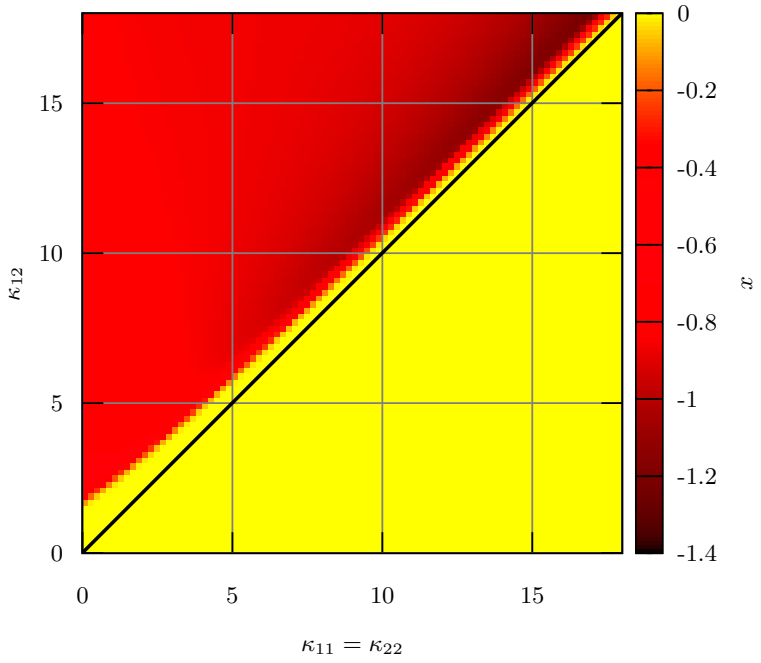

Figure 6.4: State diagram for the state separation. The color code gives the x-position of the peak of one of the condensates. The x-axis gives the value for $\kappa_{11} = \kappa_{22}$, y-axis for κ_{12}. Yellow means no shift and black a very large shift. One can also see that for large interactions the state separation takes place for $\kappa_{12}^c \approx \sqrt{\kappa_{11}\kappa_{22}}$ since the black line approaches the transition region of the state diagram.

6.3 Ground state approximations

To get an expression for the particle number, the integral over space of $n(x) = \Psi^*(x)\Psi(x)$ has to be calculated. For that, we need an analytic expression for the ground state $\Psi(x, t = 0)$. A variational method according to [6] can be used.

- We will first concentrate on the case of no state separation which corresponds to $\kappa_{12}^c \lesssim \kappa_{11} = \kappa_{22}$. According to the previous chapter, we know that the density is

centered around $x = 0$ and that in the case of no interactions, the GPE turns into the Schrödinger equation for the harmonic oscillator. Its ground state solution is given by a Gauss curve. In order to take the interactions into account, we choose a Gauss curve with an adjustable parameter β which adapts the width of the curve depending on the strength of the interaction. The ansatz for $\Psi(x)$ reads

$$\Psi(x) = \sqrt{\frac{1}{\sqrt{\pi}\beta}} e^{-\frac{x^2}{2\beta^2}}, \tag{6.1}$$

where β is a variational parameter. To obtain the energy, this ansatz is inserted into equation 2.49 for the 1D case. Since $\kappa_{12}^c \lesssim \kappa_{11} = \kappa_{22}$, $\Phi_1 = \Phi_2 = \Psi$, one obtains:

$$E = \int dx \ \left[|\partial_x \Psi(x)|^2 + x^2 |\Psi(x)|^2 + (\kappa_{11} + \kappa_{12}) |\Psi(x)|^4 \right] \tag{6.2}$$

All the appearing integrals can be solved with formula A.8 to get the following general expression for the energy:

$$E = \frac{1}{2} \left(\frac{1}{\beta^2} + \beta^2 \right) + \frac{(\kappa_{11} + \kappa_{12})}{\sqrt{2\pi}\beta} \tag{6.3}$$

This expression is supposed to be minimal for the ground state and consequently β has to fulfill the following equation:

$$\frac{\partial E}{\partial \beta} = \left(-\frac{1}{\beta^3} + \beta \right) - \frac{(\kappa_{11} + \kappa_{12})}{\sqrt{2\pi}\beta^2} = 0 \tag{6.4}$$

We will solve this equation numerically since it is complicated to obtain a solution analytically. For the non interacting case, the solution is $\beta = 1$ what means that equation 6.1 turns into the wave function of the harmonic oscillator what is consistent. The comparison of the Gauss ansatz and the numerical solution using imaginary time evolution is shown in figure 6.5. The interactions are set to $\kappa_{11} = \kappa_{22} = 6$ and $\kappa_{12} = 4$ for this plot which means that there is no state separation. One can see that the approximation deviates from the numerical result slightly at the slopes and around the peak. It was previously mentioned that for large interactions, the Thomas-Fermi profile is a good approximation but we concentrate on this regime where the Gauss function provides a sufficient description. We will see later how useful this approximation for dynamical processes is.

- We will now expand that ansatz to the case of state separation. In contrast to the previous case both density profiles are shifted, one to the region $x < 0$ and the other one to $x > 0$. Taking that into account and setting $\kappa_{11} = \kappa_{22}$, the width of the Gauss curves are the same. Now, the ansatz consists of two different wave functions of the form

$$\Psi_1(x) = \sqrt{\frac{1}{\sqrt{\pi}\beta}} e^{-\frac{(x+c)^2}{2\beta^2}} \tag{6.5}$$

$$\Psi_2(x) = \sqrt{\frac{1}{\sqrt{\pi}\beta}} e^{-\frac{(x-c)^2}{2\beta^2}} \tag{6.6}$$

Due to the symmetry of that system, the shift denoted by c is the same.

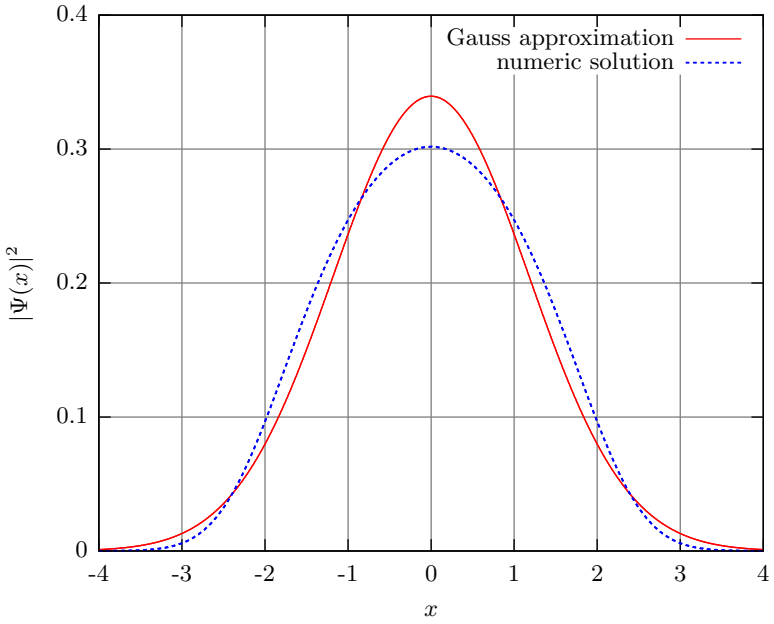

Figure 6.5: Comparison of the Gauss approximation and the numerical obtained ground state for $\kappa_{11} = \kappa_{22} = 6$ and $\kappa_{12} = 4$. There are some differences between them but a Gauss curve might be in average a good approximation for this order of the interactions.

To obtain the energy, we use formula 2.49 again for the a component BEC. After integrating over space, the energy is:

$$E = \frac{1}{2}\left(\frac{1}{\beta^2} + \beta^2\right) + c^2 + \frac{(\kappa_{11} + \kappa_{12}\, e^{-\frac{2c^2}{\beta^2}})}{\sqrt{2\pi}\beta} \tag{6.7}$$

To obtain the minimum energy, the coinciding equation has to be solved numerically again. The comparison of the Gauss ansatz and the numerical solution is shown in figure 6.6 for $\kappa_{11} = \kappa_{22} = 6$ and $\kappa_{12} = 4$.

- In order to compare the approximation with the numerical obtained state diagram, the position of the maximum of the distribution is plotted again like in figure 6.4 showing the dependency on the parameter for the intraspecies and interspecies interactions. The result is shown in figure 6.7. The black line in the diagram is for $\kappa_{12} = \kappa_{11}$. One can see how this diagram differs from 6.4 especially for large interactions. At around $\kappa_{12} = \kappa_{11} = 7$, the red area, which denotes the state separation region, crosses that line which does not occur in figure 6.4. Since one assumes a Gauss shaped particle density, the overall shape is supposed to be symmetric and a deformation of the slopes is not allowed. This deformation becomes significant above $\kappa_{12} = \kappa_{11} = 7$ which explains the difference between the figures 6.4 and 6.7.

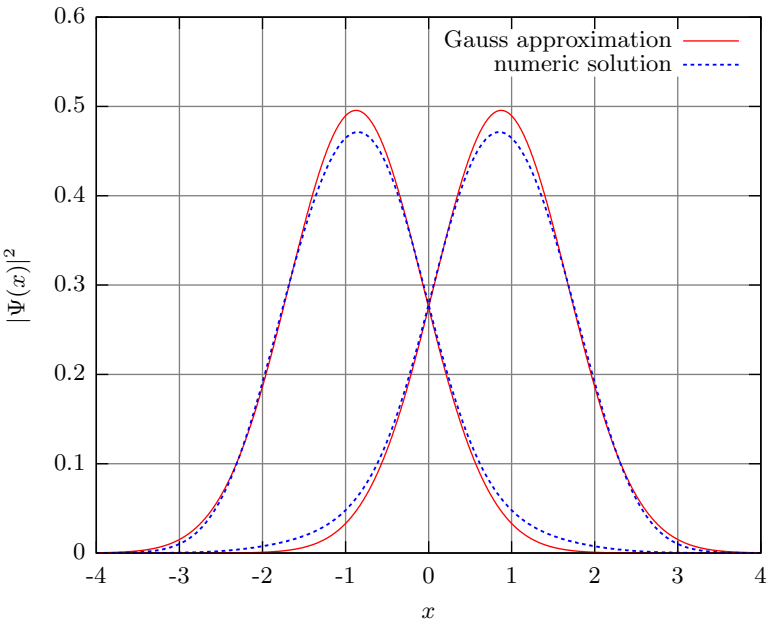

Figure 6.6: Density profiles for $\kappa_{11} = \kappa_{22} = 6$ and $\kappa_{12} = 4$ calculated numerically and with a Gauss ansatz. Despite some differences, the Gauss curves are a reasonable approximation.

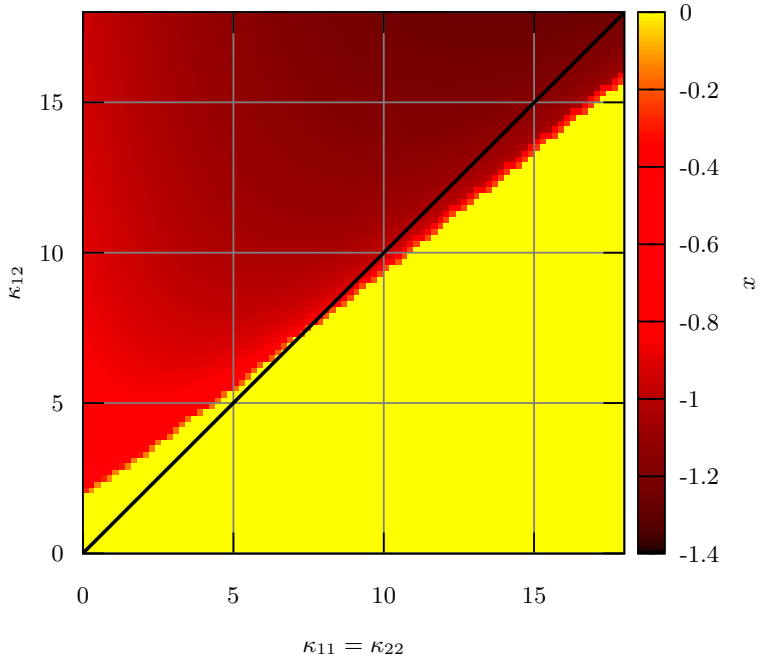

Figure 6.7: State diagram for the Gauss approximations. The red area shows the ranges of the interactions where state separation occurs and the yellow part where no shift of the density profiles appear. Compared to figure 6.4, the black line intersects the red region at around $\kappa_{11} = \kappa_{22} = \kappa_{12} = 7$.

CHAPTER 7

Dynamical properties of a two-component gas in 1D

We are going to study the evolution of the system according to the equations 3.33 and 3.34 in time. This includes the breathing mode and all effects related to dissipation. In order to explain these, a detailed analysis of the density profiles for characteristic times is necessary.

7.1 Breathing mode

In section 4.3.2, we considered the breathing mode for a one component condensate. From the numerical solution, it was found that the ratio of trapping frequency ω_0 and the mode frequency of the condensate ω is $\frac{\omega}{\omega_0} = 2$ in non-interacting regime and in the Tonks-Girardeau regime and $\frac{\omega}{\omega_0} = \sqrt{3}$ in the mean field regime. For the breathing mode of a two-level system,

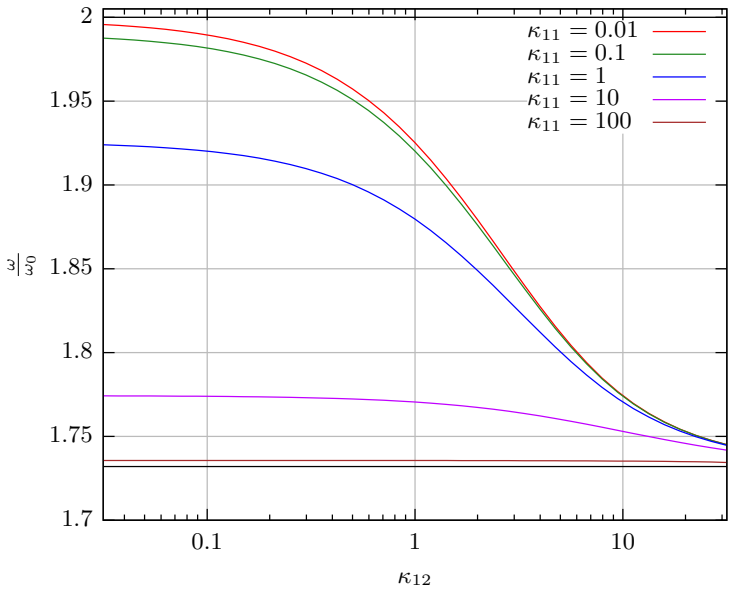

Figure 7.1: Breathing mode frequencies versus the interaction κ_{12}. For small κ_{12}, the mode frequency is dominated by the $\kappa_{11} = \kappa_{22}$ and the frequency ratio is like for the on species case. If κ_{12} increases to the order of $\kappa_{11} = \kappa_{22}$, the interspecies interaction term becomes more relevant and all curves start to converge towards $\frac{\omega}{\omega_0} = \sqrt{3}$.

the focus is on $\kappa_{11} = \kappa_{22}$. The results are shown in figure 7.1. For each line, $\kappa_{11} = \kappa_{22}$ is fixed and κ_{12} is changed. For small κ_{12}, the start values for different $\kappa_{11} = \kappa_{22}$ have to be the same as for the one-level system (see figure 4.5). In this case, the interspecies interaction is small compared to the intraspecies interaction. If κ_{12} increases to the order of $\kappa_{11} = \kappa_{22}$, the mode frequency starts then to decrease and converges afterwards towards the value of $\frac{\omega}{\omega_0} = \sqrt{3}$. One can conclude that the frequency of the breathing mode for a two component system is dominated by the largest interaction.

7.2 Atom loss dynamics for no state separation

In the following, the interactions are kept constant and the γ which is responsible for the atom losses is varied. Starting from a two component Bose gas in the ground state which was the subject of the previous chapter, the dynamics of that system will be studied when the two body losses between both species according to equations 3.33 and 3.34 begins.
Since the dissipation depends on the overlap between both species, we will be distinguish between the different types of ground states in the following as well.

7.2.1 Atom loss for different γ

Figure 7.2 shows the decay for one component for different values for γ in the case of no state separation. The values for the interaction are $\kappa_{11} = \kappa_{22} = 4$ and $\kappa_{12} = 2$. With

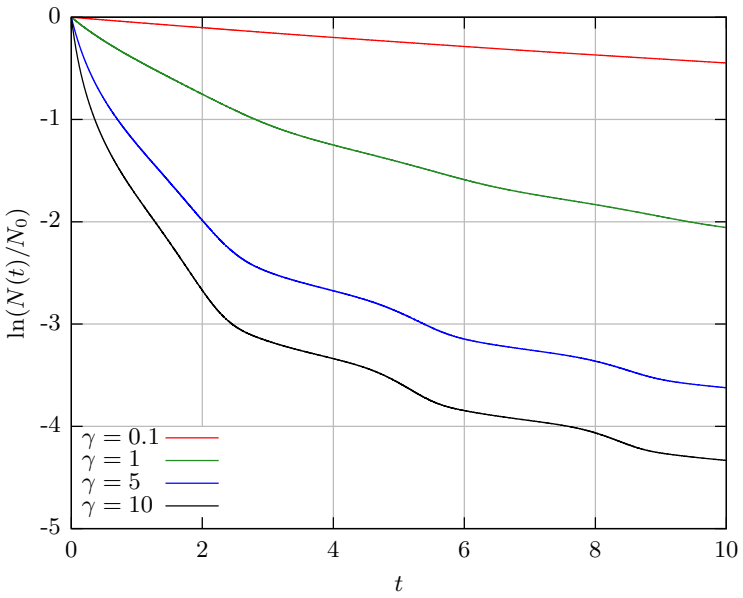

Figure 7.2: Logarithmic plot for the decay for one component for different γ, $\kappa_{11} = \kappa_{22} = 4$ and $\kappa_{12} = 2$. With increasing γ, the losses and the oscillations gets larger.

an increasing γ, the atom losses increase too. While the red curve ($\gamma = 0.1$) has a very smooth shape, the green curve ($\gamma = 1$) exhibits a slightly irregular structure at e.g. $t = 4$. This becomes even more visible for the dissipation rates $\gamma = 5$ and $\gamma = 10$ which have an oscillating character. The origin of theses oscillations in the decay curves will be explained in more detail in the following sections 7.2.2 and 7.2.4.
It is difficult to extract the frequency of this oscillation precisely. However by reading off, one can determine the periodicity of these oscillations to be $T' \approx 3$. Since the time was

rescaled by the trapping frequency ω_x, we obtain for unscaled time $T \approx \frac{3}{\omega_x}$. The most general expression for T is $T = \frac{2\pi}{\omega}$. Inserting the T from the plot gives $\omega \approx 2\omega_x$ for the oscillation frequency of the decay curve. This is of order of the breathing mode frequencies for the case of very large and no interactions.

7.2.2 Evolution of the densities

In the following, we will concentrate on the evolution of the densities in order to explain the oscillating behavior of the decay curves. For this, we consider the density profiles at different times. In figure 7.3, the interactions are set to $\kappa_{11} = \kappa_{22} = 4$ and $\kappa_{12} = 2$ and the dissipation to $\gamma = 10$. Due to the interaction, the ground state of the system ($t = 0$) has a

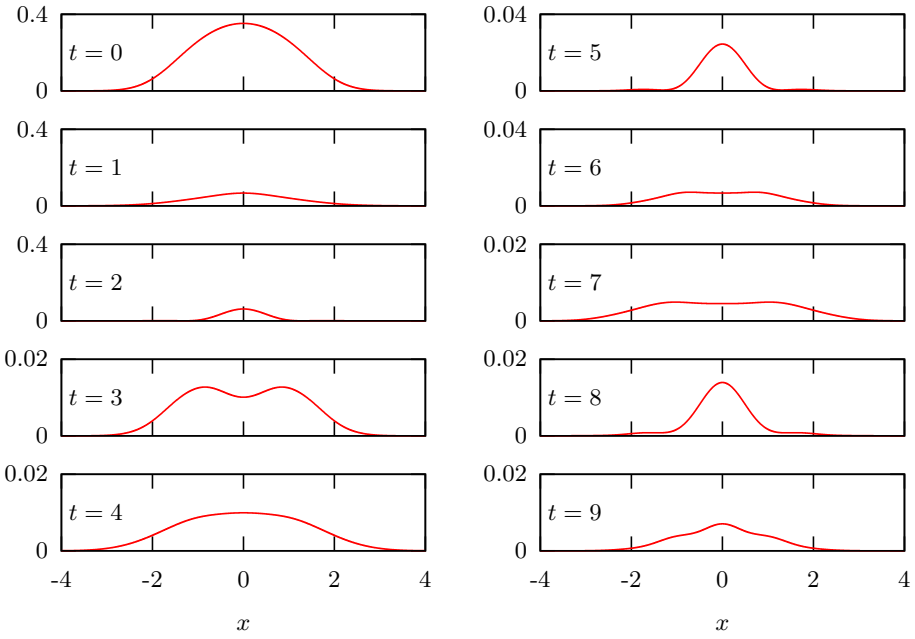

Figure 7.3: Density plots at different times for $\gamma = 10$, $\kappa_{11} = \kappa_{22} = 4$ and $\kappa_{12} = 2$. From $t = 0$ to $t = 1$, both densities shrink and at $t = 2$ the potential pushes the atoms back into the middle of the trap. For $t = 3$, the particle cloud expands again and forms a dip since they have a maximum at $x = 0$ for $t = 2$. The dissipation goes on and at $t = 5$, the densities contract again. These steps repeat for larger values of t.

wide shape and both densities overlap completely. As the dissipation starts, the densities shrink. Since in this case the dissipation for a species is the largest where the peak of the other species is, one can observe the formation of a dip at $t = 3$. In addition, a general shrinking of the profiles appears.
Due to this anisotropic decay which is proportional to $\gamma|\Psi(x)|^2$, its form exhibits now minima and maxima. At $t = 4$, these peaks start to regress due to the larger atom losses there. The density profiles have a smooth and flat shape which results in a period of less losses. The entire behavior corresponds exactly to the black curve in figure 7.2. Between $t = 0$ and $t = 2$, there is a drastic decay and as the density profile flattens, less atoms leave the BEC up to $t = 5$.
Since the atoms of both components move from the edges of the potential back to the middle

which results in a narrower and higher density for $t = 5$, a much more efficient dissipation can take place in the center afterwards. This procedure repeats and is the reason for the oscillations shown in figure 7.2. The density profile now has a similar shape as for the ground state. As a result, the following evolution is similar to the previous described one but with a continuing shrinking density.
The pulsating behavior of the density was observed earlier when the trapping potential was altered and excited the breathing mode. Now, the number of atoms is changed which generates a similar situation since this causes now the deviation from the equilibrium state. Since the frequency of this pulsating induced by the dissipation, it is reminiscent of the breathing mode. However, it is not an eigenmode in this case, since the condensate vanishes with the continuing dissipation.

7.2.3 Approximation for the decay curves

With the dissipative part of equations 3.33 and 3.34 but without taking the time dependence of the densities into account, the time evolution of the density can be written in the following form:

$$n_1(x,t) \approx n_1(x,t=0) \cdot e^{-2\gamma t n_2(x,t=0)} \tag{7.1}$$

$$n_2(x,t) \approx n_2(x,t=0) \cdot e^{-2\gamma t n_1(x,t=0)} \tag{7.2}$$

This is a very rough approximation but for very small times it should be sufficient if the system does not hardly evolve. The difference from the ground state should be then quite small. The equations 7.1 and 7.2 generate the green line in figure 7.4. The parameters of the system are set to $\kappa_{12} = 2$, $\kappa_{11} = \kappa_{22} = 4$ and $\gamma = 10$. The red curve is the numerically calculated solution of both complete GPEs.
The program calculates the ground state densities and uses these to integrate the expressions 7.1 and 7.2 over x for each time step. As one can see in figure 7.4, this crude approximation is only useful for very small times up to $t \approx 0.1$. At the beginning, the green and red curve are on top of each other. They separate when the curve for the exact solution starts to flatten.
In order to improve this, the time dependency of the dissipative parts will be taken into account. All terms in the GPEs 3.33 and 3.34 except the part describing the dissipation are neglected since it dominates the dynamics for small times:

$$i\partial_t \Psi_1(x,t) \approx -i\gamma n_2(x,t)\Psi_1(x,t) \tag{7.3}$$

$$i\partial_t \Psi_2(x,t) \approx -i\gamma n_1(x,t)\Psi_2(x,t) \tag{7.4}$$

The time derivative of the density gives:

$$i\partial_t n_1(x,t) \approx i\left((\partial_t \Psi_1^*(x,t))\Psi_1(x,t) + \Psi_1^*(x,t)(\partial_t \Psi_1^*(x,t))\right) \tag{7.5}$$

$$= (-i\gamma n_2(x,t)\Psi_1^*(x,t)\Psi_1(x,t) + \Psi_1^*(x,t)(-i\gamma)n_2(x,t)\Psi_1(x,t)) \tag{7.6}$$

$$= -2i\gamma n_2(x,t)n_1(x,t) \tag{7.7}$$

We have previously seen that for $\kappa_{12}^c \lesssim \kappa_{11} = \kappa_{22}$ the density profiles have the same shape and position in the trap. Thus, one can set for this case $n_1(x,t) = n_2(x,t) = n(x,t)$. One obtains the following differential equation.

$$\partial_t n(x,t) \approx -2\gamma n(x,t)^2 \tag{7.8}$$

By separation of variables, the solution is

$$n(x,t) \approx \frac{1}{2\gamma t + C}, \tag{7.9}$$

where C is the integration constant. We know for $t = 0$, that the calculated $n(x,t)$ has to be the ground state density $n(x, t = 0) = n(x)$ which gives:

$$n(x,t) \approx \frac{n(x,t=0)}{2n(x,t=0)\gamma t + 1} \tag{7.10}$$

Now, this expression will be compared with the ansatz from the equations 7.1 and 7.2 and the numerical result . The plot in figure 7.4 shown below is made for $\kappa_{11} = \kappa_{22} = 4$, $\kappa_{12} = 2$ and $\gamma = 10$. The ansatz according to the equations 7.1 and 7.2 is plotted as a green, the

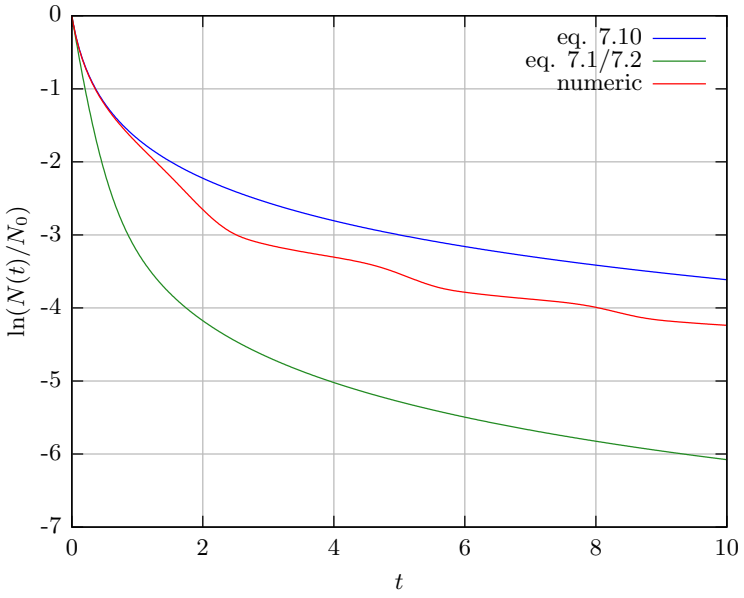

Figure 7.4: Comparison of the different approximations with the numerical result for $\kappa_{11} = \kappa_{22} = 4$, $\kappa_{12} = 2$ and $\gamma = 10$. The blue curve represents 7.10, the red one the numerical result and the green curve the approximation according to the equations 7.1 and 7.2. The analytic result provides a very good approximation up to $t = 1$ compared to the green curve which fails already around $t \approx 0.2$. For larger times, the analytic ansatz is not correct but its curve is still closer to the numeric result than the previously used approximation.

solution 7.10 as a blue and the numerical result as a red curve. The curve for the expression 7.10 starts to differ from the numerical result at $t = 1$ which is an improvement compared to the green plotted function where the deviation starts already at $t \approx 0.1$. For this time, the deviation between the numeric and analytic result is $\approx 1\%$. For $t = 4$, we see that the difference between the red and the green curve is less than 10^{-2} whereas the discrepancy between the analytic and numeric result is less than 10^{-1}.
To obtain an analytic expression for the particle number $N(t)$, one has to integrate formula 7.10 over space. In chapter 6.3, we have used a Gauss distribution in order to approximate the density profile, even for the interacting case. In section 6.3, approximations for the ground state have been studied in detail. Now, this is used in order to calculate an analytic

expression for the decay curve using only the ground state. Inserting formula 6.1 into 7.10 and calculating the integral gives:

$$N(t) \approx N_0 \frac{\sqrt{\pi}\beta}{2\gamma t} f_{1/2}\left(\frac{2\gamma t}{\sqrt{\pi}\beta}\right), \tag{7.11}$$

where $f_\nu(x) = \frac{1}{\Gamma(\nu)} \int_0^\infty dy \frac{y^{\nu-1}}{\frac{1}{x}e^y+1}$ which is also known as the polylogarithmic function $-Li_\nu(-z) = f_\nu(z)$. In case of no interaction what corresponds to the harmonic oscillator, β becomes 1, and the Gaussian function is the exact solution for the GPE.
Equation 7.11 describes the decay of a condensate mixture in the interacting case for small times for the case $\kappa_{12}^c \lesssim \kappa_{11} = \kappa_{22}$. One should be aware that for large interactions the Gaussian shaped ansatz deviates strongly from the numerical calculated ground state which was previously shown in the state diagram 6.7. This would affect also the solution for $N(t)$ in formula 7.11.
To evaluate the accuracy of that variational method for the interaction case without state separation, we use again the values $\kappa_{11} = \kappa_{22} = 4$, $\kappa_{12} = 2$ and $\gamma = 10$. By minimizing expression 6.3, the minimal energy is $E \approx 2.9398$ for $\beta \approx 1.4551$. With these values one obtains the plot in figure 7.5. The red curve gives the numerical result which is the most

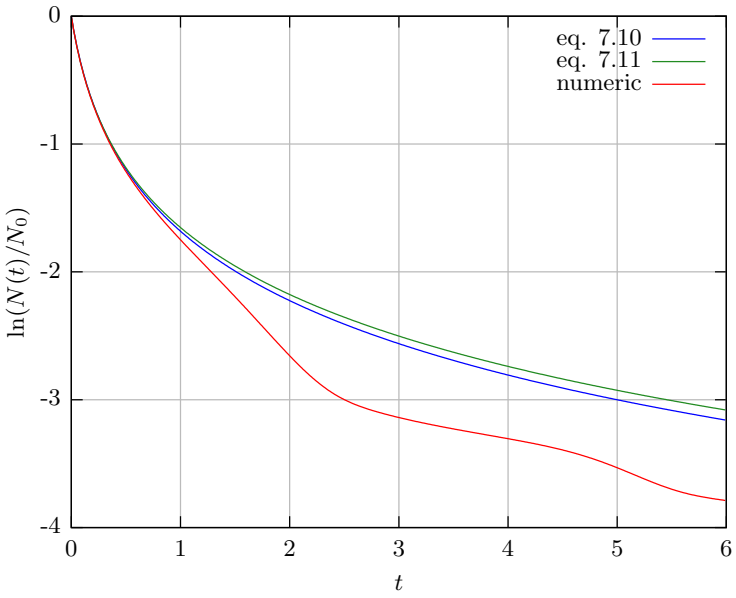

Figure 7.5: Comparison of the decay curves according to the exact solution (red), formula 7.10 (green) with a numerically calculated ground state and equation 7.11 using a variational ansatz (blue). The variational method provides also a good approximation up to $t = 1$.

precise one. The blue curve gives the decay according to formula 7.10 with $n(x, t = 0)$ obtained numerically. The green function is the expression in equation 7.11 which was found by using a Gauss shaped density with a variational method.
Both formulas 7.10 and 7.11 provide a good approximation for small times since they start deviating at nearly $t \approx 1$ significantly from the numerical result. Thus, it is irrelevant that they are not identical as long as $t < 1$.
Now, the time evolution of the Gauss approximation will be studied since we used it for

obtaining an analytical expression of the decay rate. We plot the numerically calculated density profiles and the distributions obtained by the approximation from equation 7.10 with the variational ansatz 6.1. We only consider a time range up to $t = 2$ since we know from figure 7.5 that the approximation starts deviating from the numerical result at $t \approx 1$. The red curve is the numerical result and the green curve the approximation. At $t = 0$, one

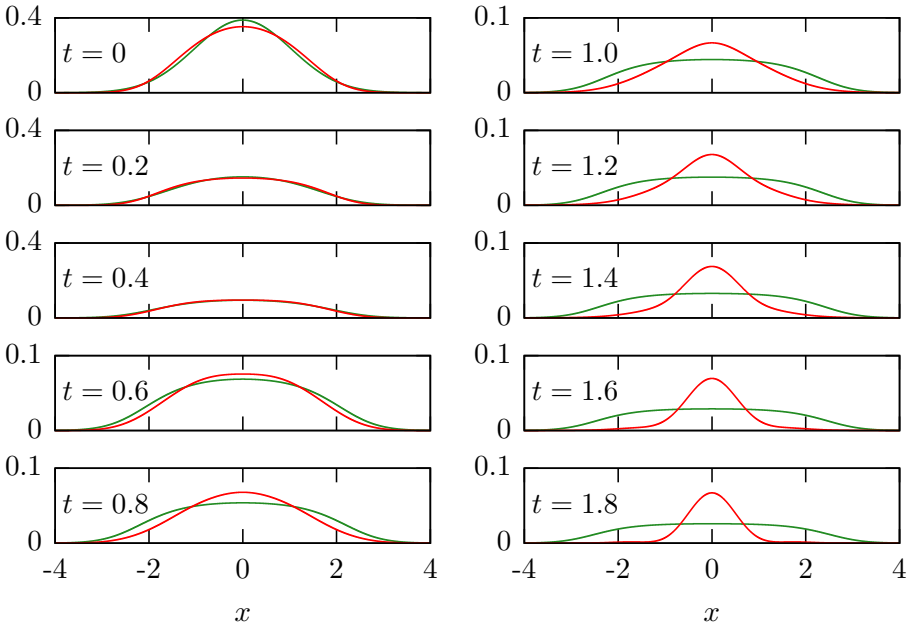

Figure 7.6: Comparison of the analytical and numerical obtained density profile for the case $\gamma = 10$, $\kappa_{11} = \kappa_{22} = 4$ and $\kappa_{12} = 2$. We used a combination of equation 7.10 for the time dependence and for the density profile formula 6.1 where β was determined by minimizing equation 6.3. For $t = 0$, one can see that the ground states are not identical but they have in average a very similar shape. As the system evolves, the curves almost overlap completely until they start to deviate at $t = 0.8$. The difference becomes severe at $t = 1.2$ since the atoms move back from the edges of the potential and the analytical treatment does not take that into account. For larger times, the analytical ansatz fails and the difference between the numerical and analytical solution for $t = 0.8$ appears also in figure 7.5 for the decay curves.

can see that the variational approach according to equation 6.1 is a good approach to the exact calculated ground state. If the dissipation starts, both profiles decrease and are still in good agreement at $t = 0.4$. The overall shape is very similar up to $t = 0.8$ and for $t = 1.0$, the numerical result looses its flat shape around $x = 0$ since the density contracts. For larger times, this maximum continues growing. At $t = 1.8$, one can see clearly the general differences between the numerical obtained density profiles and the approximation according to formula 7.10. Consequently, the analytic expression fails what is also visible in the decay curve in figure 7.5.

7.2.4 Hydrodynamic approach to a two-level system with dissipation

In order to understand the influence of the dissipation on the dynamics of the system, we come back to the hydrodynamic description of a condensate from section 2.2.

Repeating these steps for the equations 3.33 and 3.34, we obtain the following continuity equations:

$$\partial_t n_1(x,t) + \nabla j_1(x,t) = -2\gamma n_1(x,t) n_2(x,t) \tag{7.12}$$
$$\partial_t n_2(x,t) + \nabla j_2(x,t) = -2\gamma n_1(x,t) n_2(x,t) \tag{7.13}$$

Since the particle number is not conserved in this dissipative system, the right-hand side of the equations are equal to a source term depending on γ.
These equations correspond to the ansatz in formula 7.8 from the previous chapter for the case of a small or nearly spatially constant current. Now, we study the behavior of the current over the time in order to gain more knowledge about the compensation of the dissipated atoms.
The current is defined as:

$$j_1(x,t) = \frac{1}{2i}\left(\Psi_1^*(x,t)\partial_x\Psi_1(x,t) - \Psi_1(x,t)\partial_x\Psi_1^*(x,t)\right) \tag{7.14}$$
$$j_2(x,t) = \frac{1}{2i}\left(\Psi_2^*(x,t)\partial_x\Psi_2(x,t) - \Psi_2(x,t)\partial_x\Psi_2^*(x,t)\right) \tag{7.15}$$

The plots in figure 7.7 are for the special case of $\kappa_{11} = \kappa_{22} = 4$, $\kappa_{12} = 2$ and $\gamma = 10$. Both densities are represented by the red curve in the plots of figure 7.7. Since $n_1(x,t) = n_2(x,t)$, it follows $j_1(x,t) = j_2(x,t) = j(x,t)$ which is the violet curve. The plot at $t = 0$ shows the ground state. Since no particles have left the system, no atom movement takes place. Right after that, the dissipation starts. For $t = 1$, some atoms have left the condensate and a current has already formed. The atoms move towards the trapping center where the dissipation process mainly takes place. The density got smaller and $j(x,t)$ is almost in the entire trap $\neq 0$. Later at $t = 2$, the current decreases, since now a sufficient amount of atoms are in the middle of the trap. The number of atoms at $x = 0$ is so high that the form of the density profile is not very favorable. This is the reason why for $t = 3$ the atoms moving back to the edges of the potential and the current reverses leading to an expansion and the formation of a dip in the center of the density. The plots for $t = 4$ and $t = 5$ shows that the condensate started already to contract since the potential reflects the outwards directed current. For larger times, the previously described process repeats.

7.3 Atom loss dynamics for state separation ($\kappa_{11} = \kappa_{22} \lesssim \kappa_{12}^c$)

Now, the case of state separation will be considered following the same order as in the previous case. To consider this case, we set $\kappa_{11} = \kappa_{22} = 2$ and $\kappa_{12} = 6$ which means that according to the state diagram 6.4, both particle species are separated.

7.3.1 Atom loss for different γ

First, the decay curves for different γ will be considered. The corresponding plot is shown in figure 7.8.
For a very small dissipation of $\gamma = 0.1$, the decay looks on that time scale linear. The loss of atoms for $\gamma = 1$ is as expected larger and the curve looks already wavy. Oscillations become visible for $\gamma = 5$ and $\gamma = 10$ as well as the larger atom loss. The cause of these oscillations will be discussed in the following section. Their frequency is like in the case of no state separation $\omega \approx 2\omega_0$.

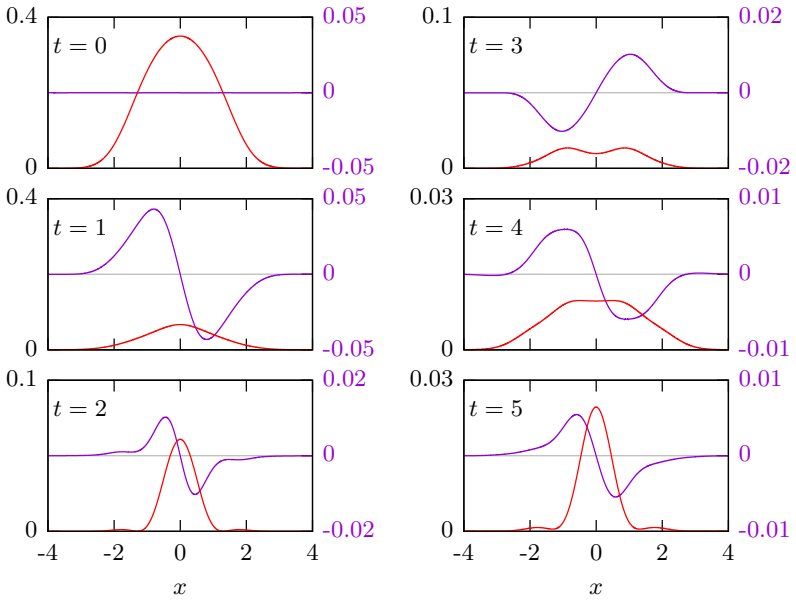

Figure 7.7: Current (violet curve) and density plot (red curve) for $\kappa_{11} = \kappa_{22} = 4$, $\kappa_{12} = 2$ and $\gamma = 10$. For $t = 0$, the current is zero which means that there is no particle movement. For $t = 1$, some atoms have left the condensate and some of the atoms move from the edges of the potential back to the center. For $t = 2$, the current decreases since too many atoms are in the center of the system and the current and the density have due to the spatially irregular dissipation a wavy structure. The current has reversed at $t = 3$ leading to an expansion of the condensate and a local minimum in the center. At $t = 4$, the current has been reflected from the edges of the potential and causes for $t = 5$ again a narrow density profile.

7.3.2 Evolution of the densities

Now, the evolution of the densities in the case of state separation influenced by dissipation will be studied. The ground states are completely different from the situation of $\kappa_{12}^c \leq \kappa_{11} = \kappa_{22}$. This process is shown in figure 7.9 for $\gamma = 10$, $\kappa_{11} = \kappa_{22} = 2$ and $\kappa_{12} = 6$ in detail. The plot for $t = 0$ shows the ground state. Due to the overlap of both components, dissipation can take place and the densities get continuously smaller up to $t = 2$. Then for $t = 3$, both components have moved towards the middle of the trap. Using the momentum coming from the potential, both distributions can exchange their position which happens between $t = 4$ and $t = 5$. The momentum is then so large compared to the repulsion between the different species, since the interspecies interaction depends on the densities in equations 3.33 and 3.34. The swapping can only happen if the maxima of the densities is initially at $x \neq 0$. During this process, they overlap completely and thus a much more efficient dissipation can take place. This results in a temporarily faster decay and explains the oscillation in the decay curves.
Both components move away from each other and are then slowed down by the potential ($t = 6$). The entire process which was previously described repeats (from $t = 6$ to $t = 9$) and both densities shrink continuously.
The evolution of the densities and the shape of the black decay curve in figure 7.8 are related to each other. In the range from $t = 0$ to $t = 4$, one can observe a steady decay which is large, due to the complete overlap of the densities around $t = 3$ and $t = 4$. At $t = 5$,

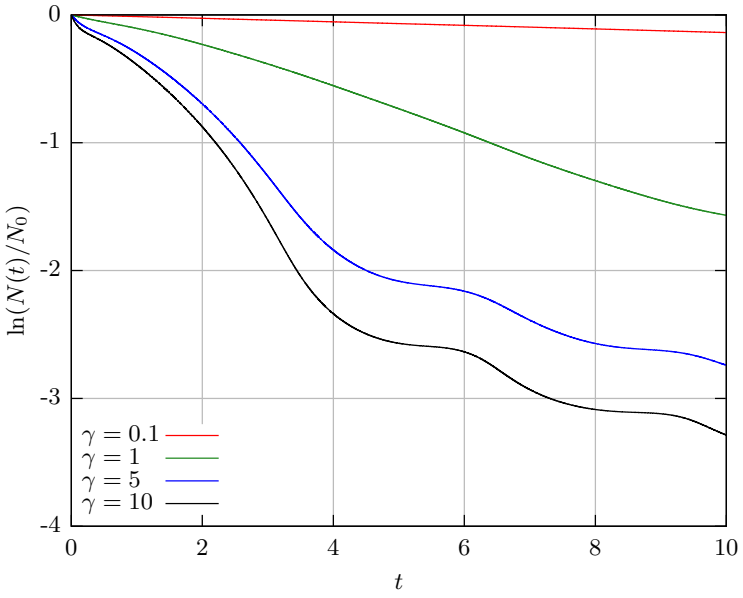

Figure 7.8: Plot for different values of γ, $\kappa_{11} = \kappa_{22} = 2$ and $\kappa_{12} = 6$. For $\gamma = 0.1$, the decay is very slow and the curve looks linear on this time scale. Increasing γ to 1 causes an oscillating behavior in the decay. For a dramatic atom loss at $\gamma = 10$, the oscillations are very well visible. Since state separation occurs while the system evolves in time, the oscillations exhibit plateaus where no dissipation can happen.

both densities are completely separated leading to a temporarily constant particle number. Starting from this, the previous events repeat.
The hydrodynamics of this effect will be discussed later in section 7.3.4.

7.3.3 Approximation for the decay curves

In order to get an analytic expression, we start with the same ansatz as in the case of no state separation. Neglecting the time dependency for the densities in the Gross-Pitaevskii equation, we obtained previously:

$$n_1(x,t) \approx n_1(x,t=0) \cdot e^{-2\gamma t n_2(x,t=0)} \tag{7.16}$$

$$n_2(x,t) \approx n_2(x,t=0) \cdot e^{-2\gamma t n_1(x,t=0)} \tag{7.17}$$

The comparison of this with the numerical solution of the entire Gross-Pitaevskii equation is shown in figure 7.10. For the values $\kappa_{12} = 6$ and $\kappa_{11} = \kappa_{22} = 2$, the red and the green curve differ already after a small time of $t \approx 0.05$. This approximation fails too, when the system starts to evolve in time because the large value of $\gamma = 10$ induces significant dynamics.
In analogy to the case of complete overlap of the density profiles, we will take now into account the time dependency and use the previous approximation and obtain two coupled differential equations.

$$\partial_t n_1(x,t) \approx -2\gamma n_2(x,t) n_1(x,t) \tag{7.18}$$

$$\partial_t n_2(x,t) \approx -2\gamma n_1(x,t) n_2(x,t) \tag{7.19}$$

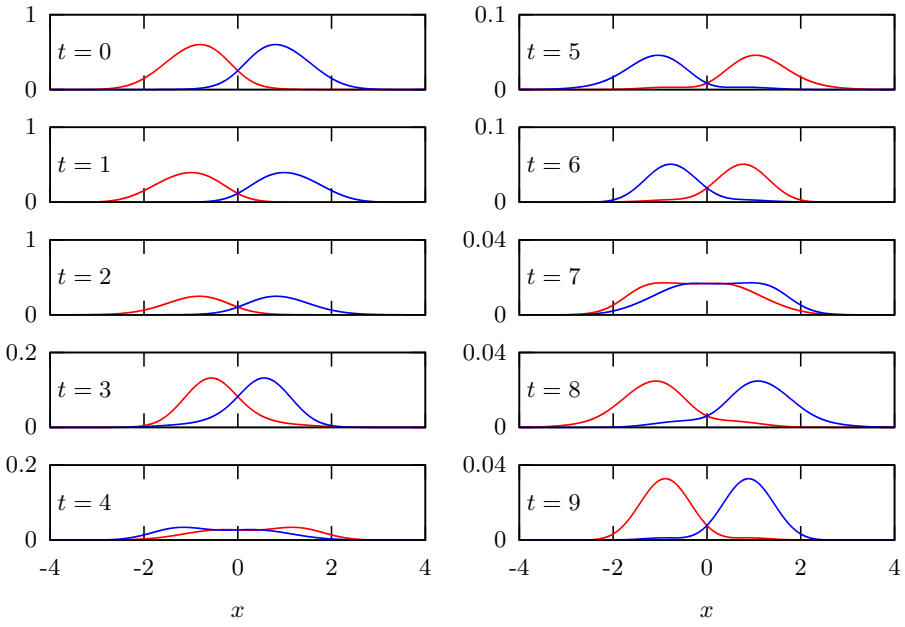

Figure 7.9: Density plots at different times for $\gamma = 10$, $\kappa_{11} = \kappa_{22} = 2$ and $\kappa_{12} = 6$. The plot at $t = 0$ shows the ground state and until $t = 3$ the densities get smaller continuously. Then, the potential forces both particle species to move to the center of the trap which gives the atoms such an amount of momentum that they are able to swap their position. Between $t = 4$ and $t = 5$, the overlap of both curves results in a temporarily larger decay until the states are clearly separated again. For $t > 6$, this process repeats constantly.

These are the continuity equations for a condensate mixture with the approximation $\nabla j_i(x,t) = 0$ and two body losses. Now, one cannot set $n_1(x,t) = n_2(x,t) = n(x,t)$, due to the separation of both components. In order to solve the equations, Mathematica is used and with the initial condition $n_1(x, t = 0) = n_1(x)$ and $n_2(x, t = 0) = n_2(x)$, the following solution is obtained:

$$n_1(x,t) \approx (n_1(x) - n_2(x)) \cdot \frac{n_1(x)}{n_1(x) - n_2(x)e^{2\gamma t(n_2(x)-n_1(x))}} \tag{7.20}$$

$$n_2(x,t) \approx (n_2(x) - n_1(x)) \cdot \left(1 - \frac{n_1(x)}{n_1(x) - n_2(x)e^{2\gamma t(n_2(x)-n_1(x))}}\right) \tag{7.21}$$

Since the ground state is unknown, we use $n(x, t = 0)$ obtained by the split step method and integrate over space numerically. To compare this approach with the ansatz in equations 7.1 and 7.2, both and the numerical result are plotted in figure 7.10. As one can see, taking the time dependency into account provides a better approximation than neglecting the time dependency in the densities and deviates at $t \approx 0.2$ significantly form the complete solved GPE.
Additionally, it was mentioned that equation 7.18 corresponds to the continuity equation for this system but without any current. Since the current is responsible for the particle movement, the blue curve exhibits an asymptotic behavior after all atoms have dissipated in the region of the overlap of both components.
Even with the Gauss shaped density, an integration of equation 7.20 in order to obtain the particle number $N(t)$ is complicated. To get an analytic expression anyway, we expand

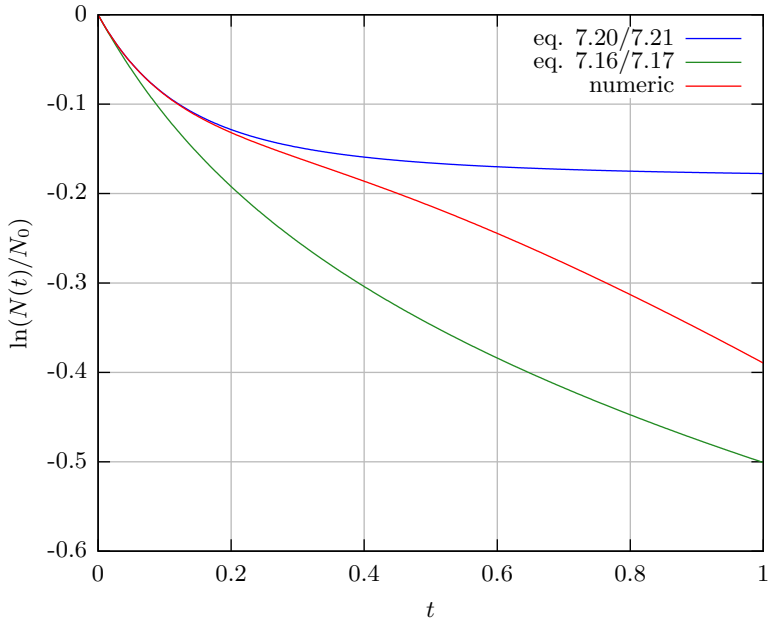

Figure 7.10: Comparison of the complete solution of the GPE (red), the analytically obtained solution in equation 7.20 (blue) and the approximation according to equations 7.1 and 7.2 (green). The time dependent ansatz improves the approximation considerably but since it is the continuity equation with a neglected current, the missing movement of the atoms leads to a stop of losses.

formula 7.20 for small γt up to the second order.

$$\begin{aligned} n_1(x,t) \approx\ & n_1(x) - 2 \cdot n_1(x) \cdot n_2(x)\gamma t \\ & + 2 \cdot (n_1(x)^2 \cdot n_2(x) + n_1(x) \cdot n_2(x)^2)\gamma^2 t^2 + \mathcal{O}(\gamma^3 t^3) \end{aligned} \tag{7.22}$$

Assuming a Gauss shaped distribution for the state separation case according to section 6.3, the integration over space can be done and one obtains for the single particle decay:

$$N(t) \approx 1 - \sqrt{\frac{2}{\pi}}\frac{\gamma t}{\beta} e^{-\frac{2c^2}{\beta^2}} + \left(\frac{2\gamma t}{\beta}\right)^2 \frac{e^{-\frac{8c^2}{3\beta^2}}}{\sqrt{3}\pi} + \mathcal{O}(\gamma^3 t^3) \tag{7.23}$$

Due to the form of formula 7.23, the decay curve starts to increase after a the time

$$t = \sqrt{\frac{3\pi\beta^2}{32\gamma^2}} e^{\frac{2c^2}{3\beta^2}} \tag{7.24}$$

which is unphysical. In addition, this approximation fails already earlier.
Figure 7.11 shows the behavior of the particle number over the time for $\kappa_{12} = 6$, $\kappa_{11} = \kappa_{22} = 2$ and $\gamma = 10$. The complete analytic expression according to equation 7.23 (green curve) deviates at approximately $t \approx 0.05$ from the numeric solution (red curve) of the entire GPEs because it decreases slightly faster. In contrast to this, equation 7.20 (with the numerically obtained ground state) fails around $t = 0.2$. Compared to the case of no state separation, all these approximations are only valid for very small times since the dynamic starts much earlier due to the potential which squeezes the separated components much harder together.

Despite the assumption of small γt used in equation 7.23, it provides a fair approximation

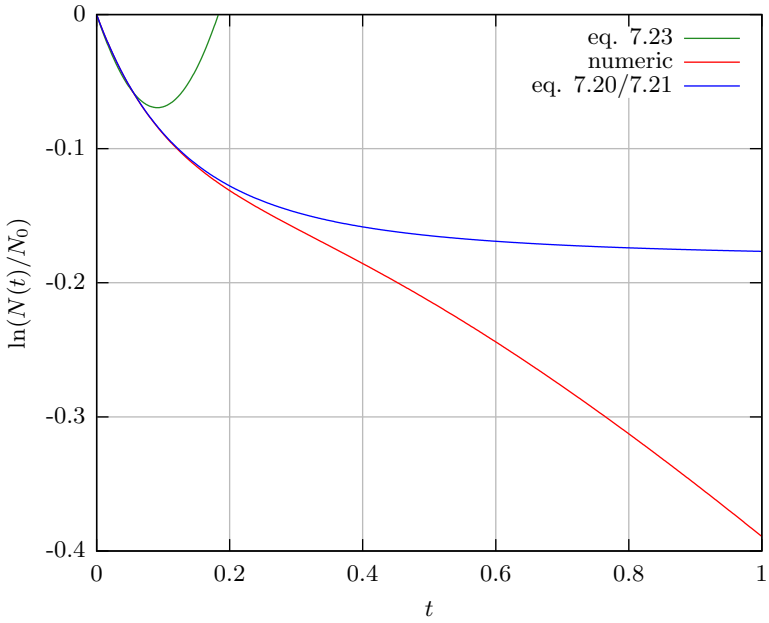

Figure 7.11: Comparison of the approximations according to formulas 7.23 and 7.20 using the numerical obtained ground state with the numerical solution of the GPE. Due to the polynomial form, the analytical expression fails after a time of $t = 0.02$ and becomes unphysical for a certain time which is given by 7.24. Since the current for formula 7.20 was neglected, no particle movement occurs which avoids any further evolution in time and converges to an constant particle number in the system after a large time.

even for a relatively large dissipation of $\gamma = 10$.
Now, the consequences of neglecting the current will be discussed. The analytic expression for the density decay in the case of a separation according to the variational method is combined with the equations 7.20 and 7.21, which are known analytic results, and is compared to the complete numerical solution. It is shown in 7.12.
Since the expansion in formula 7.23 is only a good approximation for small times, both curves do not overlap after a short time. In figure 7.12, one can see a comparison of the Gauss shaped approximation and the numerical obtained ground state. For $t = 0$, the approximation and the numerical result are in a good agreement. After a time of $t = 0.6$, the deviation between the density profiles become apparent, especially at the maxima. For $t = 0.8$, that difference between them is visible around $x = 0$ and at the peaks. The densities of the approximation stop evolving since the current was neglected and hence, no particle movement occurs.

7.3.4 Hydrodynamic approach to a two-level system with dissipation

Figure 7.13 shows the densities for the two components $n_1(x,t)$ (blue) and $n_2(x,t)$ (red) and the current $j_2(x,t)$ (violet) for $\gamma = 10$, $\kappa_{11} = \kappa_{22} = 2$ and $\kappa_{12} = 6$ which is the case of state separation. Due to the symmetry of the form $j_1(x,t) = -j_2(-x,t)$, it is sufficient to consider only one current.
At $t = 0$, no dissipation happened and the plot shows the ground state. Since the dissipation rate γ is quite large, a large current is already visible for $t = 1$. It is here larger than for the

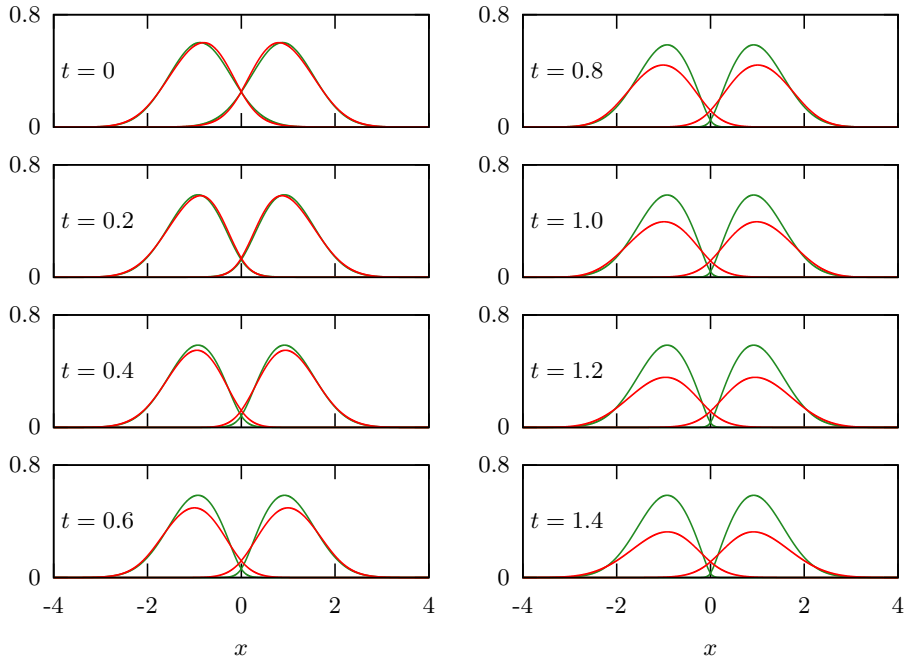

Figure 7.12: Comparison of the decay according to formula 7.20 with Gauss approximation and numerical obtained Ground state for $\gamma = 10$, $\kappa_{11} = \kappa_{22} = 2$ and $\kappa_{12} = 6$. For $t = 0$, one can see that the Gauss profile is an accurate approximation. If the dissipation starts, the region where both density profiles overlap becomes smaller. Since we neglected the current for the approximation shown here, there is no particle movement towards the trap center. This becomes visible at $t = 0.6$, since then the overlap of the Gauss shaped curves almost completely disappeared. For larger times, these density curves do not decrease further and the height of the peak does not decrease either. While there is no continuing evolution of the approximation, the numerically calculated density profiles are able to loose atoms since the existence of a current allows particles to move from the edges towards the center of the trap for larger times.

case of no state separation since the spatial extent of the condensate is larger and, therefore, the squeezing of the potential, too. The particles of the second component compensate the loss of atoms in the center of the trap by this movement of atoms. The reason for the formation of a minimum in the current around $x = -2$ is not clear. Its strength increases with an increasing value of κ_{12} and γ. A possible reason might be that too many atoms start moving in order to compensate the losses and this leads to a partial reflection of the current.
The densities get smaller and the current still transports atoms in order to compensate the loss and the minimum of the current travels towards the edges of the trap. At $t = 2$, this minimum has vanished but the current pushes atoms continuously towards the center of the potential. Since the interspecies interaction term in the Gross-Pitaevskii equation $\kappa_{ij}|\Psi_i(x,t)|^2\Psi_j(x,t)$ depends on the density, the current at $t = 2$ is so large that the density profiles start to swap their positions at $t = 3$. The plot for $t = 4$ shows the moment of the densities passing each other and that the current has already decreased. For $t = 5$, this has been finished and since the dissipation process takes now place at the left slope of the red density and the potential pushes the atoms back towards the middle of the trap, the current starts to reverse. For $t = 6$, the current is completely negative and the entire process starts

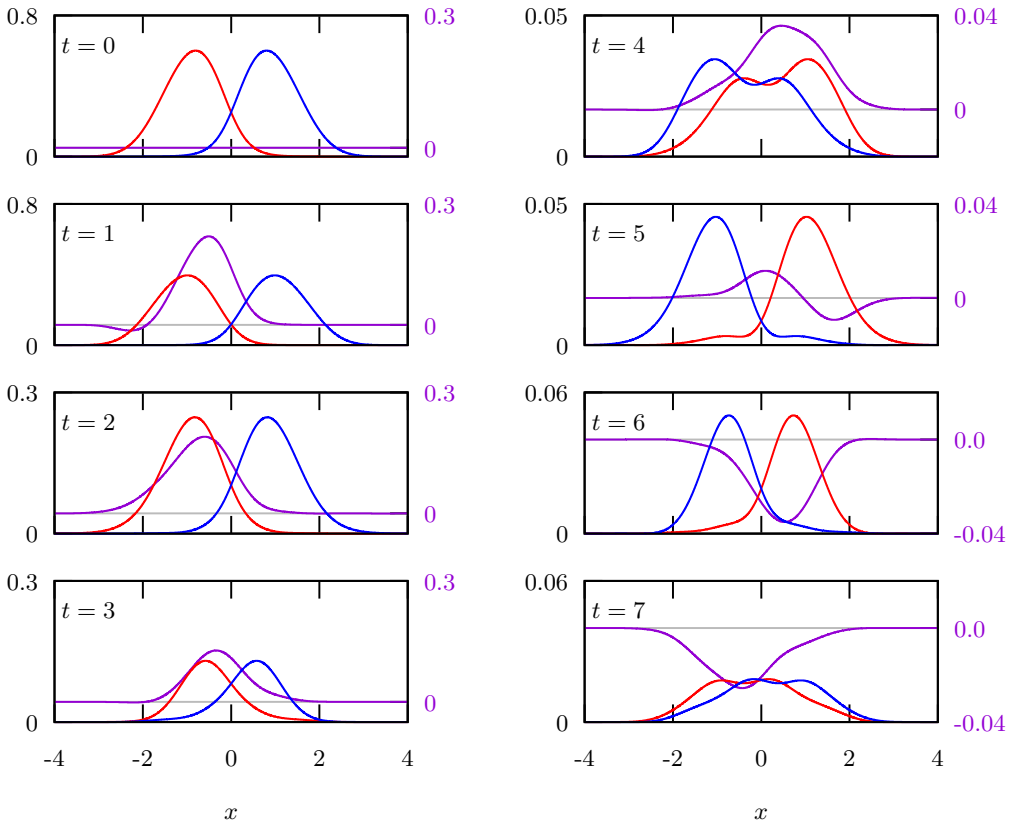

Figure 7.13: Current $j_2(x,t)$ (violet curve) for the case of the separation of the densities $n_1(x,t)$ (blue) and $n_2(x,t)$ (red). Since for $t = 1$ some atoms have left the trap, a current occurs in order to compensate this. The current grows and at $t = 3$, the current pushes more atoms towards the center than the dissipation can remove. Since the interspecies interaction term in the Gross-Pitaevskii equation $\kappa_{ij}|\Psi_i(x,t)|^2\Psi_j(x,t)$ depends on the density, it allows the curves to swap their position. After finishing this process between $t = 5$ and $t = 6$, the current reverses due to the potential and since $n_2(x,t)$ looses now its atoms at the left slope.

again vice versa and the next plot shows the interchange of the densities again.
This process explains the oscillations in the decay curves in figure 7.8.

7.3.5 Quantum Zeno effect

In the previous sections, the dynamics was explained and it will now help to understand the occurrence of the Quantum Zeno effect for this two component system.
Now, the values for γ are chosen to be large and the interactions are set to $\kappa_{11} = \kappa_{22} = 2$ and $\kappa_{12} = 6$. Figure 7.14 shows the plot for $N(t)$. One would expect the larger the value for γ is, the larger the decrease of the particle number would be. But the ground state has a limited region where both components overlap. If now the evolution starts, this coexistence region shrinks for e.g. $\gamma = 100$ faster than for $\gamma = 50$. But since the current requires some time to push particles to the trapping center, the loss process ends up less efficient for large γ. Smaller loss rates provide a continuous decrease of particle number. If the current starts to push the atoms to the middle and induces the swapping of both species, the particle

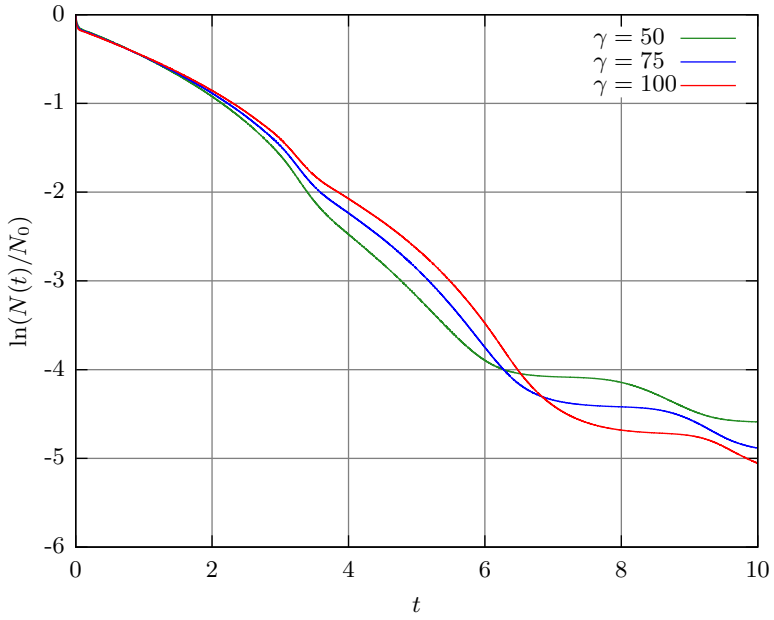

Figure 7.14: Zeno effect for $\kappa_{11} = \kappa_{22} = 2$ and $\kappa_{12} = 6$. If the particle number drops suddenly in the coexisting region of both components, the dissipation for smaller values of γ is more efficient. When the dynamics start and the densities $n_1(x)$ and $n_2(x)$ start to overlap, the atom losses increase with the values of γ.

number of drops for $\gamma = 100$ below $\gamma = 75$.
This occurs not for $\kappa_{12} < \kappa_{11} = \kappa_{22}$ due to the permanently coexisting region.

7.4 Atom loss dynamics for state separation ($\kappa_{12} = \kappa_{11} >> \kappa_{22}$)

7.4.1 Atom loss for different γ

Figure 7.15 shows the decay curves for different cases of γ for $\kappa_{11} = 2$ and $\kappa_{22} = \kappa_{12} = 6$. The behavior which was observed for the previous cases occurs here as well. For a small value of $\gamma = 0.1$, the decay curve looks almost linear on this scale. If γ is increased up to 1, the loss of atoms is even stronger and the curve shows already slight oscillations. These oscillations become more visible for higher values of γ like $\gamma = 5$ and $\gamma = 10$. As one could expect, the particle number drops faster as γ is increased.

7.4.2 Evolution of the densities

We consider now the densities at different times for $\gamma = 10$, $\kappa_{11} = \kappa_{12} = 6$ and $\kappa_{22} = 2$ which is shown in figure 7.16. It corresponds to the black decay curve in 7.15. In the ground state for $t = 0$, the densities have separated. One of the distributions has one maximum, the other one has two of them. At $t = 1$, atoms have already left the trap and the amplitude of the densities is smaller compared to the ground state. For $t = 2$, as a consequence of the existence of a potential, the blue distribution gets an additional maximum since the atoms move back from the edges of the potential. This additional maximum is the reason for a more efficient atom loss in the center. At $t = 3$, a dip in the red density forms and afterwards, the overlap of both components is minimal, which appears in the decay curve in

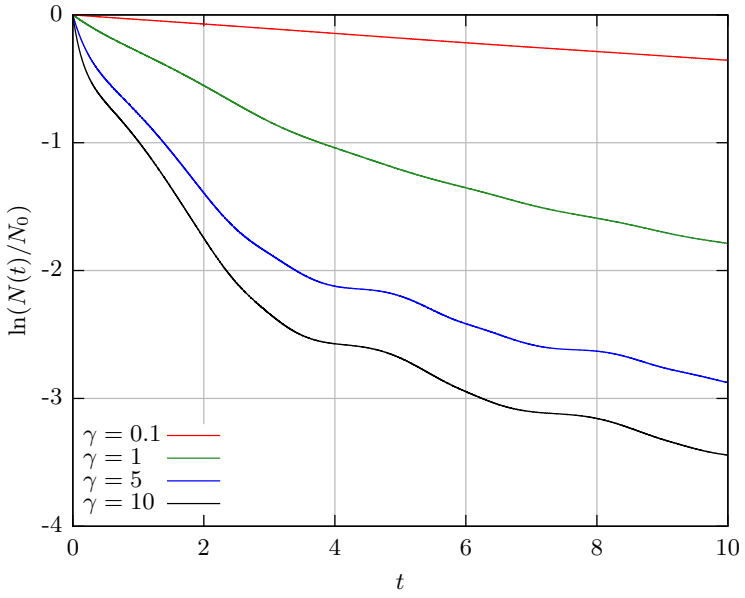

Figure 7.15: Decay curves for different values of γ and for $\kappa_{11} = 2$ and $\kappa_{22} = \kappa_{12} = 6$. As γ is increased, the particle number drops faster and the oscillating behavior in the decay curves becomes stronger.

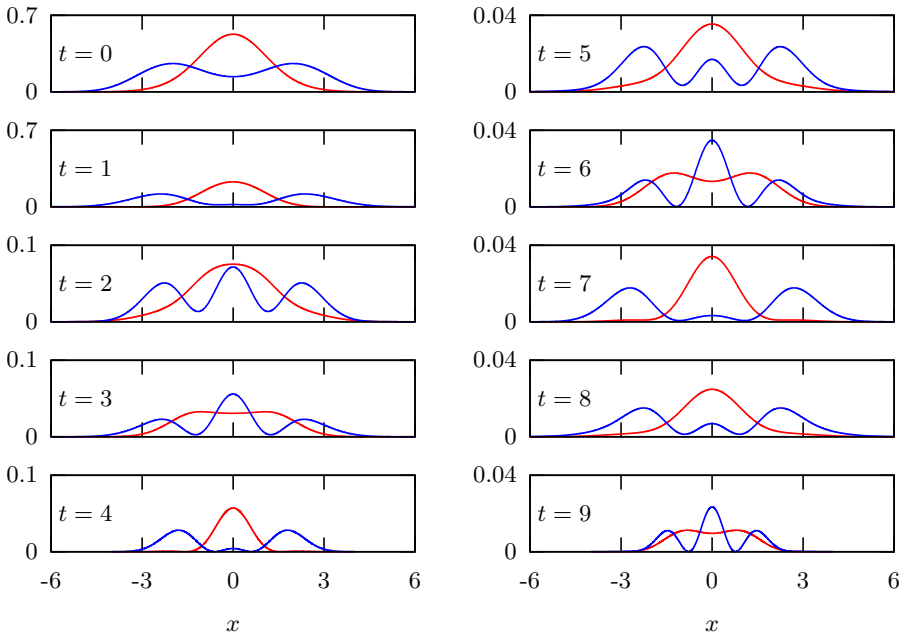

Figure 7.16: Density plots at different times for $\gamma = 10$, $\kappa_{11} = \kappa_{12} = 6$ and $\kappa_{22} = 2$. Until $t = 2$, both densities become smaller but an additional maximum in the blue density causes a larger dissipation. At $t = 3$, the red curve (species 2) has a minimum at $x = 0$ and two maxima at $|x| \approx 1.5$ and the blue density has one of its three maxima in the center. For $t = 4$, both densities have a small overlap causing a small decay. For the following times, the density profiles change like explained for $t = 1$ to $t = 4$. This periodic behavior is responsible for the oscillations in the decay curves.

figure 7.15 as a nearly constant particle number around $t = 4$. But since the dissipation continues, atoms are pushed again towards the center and an additional maximum in the blue density forms which causes again a dip in the distribution of the other component at $t = 6$. This corresponds to the section in figure 7.15 of large decay between $t = 5$ and $t = 6$. This is followed by a short period of small overlap leading to a small amount of dissipated atoms. Despite the existence of a third maximum, the temporary form of the densities looks very similar to the ground state at $t = 0$. Thus, the previously described behavior is repeated with shrinking densities.

7.4.3 Hydrodynamic approach to a two-level system with dissipation

Now, the hydrodynamics of the case for $\kappa_{11} = \kappa_{12} = 6$ and $\kappa_{22} = 2$ will be discussed. Figure 7.17 shows the densities $n_1(x,t)$ (blue curve) and $n_2(x,t)$ (red curve) and the current $j_1(x,t)$ (violet curve). Since the density profiles look completely different, both currents will be considered separately.
The plot for $t = 0$ shows the ground state of the system. The overlap of both curves

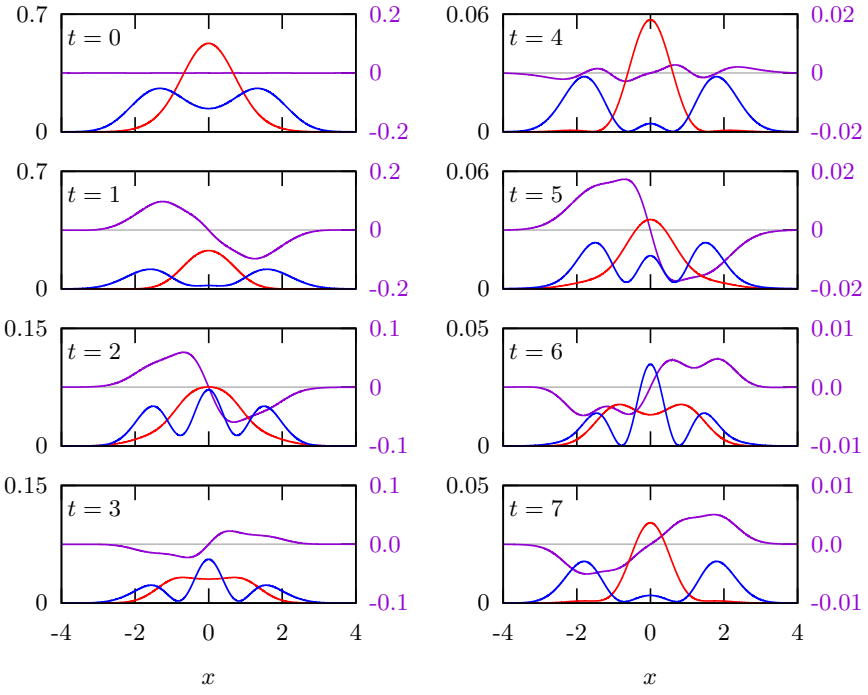

Figure 7.17: Density profiles $n_1(x,t)$ (blue curve) and $n_2(x,t)$ (red curve) and current $j_1(x,t)$ (violet curve) for different times with $\gamma = 10$, $\kappa_{11} = \kappa_{12} = 6$ and $\kappa_{22} = 2$. Starting with the ground state at $t = 0$, the potential pushes the atoms from the edges towards the center from $t = 1$ and $t = 2$ causing the formation of a third maximum in the center. At $t = 3$, this maximum is even higher than the already previously existing maxima. Consequently, $n_2(x)$ has a dip at this position due to the more efficient dissipation. The current $j_1(x)$ reverses and the atoms move towards the trap edges for $t = 4$. The contact with the trap reverses the current again inducing again the formation of a third maximum at $t = 5$ and $t = 6$.

concentrates on the range of $|x| \leq 2$ which leads to losses in that region. Since at $t = 1$ a considerably large number of atoms have left the system, the potential forces a movement

of $n_2(x,t)$ from the edges towards the center of the trap. The result is an accumulation of atoms around $x = 0$, which can be seen from the formation of a third maximum at $t = 2$. Since this is also a very unstable profile, the current stops and the atoms start moving towards the edges of $V_{ext}(x)$ which is shown in the plot for $t = 3$. But due to the shape of both densities, a small dip in $n_1(x)$ appears accompanied by an overall shrinking. For $t = 4$, the current starts to reverse because this intermediate state has a shape similar to the ground. This is the reason for the movement of the atoms back from the edges of the potential for $t = 5$. At time $t = 6$, the current is reversed again. This process continues over and over and causes the oscillations in the decay curve shown in figure 7.15.
Due to the unusual shape of $n_2(x)$ and the influence of $n_1(x)$, the current $j_1(x)$ exhibits a very wiggly structure. Further, it is mentionable that after the first formation, the centered maximum of $n_1(x,t)$ never fully disappears although a continuous dissipation occurs.
The current $j_2(x,t)$ (violet curve) is shown in figure 7.18 at the same values for t, κ_{ij} and γ as in figure 7.17 . The first plot for $t = 0$ shows the ground state. When the dissipation starts, the two body losses take mainly place in the slopes of $n_2(x)$. The atoms start moving away from the center of the trap which is shown for $t = 1$. At $t = 2$, $j_2(x)$ decreases, since now too many atoms have been shifted what can be seen from the wider density profile compared to $t = 0$. Additionally, the current $j_1(x)$ is still directed towards $x = 0$ what is the reason for the third maximum of $n_1(x)$ (see figure 7.18). As previously mentioned, this leads to the dip in $n_2(x)$ at $t = 3$. $j_2(x)$ needs to compensate this unfavorable profile and hence, the current is now negative (positive) for $x > 0$ ($x < 0$). At $t = 4$, $n_2(x)$ and $n_1(x)$ have a shape similar to the ground state and the current has already decreased. For $t = 5$, $j_2(x)$ compensates the atom losses at the slopes and the current is now > 0 (< 0) for $x > 0$ ($x < 0$). Due to the third maximum of $n_1(x)$, $n_2(x)$ has again a dip in the middle at $t = 6$ leading to a reverse of $j_2(x)$. The density profiles at $t = 7$ are similar to the state at $t = 4$ which will lead to repetition of the previously described behavior for the times $t = 2$ to $t = 4$.
Again, one can see that the periods of small atom losses in figure 7.15 correspond to a small overlap in the density profiles.

7.5 Decay for different $\kappa_{11} = \kappa_{22}$

In order to compare the efficiency of dissipation for different interactions, figure 7.19 shows the decay of a two-level system in a harmonic trap for $\gamma = 10$ and $\kappa_{12} = 6$ over time for different $\kappa_{11} = \kappa_{22}$. The strength of the decay depends strongly on the ratio of the interactions $\kappa_{11} = \kappa_{22}$ and κ_{12}. This can be explained using the state diagram.
For the cases $\kappa_{11} \lesssim \kappa_{12}^c$, the decay increases since the overlap becomes larger due to the increasing interaction among each particle species. This behavior is the consequence of the $i\gamma|\Psi_i(x)|^2\Psi_j(x)$ terms in the GPEs.
If the interactions are the same (the case $\kappa_{11} = \kappa_{12} = 6$), the distributions overlap completely, so that the position of the peaks are the same. This causes the most efficient dissipation.
Further, if $\kappa_{11} \gtrsim \kappa_{12}^c$ the decay effect is smaller compared to the previous cases. This is related to the broad and flat density profile as a consequence of the high value of κ_{11}. Due to that shape of the density, the probability for the scattering process between both species, which is responsible for the dissipation, decreases. The stability increases as the overlap of both components decreases.

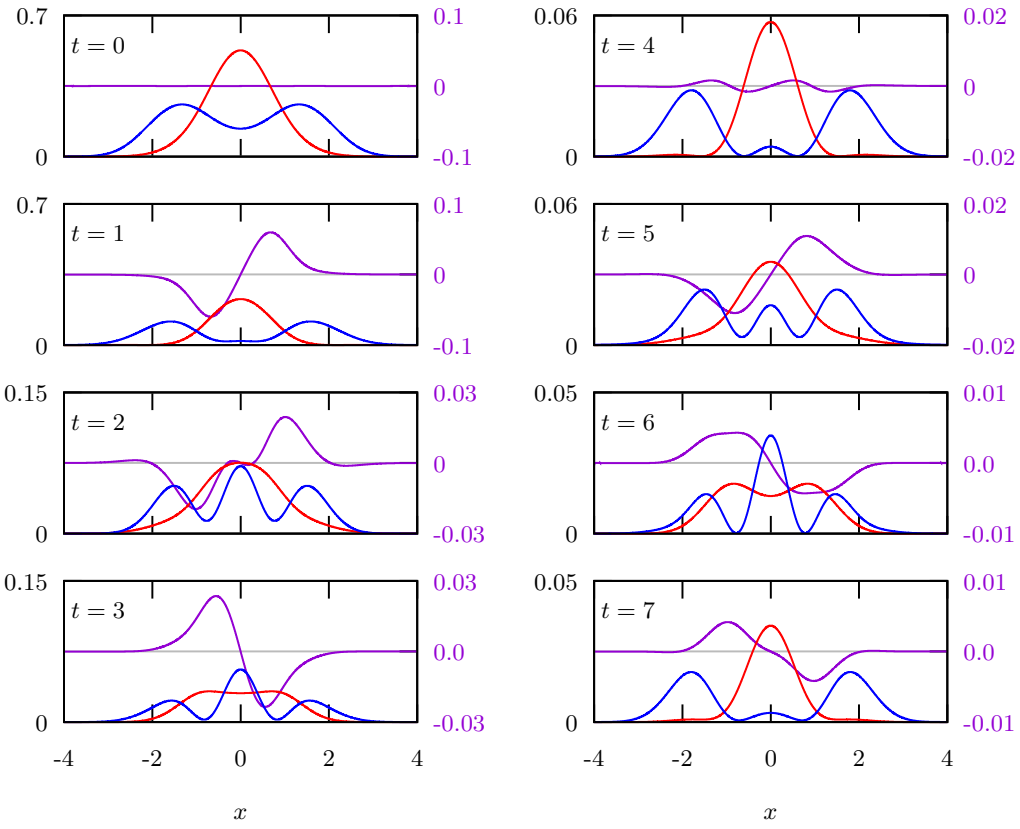

Figure 7.18: Density profiles $n_1(x,t)$ (blue curve) and $n_2(x,t)$ (red curve) and current $j_2(x,t)$ (violet curve) for different times with $\gamma = 10$, $\kappa_{11} = \kappa_{12} = 6$ and $\kappa_{22} = 2$. Due to the shape of the ground state at $t = 0$, the particles of the density $n_1(x)$ move towards the potential edges since the dissipation happens mainly at the slopes. The current $j_2(x)$ decreases for $t = 3$ in order to compensate the loss of atoms in the trap center caused by the third maximum of $n_2(x)$. At $t = 3$, a dip has formed and $j_2(x)$ has reversed. It decreases already at $t = 4$ in order to compensate the losses at the slope for $t = 5$. The current $j_1(x)$ creates again a dominating maximum at $x = 0$ in $n_1(x,t)$ for $t = 6$. Thus, a dip in the density $n_1(x)$ forms and $j_2(x)$ reverses again. The plot for $t = 7$ shows the decrease of the current since this compensation process is finished.

7.6 Decay for different $\kappa_{11} = \kappa_{12}$ and $\kappa_{22} = 0$

As in the previous chapter 6.1 mentioned, there is an other situation of state separation which does not break the symmetry. Since there is now no intraspecies interaction κ_{22}, all ground states have a similar shape shown in figure 6.2. In figure 7.20, the decay is shown for $\kappa_{11} = \kappa_{12}$ and different $\kappa_{22} = 0$. The larger $\kappa_{11} = \kappa_{12}$ gets, the components separate even more. This is the reason for the small initial dissipation at large values of $\kappa_{11} = \kappa_{12}$. But as atoms leave the system and the remaining ones move towards the coexistence region, the losses are equivalent even for a strong initial separation.

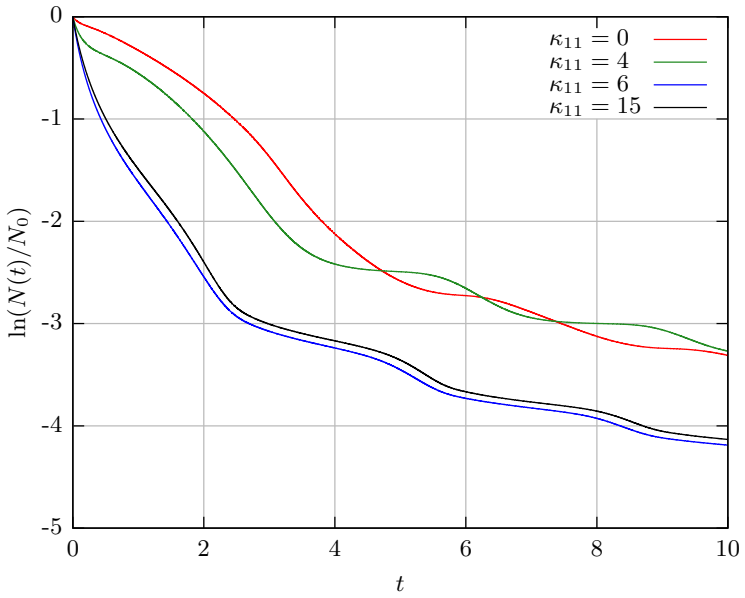

Figure 7.19: Logarithmic plot for different $\kappa_{11} = \kappa_{22}$ a fixed $\kappa_{12} = 6$ and $\gamma = 10$. Due to the oscillations, the decays for small $\kappa_{11} = \kappa_{22}$ are alternately smaller or larger. The larger κ_{11} gets with $\kappa_{11} \gtrsim \kappa_{12}$ the smaller the decay becomes.

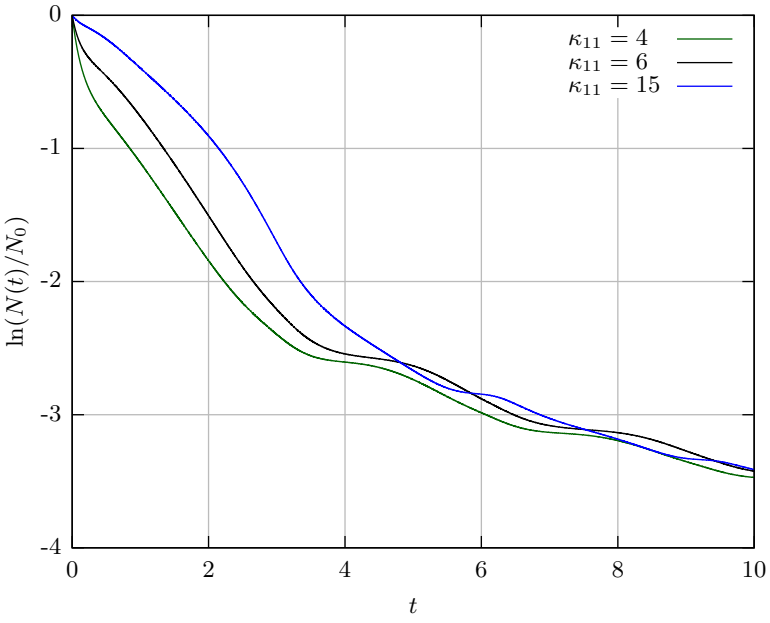

Figure 7.20: Decay for the case of state separation and conservation of symmetry. This decay exhibits oscillations too. As $\kappa_{12} = \kappa_{11}$ gets larger, the state separation increases and the decay decreases at the beginning. Since the local density increases for strong κ_{12}, the losses are larger afterwards until they are equals to these for smaller interactions.

CHAPTER 8

Static properties of a two-component gas in 2D

After the discussion of the one-dimensional Bose gas consisting of two components, the two-dimensional case will be discussed in this chapter following the same procedure as before. For this, we start with the static properties of the ground state, since this is from where the dynamics start. For these purposes, equations 3.35 and 3.36 will be solved again with the combination of split step algorithm and imaginary time evolution, but now adapted to the two-dimensional case.

8.1 State separation

There are two different kinds of interaction, the interspecies interaction κ_{12} and the intraspecies interactions κ_{11} and κ_{22}. It depends on their ratio whether the two components are miscible or immiscible. Several examples for different cases are shown in figure 8.1.

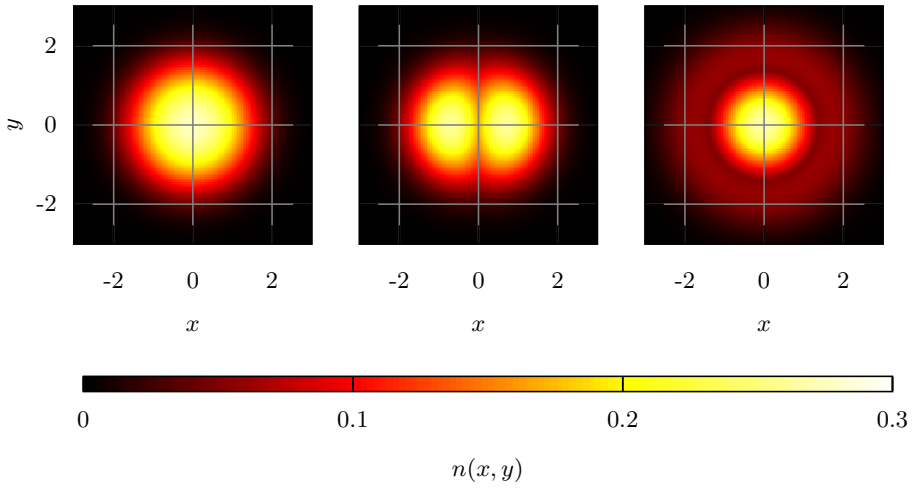

Figure 8.1: Different ground states for two-dimensional BEC in a harmonic trap. In the left plot, the interactions are set for a miscible ground state whereas in the middle plot both components separate. The right plot shows the separation of the two species admitting a rotational symmetry.

- Analogously to the one-dimensional case, the Bose gas will separate both components, if it is energetically favorable. If now $\kappa_{11} = \kappa_{22}$ and $\kappa_{12}^c \lesssim \kappa_{11}$, the contribution of the interaction part of the two Gross-Pitaevskii equations is dominated by the intraspecies

interaction. As a consequence, both density profiles overlap and no separation occurs. The left plot in figure 8.1 shows an example for $\kappa_{11} = \kappa_{22} = 10$ and $\kappa_{12} = 4$.

- Increasing the interaction up to $\kappa_{11} = \kappa_{22} \lesssim \kappa_{12}^c$, both components of the gas separate since it costs more energy to keep them at the same position than placing them at the edges of the potential. An example for this case is shown in the middle of figure 8.1 using $\kappa_{11} = \kappa_{22} = 4$ and $\kappa_{12} = 10$.
  Similar to the one-dimensional case, the initial function for the ground state calculation is a Gauss distribution already shifted along the x-axis. Setting the start values according to $e^{-(x-1)^2-y^2}$ and $e^{-(x+1)^2-y^2}$ makes sure that the computation time will be small but it forces the symmetry breaking to occur in one direction. If the initial values are arbitrary, the direction of the symmetry breaking depends on numerical effects. In contrast to the one-dimensional case, where the maximum of the density was limited on a single x value, the peak of a distribution can now be on a circle in the xy-plane, if no initial condition influences the symmetry breaking.
- In the case of $\kappa_{22} << \kappa_{11} = \kappa_{12}$ state separation occurs without breaking the rotational symmetry of the system. Due to the very small interaction of the second species, its atoms are in the center of the trap. The atoms of the other species are arranged between the first component and the edges of the potential. Figure 8.1 shows this for $\kappa_{11} = \kappa_{12} = 30$ and $\kappa_{22} = 8$ in the right-hand side plot.
- In two dimensions, it is also possible to take trapping asymmetries into account. Let us denote $a_t = \frac{\omega_y}{\omega_x}$. Figure 8.2 shows the ground states for the same set of interactions as for figure 8.1 but now with $a_t = 2$. As expected, an increase of the trap in the

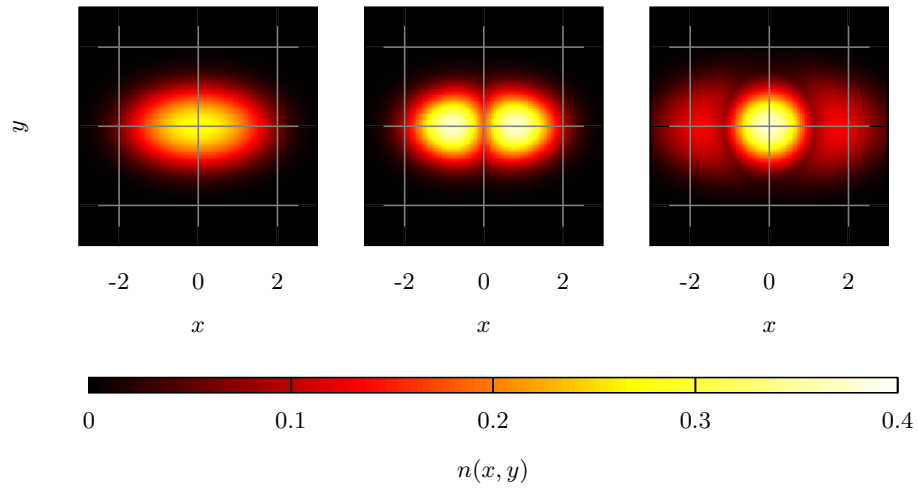

Figure 8.2: Densities for the same values as in figure 8.1 but with $a_t = 2$. The compression y-direction leads to an increase of the densities in the region of the trap center.

y-direction presses the condensate into the same direction. The spatial extension is smaller compared to $a_t = 1$ but the value of the density itself is larger.

8.2 State diagram

To summarize the previous situation for several values of the interactions, a state diagram in the same way for the one-dimensional case is now plotted for 2D. It is reasonable to use the radius given by $r = \sqrt{x_{max}^2 + y_{max}^2}$ where x_{max} and y_{max} are the coordinates of

the maximum of the density. To ensure a fast convergence, the initial wave function is a two dimensional Gauss profile shifted along the x-axis for $y = 0$. This reduces the shift to $r = x_{max}$. The state diagram for the two-dimensional case is shown in figure 8.3. The color corresponds to the shift of the maximum of the density profile of one component of the gas. No shift is denoted by the yellow color whereas the different shades of red mean a different strength of displacement of the maximum.
Similar to the one-dimensional case, the black line separates the area of state separation

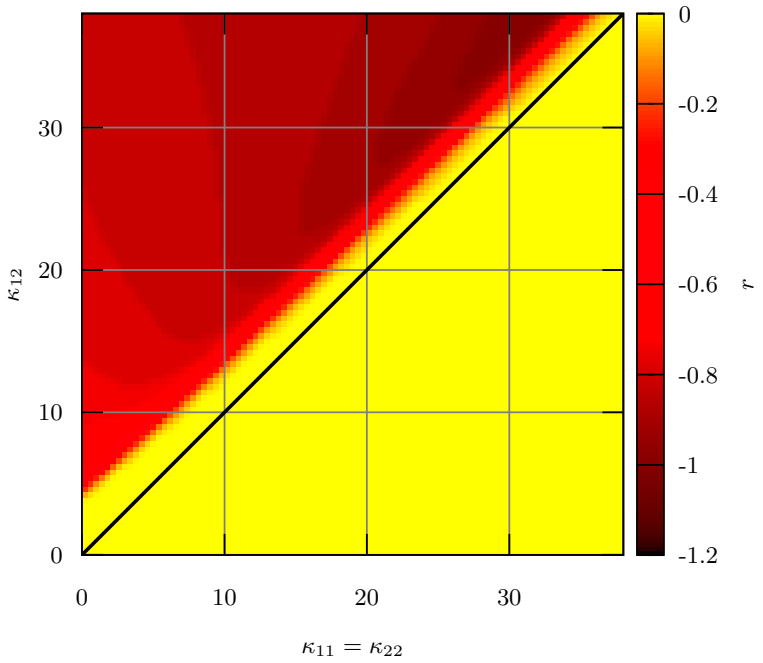

Figure 8.3: State diagram for the two-dimensional case. The black line gives the critical value for κ_{12} for the homogeneous case. The yellow area means no shift of the maximum of one species. For small interactions, κ_{12} has to be considerably larger than κ_{11} to lead to a state separation since such separation leads to a spatial extension and the potential works against it. As the interactions increase, they become the dominating terms in the GPE and the κ_{12} approaches the value κ_{12}^c of the homogeneous case.

from the cases of no separation of the components in the homogeneous case. For the trapped case, the transition area is not on top of the black line. For small interactions, a much larger interspecies interaction than the intraspecies interaction is necessary to lead to a state separation. As already explained, this is due to the existence of the potential since two separated densities require more space in the trap. This leads to a higher contribution of potential energy.
For large interactions, κ_{12}^c approaches $\kappa_{11} = \kappa_{22}$ which was also observed in the one-dimensional case. In the following, we will use κ_{12}^c to denote the critical value for the interspecies interaction for which both components of the condensate will separate.

8.3 Ground state approximations

In the following, the approximations carried out for the one-dimensional case will be repeated for the two-dimensional situation. This provides an initial state for the time-dependent

considerations.

- First, we concentrate on the case of no state separation, hence we use $\Psi(x,y) = \Phi_1(x,y) = \Phi_2(x,y)$ again. Assuming a Gauss shaped function in two dimensions, we can introduce $\Psi(x,y)$ as

$$\Psi(x,y) = \frac{1}{\sqrt{\alpha\beta\pi}}\, e^{-\frac{x^2}{2\alpha^2}-\frac{y^2}{2\beta^2}}, \tag{8.1}$$

which is a normalized wave function. The parameters α and β are the widths for the

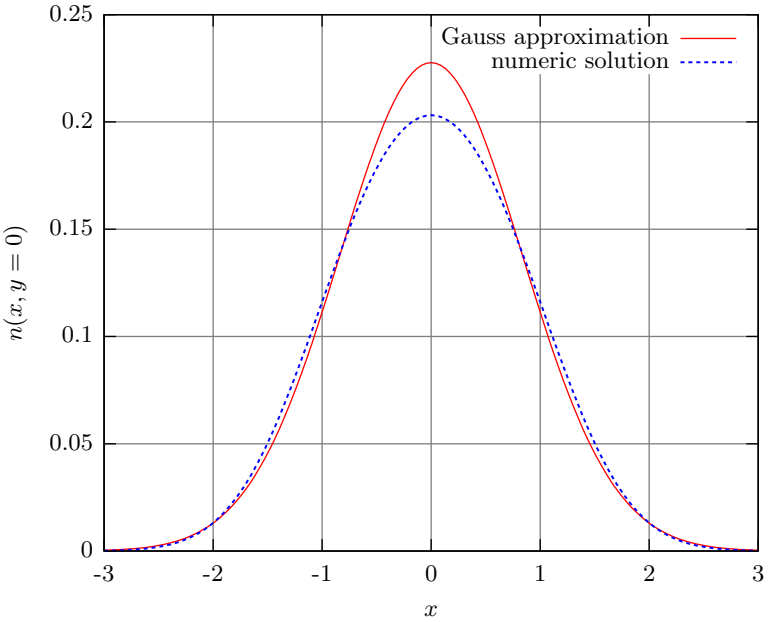

Figure 8.4: Comparison of the Gauss approximation with the numerically obtained solution. Since these ground states have a rotational symmetry it is sufficient to consider only $n(x, y = 0)$. The largest difference between the approximation and the numerical solution is around the peak.

x and y-direction. We are then able to take an asymmetric potential into account. The energy for the two-dimensional case is given by

$$E = \int dx\ dy\ \left[|\partial_x\Psi(x,y)|^2 + |\partial_y\Psi(x,y)|^2 + x^2|\Psi(x,y)|^2 + (a_t \cdot y)^2|\Psi(x,y)|^2 + (\kappa_{11}+\kappa_{12})|\Psi(x,y)|^4\right]. \tag{8.2}$$

Inserting formula 8.1 and calculating the integrals gives an expression for the energy depending only on α, β and the trapping asymmetry a_t.

$$E = \frac{1}{2}\left(\frac{1}{\alpha^2} + \alpha^2 + \frac{1}{\beta^2} + (a_t\beta)^2\right) + \frac{\kappa_{11}+\kappa_{12}}{2\alpha\beta\pi} \tag{8.3}$$

Equation 8.3 needs to be minimized numerically with respect to α and β. Figure 8.4 shows the Gauss approximation (red curve) and the numerically obtained ground state (blue dashed line) for the parameters $\kappa_{11} = \kappa_{22} = 4$ and $\kappa_{12} = 2$.

- For the case of state separation, we assume for the wave functions again a Gauss function. However, we assume now a shift in x-direction with the following ansatz:

$$\Psi_1(x) = \frac{1}{\sqrt{\alpha\beta\pi}} e^{-\frac{(x+c)^2}{2\alpha^2} - \frac{y^2}{2\beta^2}} \tag{8.4}$$

$$\Psi_2(x) = \frac{1}{\sqrt{\alpha\beta\pi}} e^{-\frac{(x-c)^2}{2\alpha^2} - \frac{y^2}{2\beta^2}} \tag{8.5}$$

It defines already the symmetry axis which can be actually chosen to be arbitrarily. With this approximation, the energy given by formula 8.3 becomes:

$$E = \frac{1}{2}\left(\frac{1}{\alpha^2} + \frac{1}{\beta^2} + \alpha^2 + (a_t\beta)^2\right) + c^2 + \frac{\kappa_{11} + \kappa_{12}\, e^{-\frac{2c^2}{\alpha^2}}}{2\pi\alpha\beta} \tag{8.6}$$

This has to be minimized numerically again with respect to α, β and c.
An example is shown in figure 8.5 for $\kappa_{11} = \kappa_{22} = 4$ and $\kappa_{12} = 10$. The left plot shows the Gauss shaped profile whereas as the plot in the middle is the numerical solution. The difference of both is shown in the right figure. The minimization of formula 8.6

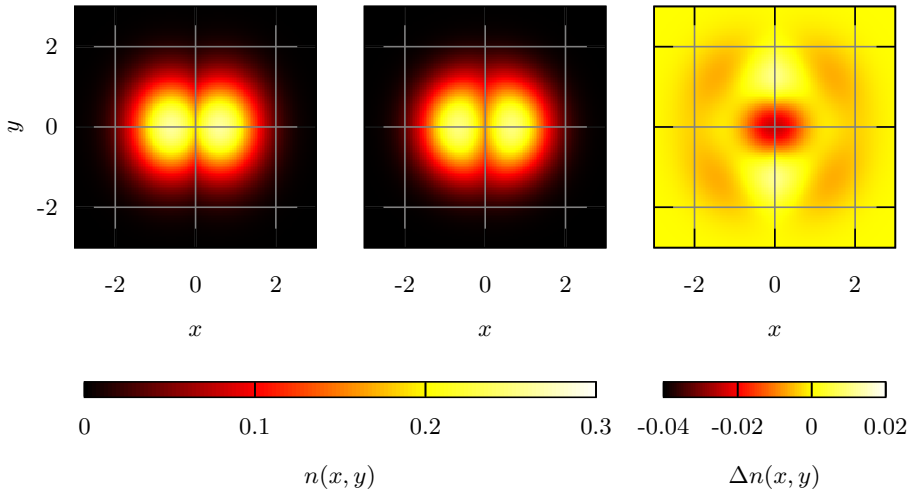

Figure 8.5: Gauss approximation, numerical calculated density profile and their difference $\Delta n(x, y)$ for $\kappa_{11} = \kappa_{22} = 4$ and $\kappa_{12} = 10$. Again, the numerical density profiles are smoother compared to the Gauss shaped ones which explains the negative values for $\Delta n(x, y)$ in the trap center shown in the right plot. Since the approximated densities have the form of an ellipse, it deviates from the numerical one at the trap edges which is shown by the red areas of the $\Delta n(x, y)$ plot.

leads also to the separation of both components. The numerically obtained figure has smoother shape compared to the Gauss approximation and since in the Gauss ansatz only the parameters α and β take a deformation into account, the density profiles have still an elliptic shape. This leads to the white and red areas in the trap center in the plot for $\Delta n(x, y)$. The difference between approximation and exact solution are ≈ 10 %.

- In order to summarize and compare this approximation in general to the numerical solution, a state diagram is plotted which is shown in figure 8.6. The black line denotes

the critical value for κ_{12} for the homogeneous case.
The transition region from no state separation to a separation of both components

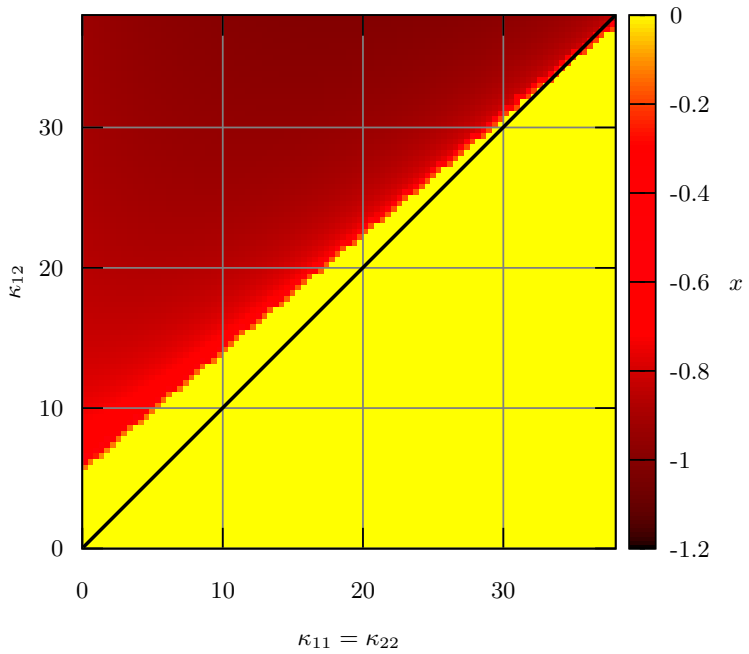

Figure 8.6: State diagram in two dimensions using equations 8.4 and 8.5. For small interactions, it is very similar to 8.3 but then the black line crosses the transition area. Here, the absolute value of the shift increases continuously since the deformation of the densities is limited to the parameters α and β.

is not as smooth as in figure 8.3 which is a consequence that the deformation of the Gauss shaped density is limited. Further, the black line crosses the transition region in the diagram which was not observed in figure 8.3.

CHAPTER 9

Dynamical properties of a two-component gas in 2D

9.1 Breathing mode

In order to check the accuracy of the program for two dimensions, the breathing mode was studied too. For the modes in 1D, varying the interaction strength leads to $\omega^2 = 4\omega_0^2$ and $\omega^2 = 3\omega_0^2$ for the Tonk-Girardeau and the 1D mean-field regime.
For the two-dimensional case, it was shown in [10] numerically that the mode frequency is $2\omega_0$ and independent of the interaction strength. The program confirms these results for a single component BEC and also for a condensate with two components.

9.2 Atom loss dynamics for no state separation

This section concentrates on the dynamics caused by the dissipation in two dimensions.

9.2.1 Atom loss for different γ

In two dimensions, the interactions are highly relevant too since the losses depend on the overlap of the two densities. We will start with the case of no state separation and choose now $\kappa_{12} = 2$ and $\kappa_{11} = \kappa_{22} = 4$. The decay for this case is shown in figure 9.1. The overall shape and the behavior of the decay curves is very similar to the 1D case. For $\gamma = 0.1$, the losses are very small compared to higher values. On this time scale, the curve looks almost linear. If γ is increased up to a value of 1, the green curve shows already some small oscillations.
The oscillations mentioned earlier are for $\gamma = 5$ and $\gamma = 10$ even more visible. The larger γ gets the higher are the losses which is consistent, since γ is the dissipation rate.

9.2.2 Evolution of the density

Now, we want to discuss the cause of the oscillation occurring in the decay curves for the case $\kappa_{12}^c \lesssim \kappa_{11} = \kappa_{22}$ and $a_t = 1$ on the basis of the density plots shown in figure 9.2.
The plot for $t = 0$ shows the ground state for the values $\kappa_{11} = 4$ and $\kappa_{12} = 2$. By the choice of the interactions, it is an immiscible condensate. Due to the dissipation parameter of $\gamma = 10$ and the complete overlap of both components, at $t = 1$ the loss is quite visible. This continues until $t = 4$. The majority of the loss happens in the middle of the trap. Similar to the one-dimensional case, the atoms move from the edge of the trap towards the center, in order to compensate the losses. At $t = 3$, the majority of the atoms is in the middle which

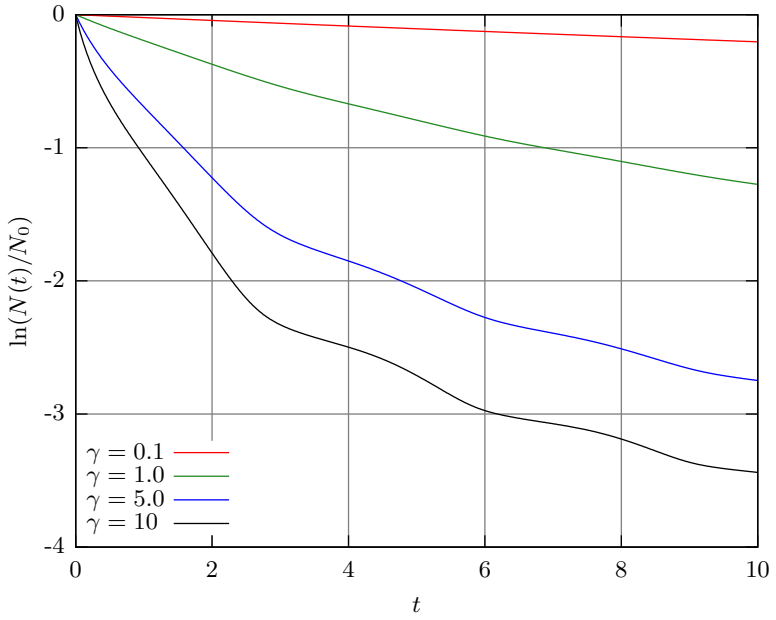

Figure 9.1: Logarithmic plot for the particle number of one component for different γ, $\kappa_{12} = 2$ and $\kappa_{11} = \kappa_{22} = 4$ in 2D. As γ gets larger, the loss of particles and the visibility of the oscillations increases.

leads to a large dissipation there and causes an increase of the radius of the cloud at $t = 4$ (not seen in figure 9.2). Since the color scale for the density is not adapted for the plots between $t = 3$ and $t = 5$, the contraction of the gas becomes visible from $t = 4$ to $t = 5$. At $t = 6$, the density has already has decreased since the previous contraction allowed a more efficient dissipation in the center of the trap. At $t = 7$, the gas expands again and contracts for $t = 8$. The periods during the contractions occur in the decay curves as a high decrease and the phases of expansions as a low decrease of particle number.

9.2.3 Approximation for the decay curves

In analogy to the 1D case, we try to approximate the decay curve using only the numerical obtained ground state. The formulas 7.1 and 7.2 for the one-dimensional case can be simply adapted to the two-dimensional situation.

$$n_1(x, y, t) \approx n_1(x, y, t = 0) \cdot e^{-2\gamma t n_2(x,y,t=0)} \tag{9.1}$$

$$n_2(x, y, t) \approx n_2(x, y, t = 0) \cdot e^{-2\gamma t n_1(x,y,t=0)} \tag{9.2}$$

Again, the time dependency of the densities in the exponent is neglected.
The resulting plot is shown in figure 9.3. The red curve shows the result obtained by the split step algorithm and the green curve shows the result according to equations 9.1 and 9.2. Since there is no state separation, we can set $n_1(x, y, t = 0) = n_2(x, y, t = 0) = n(x, y, t = 0)$ in the following.
The approximation is very rough and both curves deviate already after $t \approx 0.1$. As the system starts to evolve further and differs from the ground state, equations 9.1 and 9.2 are not reasonable approximations anymore.
We use the same ansatz as in the one-dimensional case taking the time dependency of the

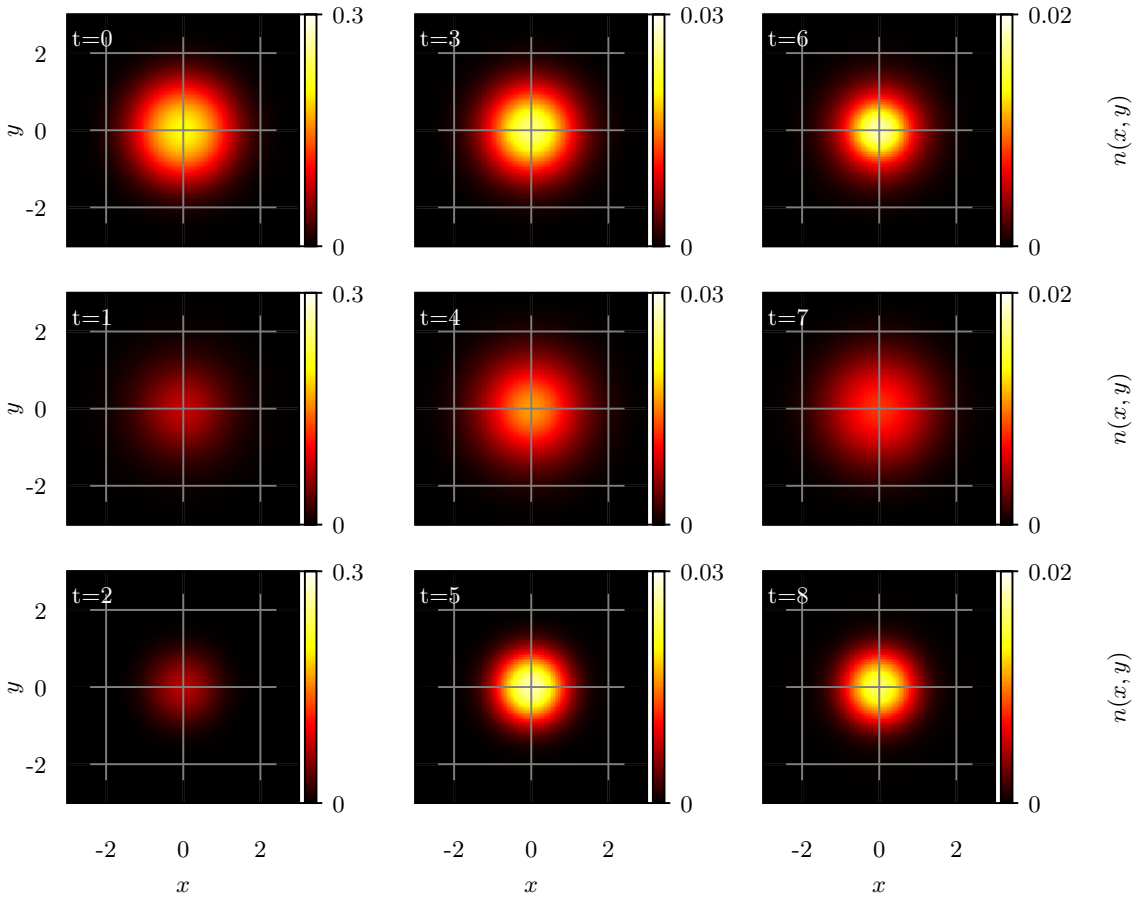

Figure 9.2: Evolution of the densities for $\gamma = 10$, $\kappa_{11} = \kappa_{22} = 4$ and $\kappa_{12} = 2$. Our considerations start with the ground state at $t = 0$. After switching on the dissipation, the density drops until $t \approx 2$ and due to the anisotropic dissipation which happens predominantly in the trap center, the atoms move towards the trapping center. At $t = 3$, too many atoms are now in the middle of the trap. This leads to a slight expansion which is shown in the plot at $t = 4$. Since the condensate has contracted at $t \approx 5$, the particles moved again back from the edges of the potential. One can see the same process from $t = 6$ to $t = 8$, but the density decreases further.

density into account but neglecting all other terms in equations 3.35 and 3.36 to get an improved approximation.

$$i\partial_t \Psi_1(x, y, t) \approx -i\gamma n_2(x, y, t)\Psi_1(x, y, t) \tag{9.3}$$
$$i\partial_t \Psi_2(x, y, t) \approx -i\gamma n_1(x, y, t)\Psi_2(x, y, t) \tag{9.4}$$

This leads to

$$\partial_t n_1(x, y, t) \approx -2\gamma n_1(x, y, t)n_2(x, y, t) \tag{9.5}$$
$$\partial_t n_2(x, y, t) \approx -2\gamma n_1(x, y, t)n_2(x, y, t). \tag{9.6}$$

For the case $\kappa_{11} = \kappa_{22} \lesssim \kappa_{12}^c$, one can set $n(x, y, t) = n_1(x, y, t) = n_2(x, y, t)$. Similar to the 1D case, the solution of the differential equation is:

$$n(x, y, t) \approx \frac{n(x, y, t = 0)}{2\gamma t n(x, y, t = 0) + 1} \tag{9.7}$$

In figure 9.3, the comparison of the numerical solution (red) and formulas 9.1/9.2 (green)

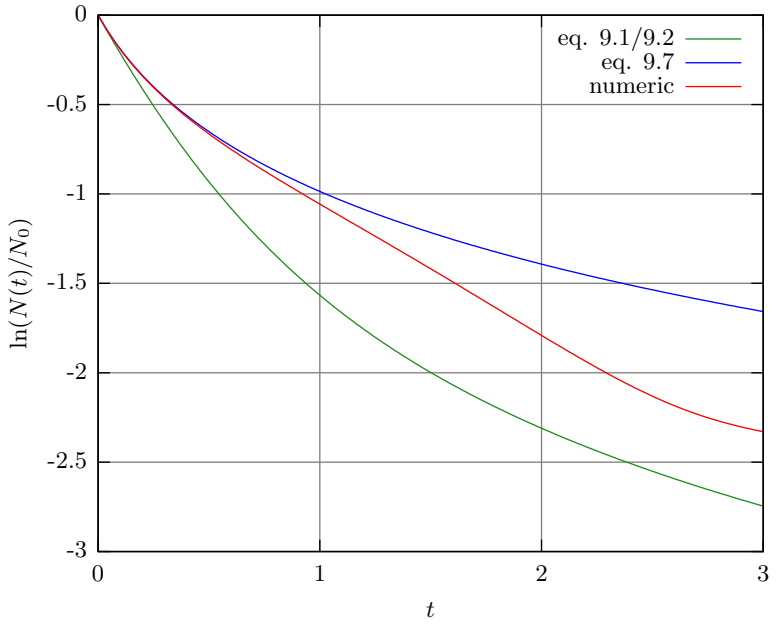

Figure 9.3: Comparison of the exact decay curve for $\gamma = 10$, $\kappa_{11} = \kappa_{22} = 4$ and $\kappa_{12} = 2$ with the approximations according to the equation 9.1 (green), 9.7 (blue) and the numerical result (red). Since equation 9.7 takes the time dependence of the density into account, it is a better approximation than equation 9.1 which fails at $t \approx 0.2$. The *analytic* decay curve provides a good solution up to nearly $t = 1$.

and 9.7 (blue) is shown. For the latter, the numerically calculated ground state was used and it was integrated over space in order to get $N(t)$. One can see clearly that the blue curve is a better approximation compared to the time independent one. It provides a fairly good approximation up to $t \approx 1$.
In section 8.3, the ground state density was described by a Gauss profile of the form

$$n(x, y) = \frac{1}{\alpha\beta\pi} e^{-\frac{x^2}{\alpha^2} - \frac{y^2}{\beta^2}}. \tag{9.8}$$

Using this, an expression for the absolute particle number $N(t)$ can be obtained. The integral gives

$$N(t) \approx N_0 \frac{\alpha\beta\pi}{2\gamma t} f_1\left(\frac{2\gamma t}{\alpha\beta\pi}\right). \tag{9.9}$$

Its form is very similar to formula 7.11, but one has to integrate over an additional dimension. This leads to $f_1(x)$ instead of $f_{1/2}(x)$. The parameters α and β are determined by minimizing equation 8.3. In figure 9.4, one can see the magnitude of the differences between equations 9.9 (green), 9.7 with the numerical ground state (blue) and the complete solution (red). Both approximations are on top of each other up to $t \approx 1$ and start to deviate from the red

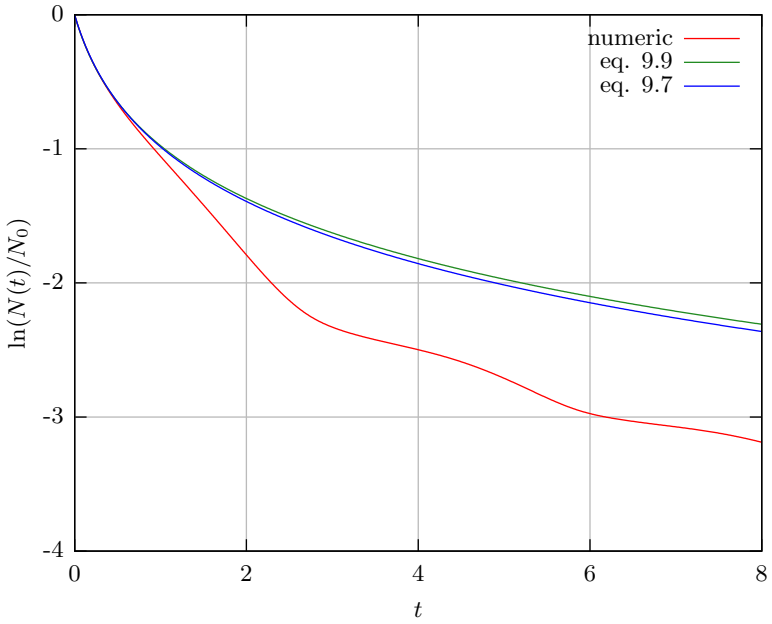

Figure 9.4: Plot of the complete numerical solution, equations 9.7 with a numerical ground state and 9.9 for $\gamma = 10$, $\kappa_{11} = \kappa_{22} = 4$ and $\kappa_{12} = 2$. Both are good approximations but they fail at $t \approx 1$

curve afterwards. At the beginning, the blue and green curve are on top of each other and differ from the numeric solution for $t \approx 1$. Later for $t \approx 2$, they separate.
In the following, the validity of the Gauss density itself during evolution is checked. This is shown in figure 9.5 for the values $\gamma = 10$, $\kappa_{11} = \kappa_{22} = 4$ and $\kappa_{12} = 2$ where the green curve denotes the Gauss shaped function and the red one the numerical solution.
The difference between the ground states obtained by the Gauss approximation and the fully numerically calculated is shown in the plots for $t = 0$. Due to the symmetry of the system, only $n(x, y = 0)$ is considered. As the system evolves, both the approximation and the numerical density shrink. At $t = 0.6$, the entire green curve drops completely below the red one. At $t = 0.8$, the contraction of the condensate starts and leads to a larger deviation at the center and a smaller deviation at the slopes. The contraction continues and causes a lower density at the edges of the potential which is the reason for the big difference at $t \approx 1.0$. From this time on, equation 9.9 is not a good approximation, as we have already seen in figure 9.4. Since the atoms continue moving towards the trapping center, $t = 1.8$ shows for the Gauss profile a flat density, whereas the red curve has a very distinct peak.
Despite these large deviations between the complete numerical solution and approximation, formula 9.9 provides for small times a good description of the decay curve for such a system. A possible reason for that might be that these local differences compensate each other when taking the average.
In the two-dimensional case, the behavior of such system for an asymmetric trapping potential can be studied. In formula 9.9, this is taken into account via the values of α and β. The comparison of a symmetric and an asymmetric trap with the numerical results can be found in figure 9.6. As one can see, the asymmetry is taken into account but the approximation is not as reliable as for $a_t = 1$ because it deviates slightly earlier. However, it describes the initial drop of particle number quite good.

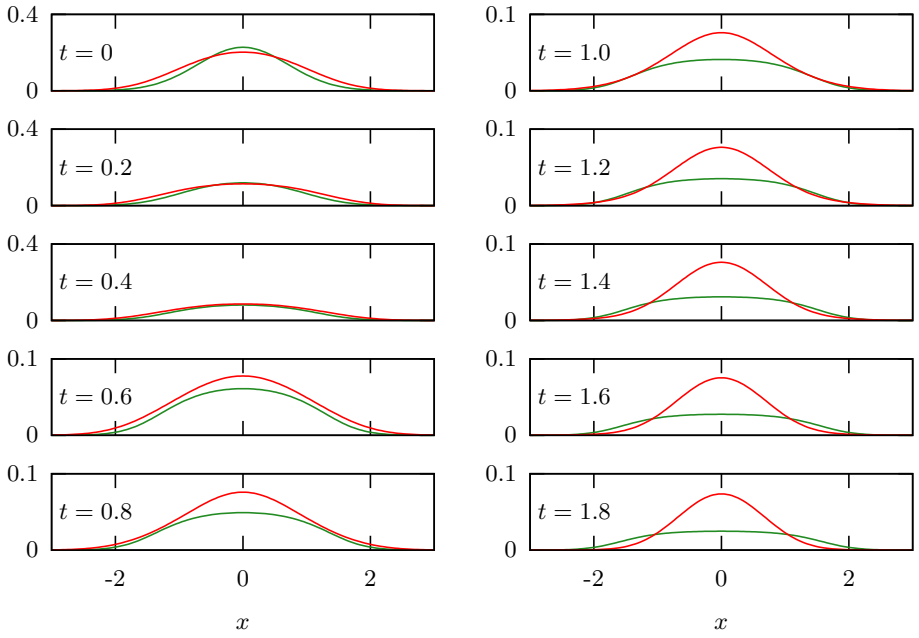

Figure 9.5: Comparison of the Gauss shaped approximation with the numerical solution of the Gross-Pitaevskii equation for $\gamma = 10$, $\kappa_{11} = \kappa_{22} = 4$ and $\kappa_{12} = 2$. The approximation starts to deviate at $t = 0.6$ slightly. For $t = 1$, that difference becomes significantly large as the numerically obtained density starts to contract.

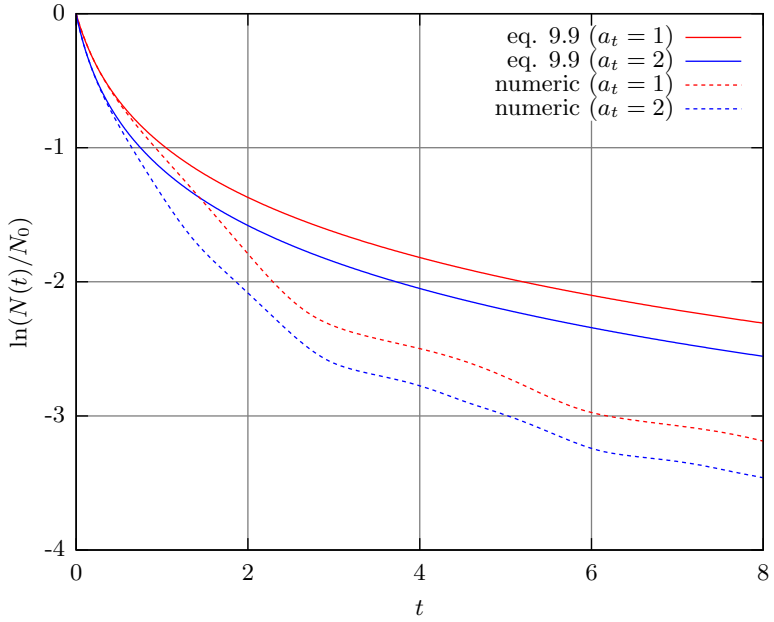

Figure 9.6: Plot of the numerical solution and the expression 9.9 for $\gamma = 10$, $\kappa_{11} = \kappa_{22} = 4$ and $\kappa_{12} = 2$ for a trap with no asymmetry and a frequency ratio $\frac{\omega_y}{\omega_x} = 2$. The analytic expression provides a good description even for asymmetric traps although it becomes inaccurate after a shorter time compared to the case $\omega_y = \omega_x$.

9.2.4 Hydrodynamic approach to a two-component system with dissipation

In analogy to the one-dimensional case, the movement of the particles will be studied using the current. For two dimensions, it is defined for each particle species as:

$$\vec{j}_1(x,y,t) = \frac{1}{2i}(\Psi_1^*(x,y,t)\vec{\nabla}\Psi_1(x,y,t) - \Psi_1(x,y,t)\vec{\nabla}\Psi_1^*(x,y,t)) \tag{9.10}$$

$$\vec{j}_2(x,y,t) = \frac{1}{2i}(\Psi_2^*(x,y,t)\vec{\nabla}\Psi_2(x,y,t) - \Psi_2(x,y,t)\vec{\nabla}\Psi_2^*(x,y,t)) \tag{9.11}$$

The current has now the form of a vector field and due to the symmetry of the system, one can set $\vec{j}_1(x,y,t) = \vec{j}_2(x,y,t) = \vec{j}(x,y,t)$. In plot 9.7, the density profile and the current (red arrows) are shown for different times using $\gamma = 10$, $\kappa_{11} = \kappa_{22} = 4$ and $\kappa_{12} = 2$. The

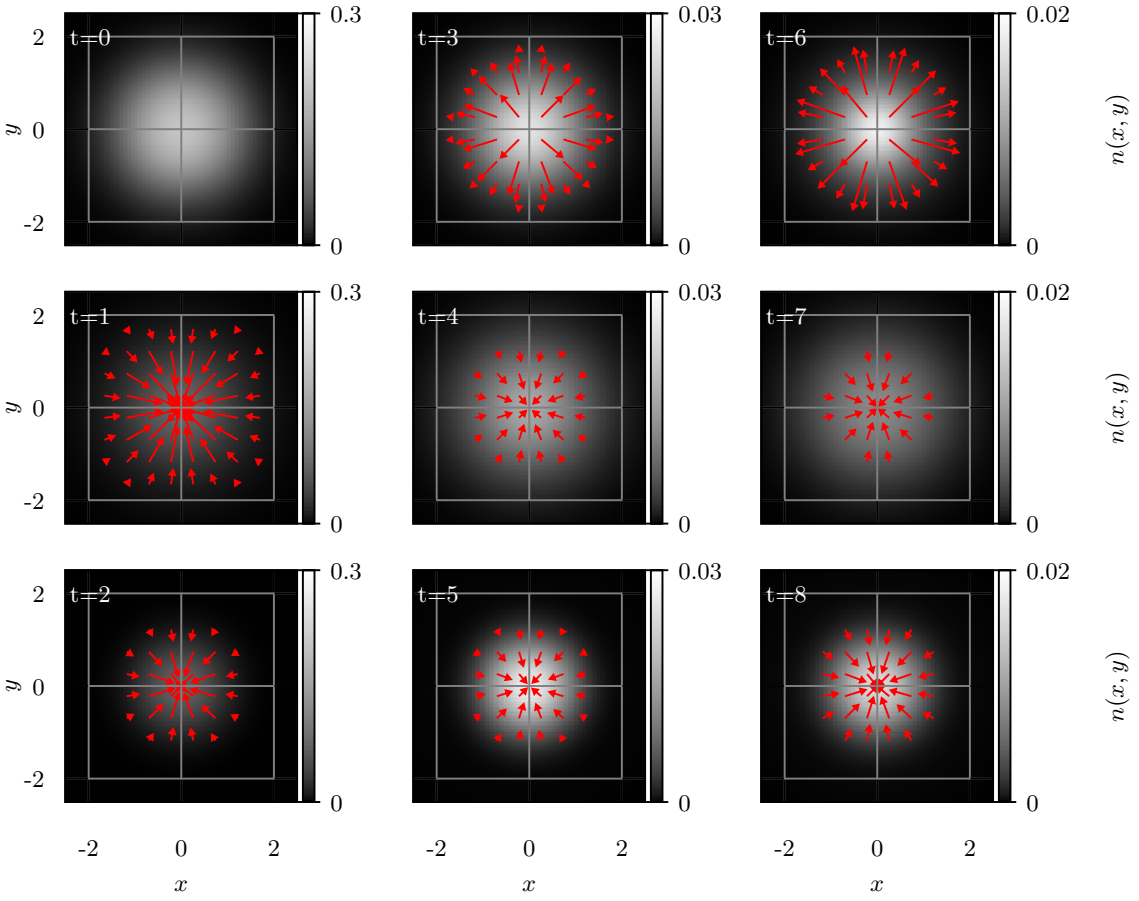

Figure 9.7: Current and density plots for different times with the settings $\gamma = 10$, $\kappa_{11} = \kappa_{22} = 4$ and $\kappa_{12} = 2$. Since the dissipation induces the dynamics, the ground state $t = 0$ shows no current. When the dissipation starts, a large current towards the center of the condensate starts and decreases at $t = 2$, especially at the edges. After this contraction, the gas expands again at $t = 3$ which causes an decreasing loss rate until it contracts again between $t = 4$ and $t = 5$. The previously described process would repeat until all atoms have left this system.

scale for the density and current are changed simultaneously. For the ground state at $t = 0$, no dynamic has taken place and hence, no current appears. If the dissipation starts, a current directed towards the trap center forms. The absolute value of $\vec{j}(x,y)$ gets larger towards the center of the trap since the dissipation takes place mainly there.

The plot for $t = 2$ shows the decreasing current since the movement of the particles have already compensated the previous losses and the contraction of the density slows down. Later at $t = 3$, the current has reversed again and causes now an expansion of the density. During the period of the reversal of the current, the most efficient dissipation happens, since the majority of the atoms of both species are in the middle of the potential. The velocity of expansion is in the middle much higher than in the outer regions, since the atoms are slowed down there due to the smaller density again.
At $t = 4$, the current has turned back and all its components point now towards the center of the condensate. This leads to a contraction which becomes especially visible at time $t = 5$. For $t = 6$, the expansion process starts again and avoids an efficient dissipation until both components contract again at $t = 8$. This cycle of contraction and expansion repeats until no atoms are left in the condensate.
The overall dynamics are very similar to the one-dimensional case. This alternating behavior of the particle movements, which is inwards or outwards directed at some times, was previously observed. It leads to an oscillating form of the decay curves in both cases.
The breathing mode is a deviation from the equilibrium state and was excited by a change of the trapping frequency. In the case of such a dissipative system, the particle number was changed instead of the potential. This leads to similarity between both the change of the trapping potential and the continuous dissipation of the condensate mixture.

9.2.5 Asymmetric trapping potential

Since the two-dimensional case offers an additional degree of freedom, the asymmetric trapping potential will be considered in the following. For figure 9.8, the settings $\kappa_{11} = \kappa_{22} = 7$, $\kappa_{12} = 2$ and $\gamma = 50$ are used. The ratio of the trapping frequencies $\frac{\omega_y}{\omega_x}$ is increased to reach various values. In order to have a reference, the case of no asymmetry $a_t = 1$ is plotted as well. For $a_t = 1$, the decay curve has the familiar oscillating shape and shows periods of large and small particle losses. In this example, these oscillations occur between $t \approx 3$ and $t \approx 6$. Considering now highly asymmetric traps e.g $a_t = 8$ and $a_t = 12$, we observe on the one hand a higher loss of atoms due to the squeezing of the condensate in y-direction and on the other hand a combination of two kinds of oscillations.
For a symmetric trap, the frequency is $\omega \approx 2\omega_x \approx 2\omega_y$ what is the frequency of the breathing mode in two-dimensions. Reading off the frequency for the small oscillations gives us $\omega_{small} \approx 2\omega_y$. This means that a combination of the same effect observed for the one-dimensional case for both directions takes place.
In order to verify the mechanism behind, the hydrodynamic description of a Bose gas is used again. Figure 9.9 shows the density and the current (red arrows) for different times for $\kappa_{11} = \kappa_{22} = 7$, $\kappa_{12} = 2$, $\gamma = 50$ and an asymmetry of $a_t = 2$. The vectors are normalized and scaled since we are only interested in the direction of the current but not in its absolute value. Since for $t = 0$ the ground state is shown, no dynamic occurs, but it is visible how the larger frequency influences the shape of the condensate. As the dissipation starts, the current consisting of the component $j_x(x, y)$ and $j_y(x, y)$ is directed towards the center in order to compensate the loss there and the particles move away from the edges of the potential. This continues until $t = 0.8$. This is very similar to the symmetric case which was shown in figure 9.7.
For $t = 1.2$, the $j_y(x, y)$ components have changed their signs but the $j_x(x, y)$ component has not. The condensate starts contracting along the x-direction and elongating along the y-direction which becomes even more apparent for $t = 1.6$. At $t = 2$, the current points

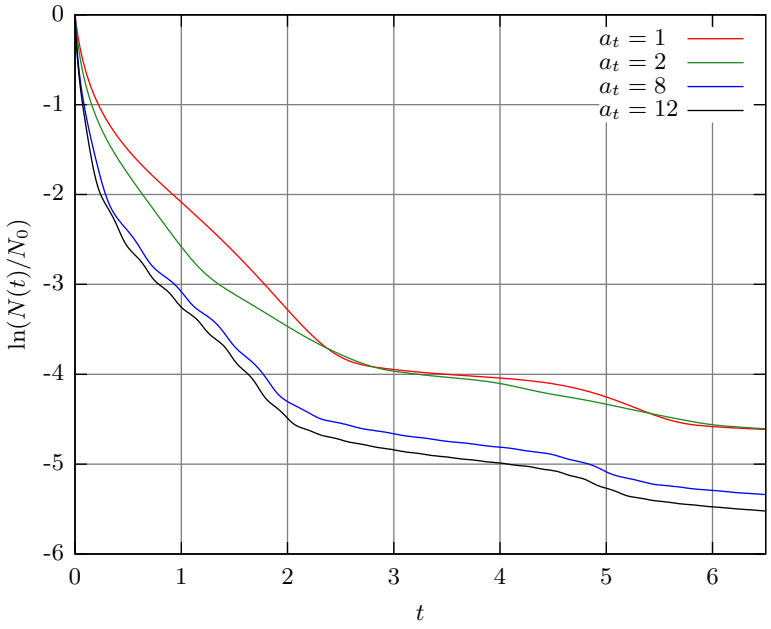

Figure 9.8: Decay curves for $\kappa_{11} = \kappa_{22} = 7$, $\kappa_{12} = 2$, $\gamma = 50$ and different a_t. As the asymmetry is increased, the losses increase too and oscillations occur additionally to the ones observed in the case $a_t = 1$. Estimating their frequency gives $\omega_{small} = 2\omega_y$. The asymmetry also influences the loss rate since the larger the asymmetry gets, the more the condensate is squeezed.

mainly towards the trapping center but at the edges one can see that now j_x starts to change its sign. Now, the plot for $t = 2.4$ shows the reversing process starting in x-direction, then in y-direction. This was not observed in e.g. figure 9.7 where the current resembled the symmetry of the system and the condensate pulsated symmetrically. As j_y reverses, the condensate expands in all directions for $t = 2.8$ and $t = 3.2$. This continues for larger times. Since j_y and j_x oscillate with different frequencies, this becomes visible in the decay curve. If the condensate contracts in both directions, the losses are larger compared to the contraction in only one direction . For a good visibility, the dissipation rate and the asymmetry has to be chosen rather large but it also occurs for smaller values of a_t and γ.

9.3 Atom loss dynamics for state separation ($\kappa_{11} = \kappa_{22} \leq \kappa_{12}^c$)

This section deals with the dynamics for $\kappa_{11} = \kappa_{22} \leq \kappa_{12}^c$. It will follow the same procedure as before.

9.3.1 Atom loss for different γ

Figure 9.10 shows the decay curve of one component of the condensate for different values for the dissipation rate γ. As observed in the previous cases, an increasing γ leads to more losses which is visible by the faster decrease of the particle number. It was already mentioned for the one-dimensional and the previous example in two dimensions that the oscillations are more apparent as the removal of atoms is increased. For $\gamma = 0.1$, the decay curve looks almost linear and at $\gamma = 1$, around $t = 5$, the curve exhibits a slightly oscillating behavior.

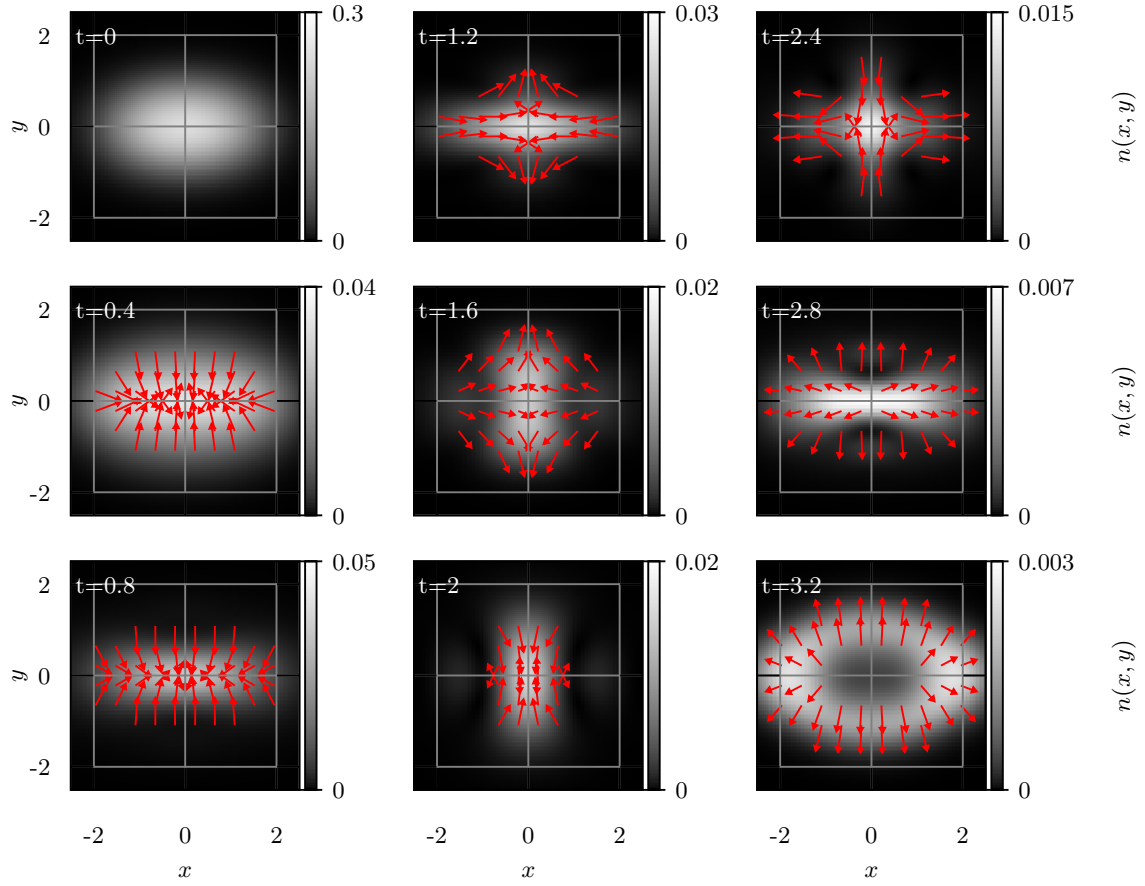

Figure 9.9: Density and current (red arrows) plots for $\kappa_{11} = \kappa_{22} = 7$, $\kappa_{12} = 2$, $\gamma = 50$ and $a_t = 2$. The vectors for the current are all normalized since we are only interested in the direction. Due to the asymmetry of the trap, the frequencies for the expansion and contraction in x and y-direction are different. This is the reason for the small oscillations in the decay curves shown in figure 9.8.

This becomes even more apparent for $\gamma = 5$ and $\gamma = 10$. The reason is explained in the following section.
The Quantum-Zeno effect occurs here too, as already explained for the 1D case. Since the mechanism is the same, it will not be further discussed here.

9.3.2 Evolution of the density

To explain the form of these curves, the evolution of the density for the values $\kappa_{11} = \kappa_{22} = 0$, $\kappa_{12} = 12$ and $\gamma = 5$ is discussed, which corresponds to the blue curve in figure 9.10. In figure 9.11, the ground state is shown for $t = 0$ and starting the dissipation leads to the figure for $t = 1$. The overall density for both components has decreased since the dissipation happens in the overlap region and the obtained space is refilled by atoms from the area where most of the atoms were.
For larger times, the dissipation continues which can be seen from the decreasing density in the $t = 2$ and $t = 3$ plots. Since the movement of atoms caused by the continuous dissipation is directed towards the trapping center, both components of the condensate start to extend into each other for $t = 4$. Later at $t = 5$, they overlap completely. This corresponds to the strong slope of the decay curve. They separate again at $t = 6$ since the momentum of the

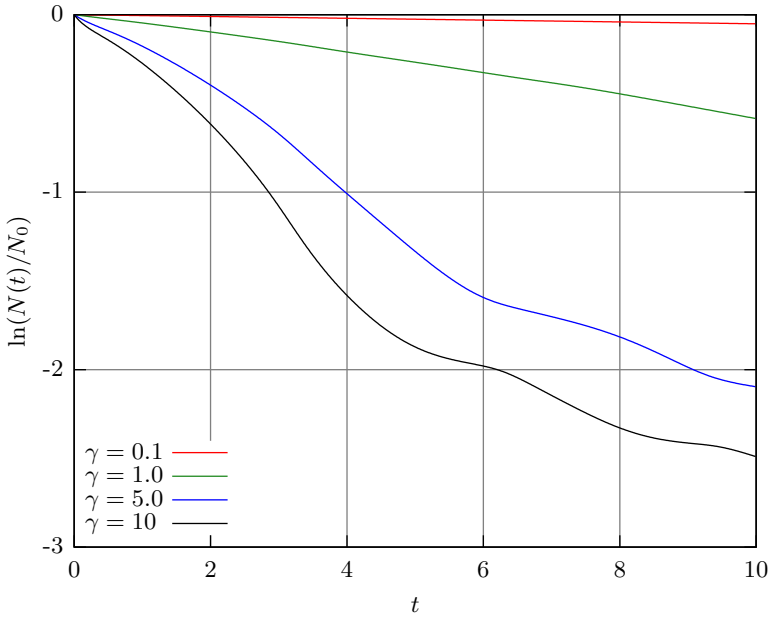

Figure 9.10: $N(t)$ for $\kappa_{11} = \kappa_{22} = 0$, $\kappa_{12} = 12$ and various values for γ. An increasing γ causes larger losses and makes oscillations more visible.

movement, which compensates the losses, is large enough that both components can slosh through each other. As it was already shown in the one-dimensional case, both species have swapped their position in the trap. Consequently, the decay curve flattens.
The momentum is reduced when the atoms strike the edges of the potential at about $t = 7$ and are reflected. Since this is very similar to the initial situation, the process repeats until all atoms have left the condensate.

9.3.3 Approximation for the decay curves

Again, by neglecting the time dependence of the other component of the gas, one can obtain equations 9.1 and 9.2. Figure shows 9.12 both the numeric solution of the entire GPEs (red) and the decay curve according to the approximation for $\kappa_{11} = \kappa_{22} = 0$, $\kappa_{12} = 10$ and $\gamma = 5$ (green). As always, this ansatz gives the initial behavior of the decay. When the system starts evolving and deviating from the ground state, the ansatz fails.
It was shown in section 8.3 that it is possible to approximate the ground state of a two component Bose gas in two dimensions with a Gauss function. Repeating these steps for two-dimensions, our ansatz is then

$$i\partial_t \Psi_1(x,y,t) \approx -i\gamma n_2(x,y,t)\Psi_1(x,y,t) \tag{9.12}$$
$$i\partial_t \Psi_2(x,y,t) \approx -i\gamma n_1(x,y,t)\Psi_2(x,y,t) \tag{9.13}$$

The solutions for $n_1(x,y,t)$ and $n_2(x,y,t)$ have the same form like equations 7.20 and 7.21 and read:

$$n_1(x,y,t) \approx (n_1(x,y) - n_2(x,y)) \cdot \frac{n_1(x,y)}{n_1(x,y) - n_2(x,y)e^{2\gamma t(n_2(x,y)-n_1(x,y))}} \tag{9.14}$$
$$n_2(x,y,t) \approx (n_2(x,y) - n_1(x,y)) \cdot \left(1 - \frac{n_1(x,y)}{n_1(x,y) - n_2(x,y)e^{2\gamma t(n_2(x,y)-n_1(x,y))}}\right) \tag{9.15}$$

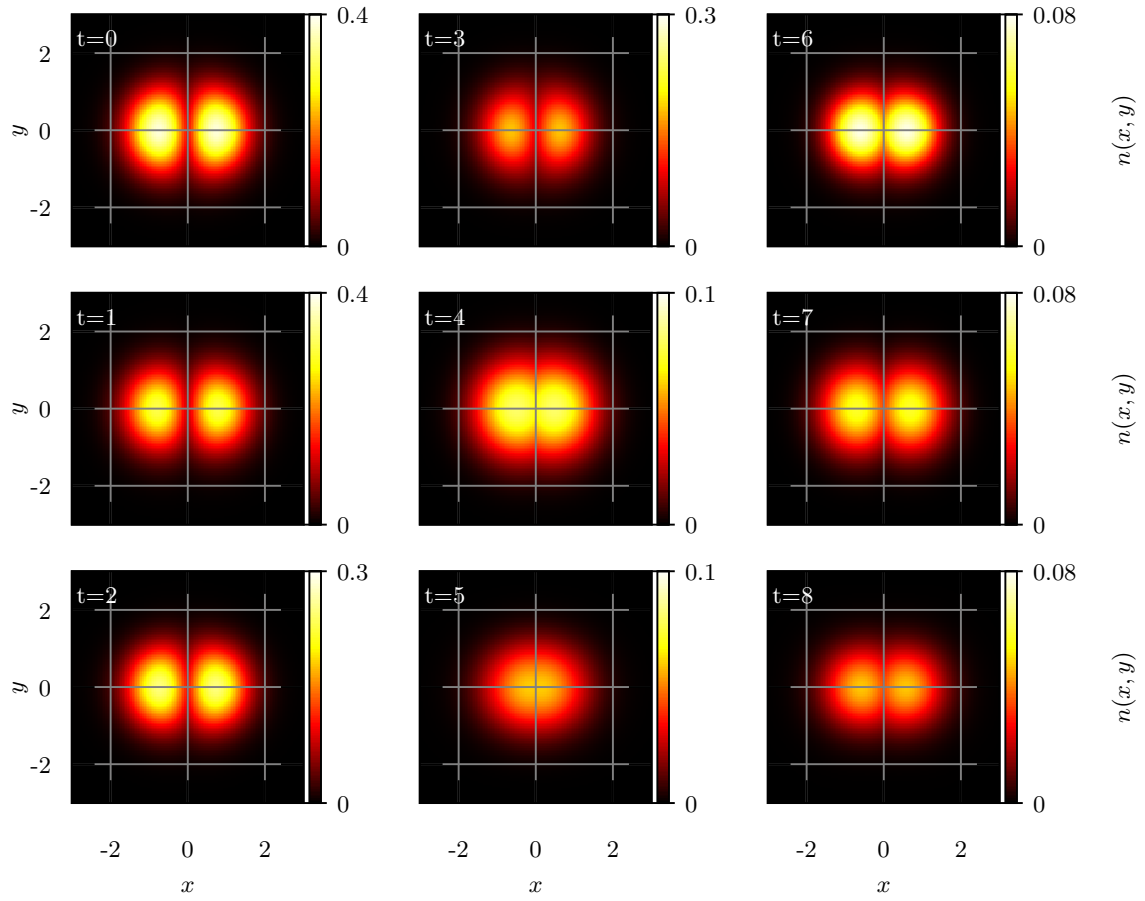

Figure 9.11: Evolution of the density over time for $\kappa_{11} = \kappa_{22} = 0$, $\kappa_{12} = 12$ and $\gamma = 5$. Starting from the ground state the density of the gas decreases constantly. For $t = 4$, both components start to merge and at $t = 5$, one cannot distinguish between both components. Later at $t = 6$, they separated again leading to a decrease in the decay.

In figure 9.12, one can see that $N(t)$ according to equations 9.14/9.15 (blue curve) starts to approach a constant value since the current is neglected. This is an improvement compared to the equations 9.1/9.2 since it fails significantly at about $t = 0.5$ whereas the green curve differs from the numerical solution already at $t \approx 0.1$.
In order to use the Gauss profile for this case, the integral over the x and y coordinate has to be calculated. Since one obtains a complicated integral, this is expanded for small γt up to second order which was already done for the one-dimensional case.
This gives for $N(t)$:

$$N(t) \approx 1 - \frac{\gamma t}{\alpha\beta\pi} e^{-\frac{2c^2}{\alpha^2}} + \frac{1}{3}\left(\frac{2\gamma t}{\alpha\beta\pi}\right)^2 e^{-\frac{8c^2}{3\alpha^2}} + \mathcal{O}(\gamma^3 t^3) \tag{9.16}$$

This expression becomes unphysical for its minimum which is given by:

$$t = \frac{3\alpha\beta\pi}{4\gamma} e^{\frac{2c^2}{3\alpha^2}} \tag{9.17}$$

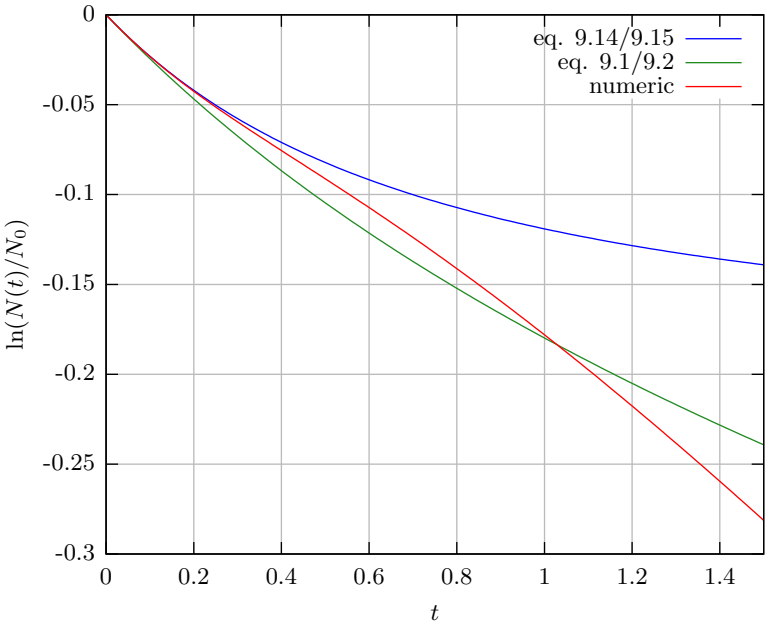

Figure 9.12: This plot compares equations 9.14/9.15, 9.1/9.2 and the numeric result for $\gamma = 5$, $\kappa_{11} = \kappa_{22} = 0$ and $\kappa_{12} = 12$. Since equations 9.14/9.15 take the time-dependence into account, they provide a good approximation. Neglecting the current leads to an asymptotic behavior of $N(t)$.

The parameters α, β and c are determined by minimizing equation 8.3.
Figure 9.13 shows the comparison of the complete numerical solution (red), the solutions of equations 9.14 and 9.15 with a numerically obtained ground state (green) and equation 9.16 (blue). Since equations 9.12 and 9.13 only consider the dissipation part of the GPEs -

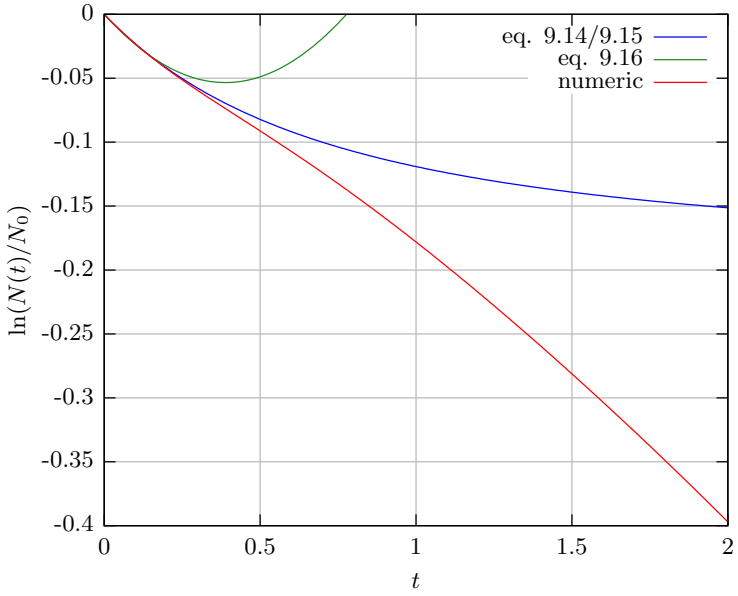

Figure 9.13: This plot shows $N(t)/N_0$ for $\gamma = 5$, $\kappa_{11} = \kappa_{22} = 0$ and $\kappa_{12} = 12$ of equations 9.16, 9.14/9.15 and the numeric result. The analytic expression fails earlier than 9.14/9.15 but it provides a useful approximation.

and not the kinetic part related to the current - the missing particle movement causes the particle number to freeze. Until the current forms, it is still a good approximation for small times. The analytic expression fails a little bit earlier but it provides a good description of the system up to $t \approx 0.3$.

9.3.4 Hydrodynamic approach to a two-component system with dissipation

We will now discuss the current. It is closely related to the form of the decay curve.
The current was previously defined in equations 9.10 and 9.11. Due to the symmetry of this system, one can set $j_{1,x}(x,y,t) = -j_{2,x}(-x,y,t) := j_x(x,y,t)$ and $j_{1,y}(x,y,t) = j_{2,y}(-x,y,t) := j_y(x,y,t)$. Figure 9.14 shows the current (red arrows) for $\kappa_{11} = \kappa_{22} = 0$, $\kappa_{12} = 12$ and $\gamma = 5$ and we define $\vec{j}(x,y,t)$ as the current of the initially right condensate. The plot for $t = 0$ shows the ground state. When the dissipation starts, the current is

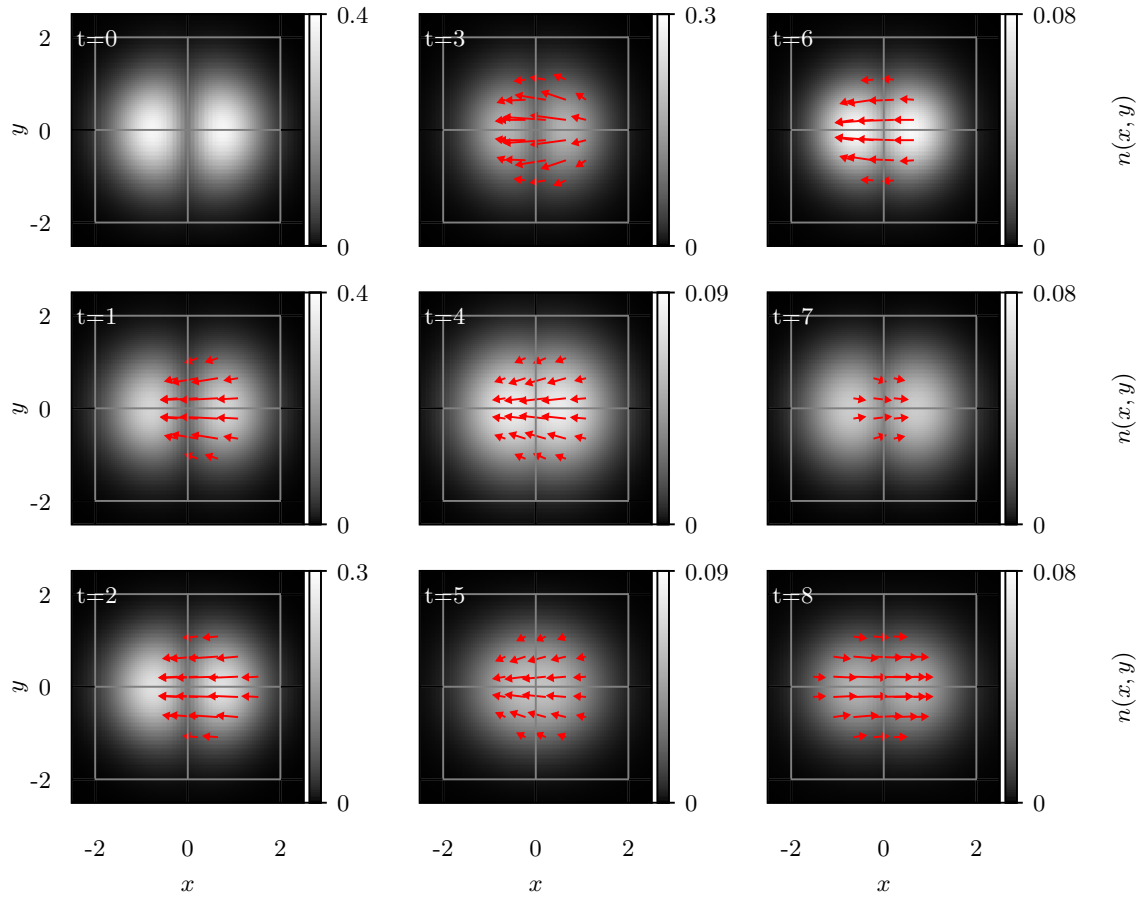

Figure 9.14: Current of the initially right component and density for $\gamma = 5$, $\kappa_{11} = \kappa_{22} = 0$ and $\kappa_{12} = 12$. As the dissipation starts, a current forms which is directed towards the region where the losses take place. At $t = 5$, both components overlap completely which causes an efficient dissipation. After they have swapped, the current reverses at $t = 7$ and initiates the previous procedure.

directed to the center of the trap which means that the overall movement of the particles is dominated by the atom losses. Later at $t = 2$, the current has extended to the right edge of the condensate. Since the dissipation happens mainly at the center of the condensate, the current there is larger than at the edges and points towards the center.

At time $t = 3$, the current adapts to the shape of the rotationally symmetric potential. The maxima of both components start to approach the center of the potential for $t = 4$. If $t = 5$ and $t = 6$, both components fuse temporarily and the current directs still to the $x < 0$ region. During that time, the decay curve shows a large loss of atoms (see figure 9.10). Later, the components separate completely and the atoms are slowed down by the potential. The dissipation takes place now at the right slope of the considered component and hence, a current forms around the trapping center. It is now directed towards the right edge of the potential. For large times, this swapping of the densities repeats. This effect is the reason for the oscillating structure in the blue curve 9.10.

9.3.5 Asymmetric trapping potential

Now, it will be discussed how an asymmetric trapping potential affects the dissipation in the case of state separation.
For this, we choose $\kappa_{11} = \kappa_{22} = 0$, $\kappa_{12} = 12$, $\gamma = 50$ and different values for the asymmetry. The result for the decay curve is shown in figure 9.15. The decay is considerably influenced

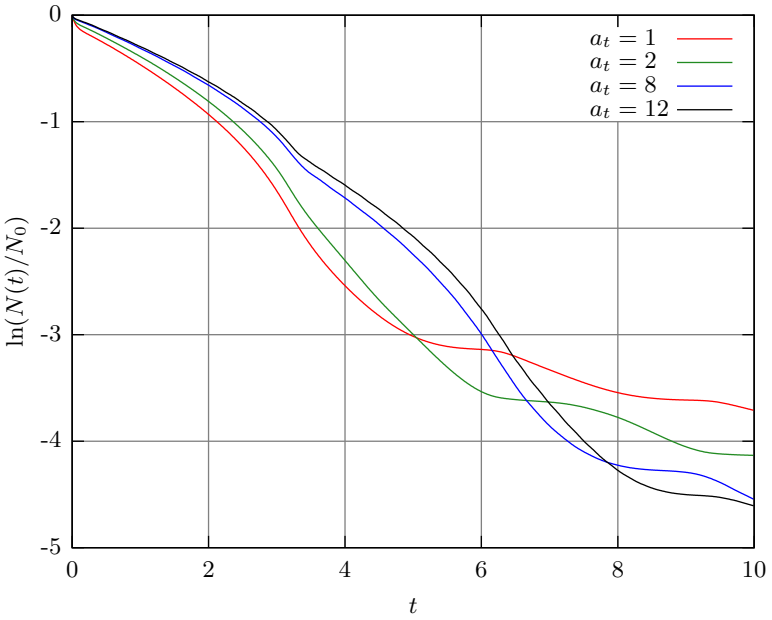

Figure 9.15: Decay curves for $\gamma = 50$, $\kappa_{11} = \kappa_{22} = 0$, $\kappa_{12} = 12$ and different values for a_t. The amount of dissipated atoms depends on asymmetry since the strong potential in y-direction limits the number of atoms which can move towards the middle of the trapping center. Due to the higher density, the losses are larger for high asymmetries. If then both components slosh through each other, the losses are even more dramatic.

by the asymmetry. The larger a_t is, the less atoms can leave the system for small times. Since both components are separated in the ground state and the potential in the y-direction is much stronger, the space where the dissipation can take place is quite small. This is the reason for the small loss of atoms at the beginning.
For $t \approx 5$, the loss in the symmetric trap becomes smaller than for $a_t = 2$. At this time, the densities of both components overlap completely. Since the space in asymmetric traps is much more limited compared to the symmetric case, the losses are much larger in this kind of potential. If a_t is increased further, the initial decay gets smaller but after a time the

losses are even higher.
In section 9.2.5, it was shown that for a large ratio of $\frac{\omega_y}{\omega_x}$, additional oscillations occur. We observed this for state separation too. Unfortunately, they are not visible on this scale in the plot 9.15 since the losses influenced by the asymmetry are too small to appear in the decay curve. In the following, the current and the densities for $\gamma = 50$, $\kappa_{12} = 12$ and $\kappa_{11} = \kappa_{22} = 0$ will be investigated. These plots are shown in figure 9.16 and correspond to the blue line in plot 9.15.
The plot for $t = 0$ shows the ground state and no current occurs. All vectors are normalized

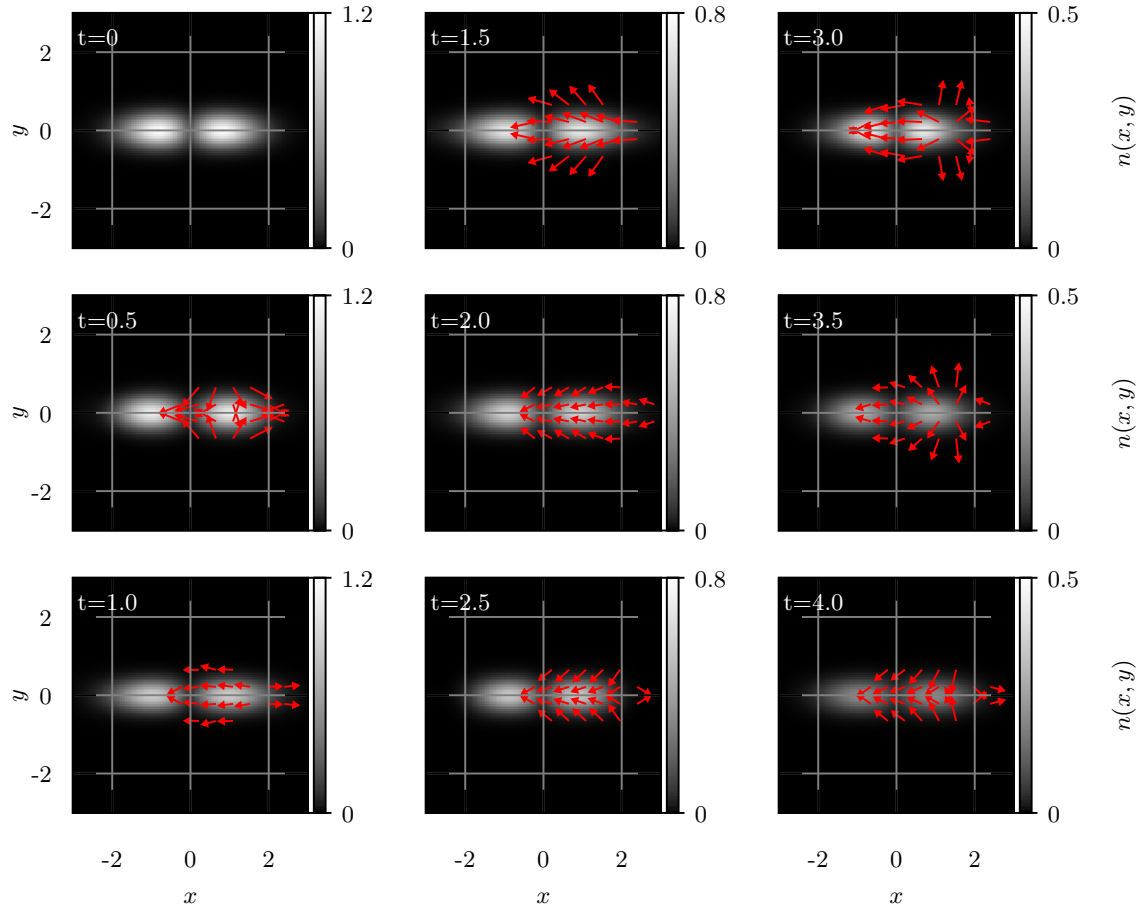

Figure 9.16: Density and current plots for $\gamma = 50$, $\kappa_{12} = 12$ and $\kappa_{11} = \kappa_{22} = 0$ and $a_t = 8$. Due to the high asymmetry, a part of the current is reflected whereas another part refills the space of the dissipated atoms at $t = 0.5$ and $t = 1$. Despite this, one can see that the components $j_x(x, y)$ and $j_y(x, y)$ oscillate with different frequencies which causes smaller oscillations in the decay curves in figure 9.15.

and scaled. When the dissipation starts, a current forms which is directed towards the region where both components coexist. Another part is heading away from the center of the condensate since more atoms moving towards the center than actually can leave the condensate. The high asymmetry of the trap generates a bottleneck, which seems to lead to a partial reflection of the current. This part of atoms moves then towards the edge of the potential in the plot for $t = 0.5$ and reaches it at around $t = 1$. The $j_y(x, y)$ component is still directed inwards but points outwards at $t = 1$ and $t = 1.5$. Later for $t = 2$ and for $t = 2.5$, the y component of $\vec{j}(x, y)$ has reversed its sign again. As in the case of no state separation, the asymmetry causes the x- and y-components of the current to oscillate with

a different frequency which leads to a sometimes less or more efficient dissipation.
This oscillating behavior of the components of the current repeats a few times until $t = 4$. Since this asymmetric potential squeezes the atoms in the y-direction and prevents also that both components overlap too much, a small part of the current is reflected once in a while and moves towards the edges of the potential. During the entire time, the largest part of $j_x(x, y)$ points to the middle of the condensate whereas the y-component changes its sign a few times.

9.4 Atom loss dynamics for state separation ($\kappa_{12} = \kappa_{11} >> \kappa_{22}$)

Now, the case of state separation will be considered but in contrast to the previous case, the rotational symmetry is conserved.

9.4.1 Atom loss for different γ

In figure 9.17, $N(t)$ is shown for $\kappa_{11} = \kappa_{12} = 20$ and $\kappa_{22} = 0$ for different values of γ. For relatively small values of γ, the curves look very smooth and do not exhibit any oscillating structure. But for $\gamma = 10$, around $t = 5.5$ and $t = 8.5$, the losses decrease temporarily.

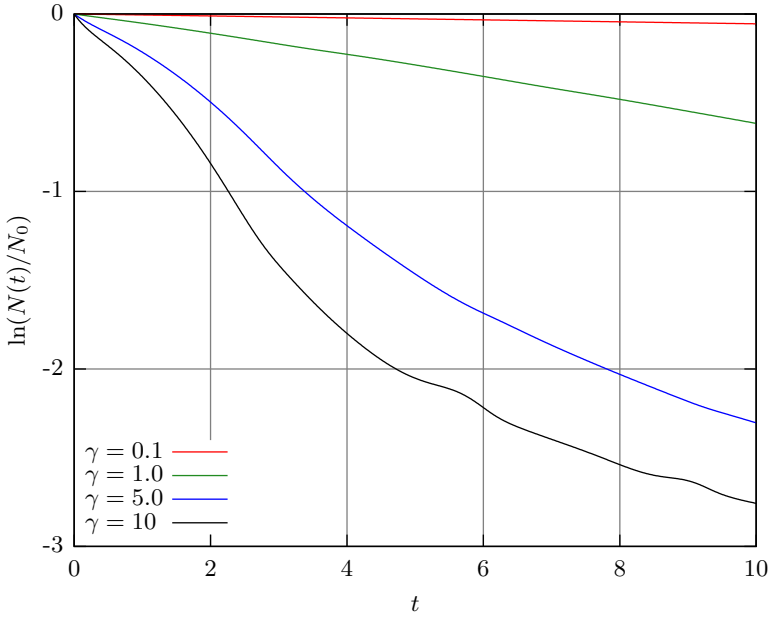

Figure 9.17: Plot for $N(t)$ for $\kappa_{11} = \kappa_{12} = 20$,$\kappa_{22} = 0$ and different γ. The particle number decreases faster as γ is increased. The black curve already shows small oscillations whereas the others have a quite smooth shape.

This is similar to the cases of no state separation and state separation with breaking of the symmetry.

9.4.2 Evolution of the density

In order to explain this form of the decay curves in this case of state separation, the evolution of the density is considered.
The plots in figure 9.18 show its behavior for $\kappa_{11} = \kappa_{12} = 20$, $\kappa_{22} = 0$ and $\gamma = 10$ which

corresponds to the black decay curve in figure 9.17. The red and blue arrows represent the current of both components and will be discussed in the next section. Starting from the ground state at $t = 0$, where one component surround the other in the trap center, the density starts to decrease continuously until $t = 2$. At $t = 3$, one can see from the plots, that $n_1(x)$ has contracted whereas $n_2(x)$ has expanded to a ring-shaped form and surrounds the first component. Around this time, the decay curve in figure 9.17 drops drastically. For $t = 4$, the previously described process reverses which means that the atoms of $n_1(x)$ move outwards and $n_2(x)$ towards the trapping center between $t = 4$ and $t = 5$. At this time, $n_1(x)$ has dropped due to the dissipation and since all remaining atoms are distributed over a larger area. Between $t = 6$ and $t = 7$ the process reverses again, leading to a contraction of $n_1(x)$ and expansion of $n_2(x)$. Like in all the previous cases, the periodic structure of the decay curve is related to an alternating overlap and separation of the densities.

9.4.3 Hydrodynamic approach to a two-component system with dissipation

Again, the current for a Bose gas is used to study the particle movement. The currents $\vec{j}_1(x, y)$ (red) and $\vec{j}_2(x, y)$ (blue) and their corresponding densities will be discussed separately. $\vec{j}_1(x, y)$ (red) is studied first.
The dissipation at the inner side of $n_1(x, y)$ causes a movement towards the center which can be seen from the current plot for $t = 1$ up to $t = 3$. At $t = 4$, the current is directed outwards and the density expands again. The current drops at $t = 5$ and points for $t = 6$ inwards. After decreasing at $t = 7$, the condensate expands again at $t = 8$.
The atoms of $n_2(x, y)$ move in the opposite way. $\vec{j}_2(x, y)$ is directed outwards at $t = 1$ and $t = 2$ and starts reversing for $t = 3$ since the expansion is limited by the potential. The plot for $t = 4$ shows how the losses of the density $n_2(x, y)$ are compensated since the dissipation takes now place in the inner region. At $t = 5$, the current decreases in the outer regions and reverses its direction at $t = 6$. Later for $t = 7$ is contracts again. Since the components swaps their position and form, the atoms of one species have to cross the other density. For this case of state separation, both densities contract and expand out of phase.

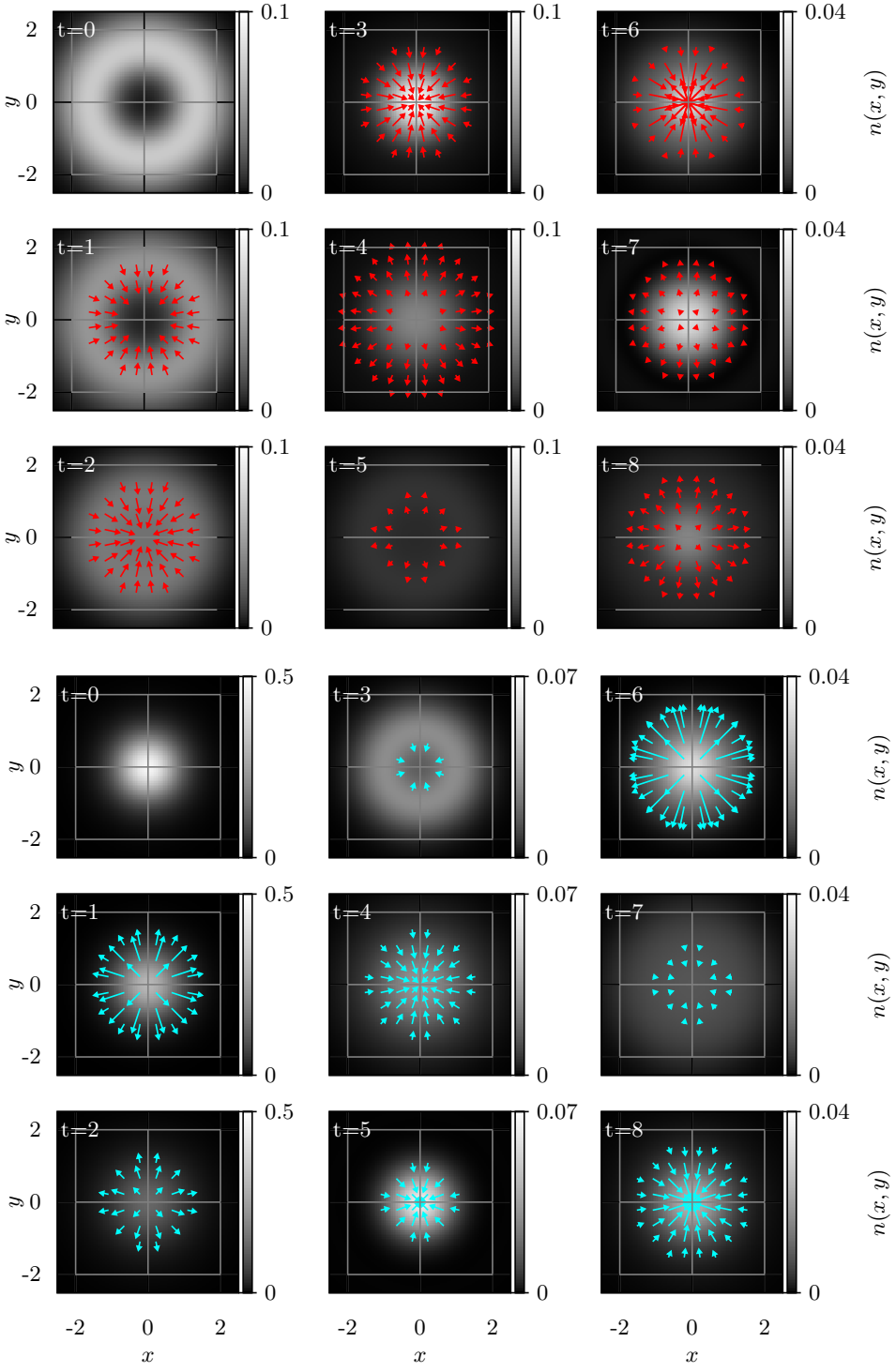

Figure 9.18: Plots for $j_1(x, y)$ (red) and $j_2(x, y)$ (blue) for $\kappa_{11} = \kappa_{12} = 20$, $\kappa_{22} = 0$ and $\gamma = 10$. The dissipation induces for $n_1(x, y)$ a contraction and an expansion for $n_2(x, y)$ between $t = 0$ and $t = 2$. Since both components have to move through each other during this process, this leads to a temporarily faster decay until they have separated again at $t = 3$. Then, both start to reverse and then $n_1(x, y)$ expands and $n_2(x, y)$ contracts between $t = 4$ and $t = 5$.

CHAPTER 10

Conclusion

In this thesis, the stability and response of a BEC consisting of two components with two body losses among them was studied.
In order to describe such system, two coupled Gross-Pitaevskii equations which are modified by a loss term were used. Since an analytical treatment is quite complicated, the numerical method of the split step algorithm was used.
First, the reliability of this algorithm for dissipative systems was checked. Since it reproduces the same results as in [16] and the program exhibited a convergence with respect to the discretization of time and space, it has been regarded as validated and ready for use. Further, the breathing mode frequencies which depend on the strength of the interaction were calculated and are in agreement with the values from the literature.
Applying the numerical method 1D and 2D, the following results were obtained.
First, the static properties of a two level system have been studied which revealed three kinds of ground states. Depending on the interspecies and intraspecies interaction, both components of the Bose gas can separate either with or without breaking of the symmetry of the system. If the interspecies interaction is too small to cause a separation, the densities of both components have the same shape and position in the trap. Since in this case the coexisting region of both components is larger than in the case of state separation, the ground state influences drastically the evolution in time when the dissipation starts. For the one-dimensional and two-dimensional case, we obtained the same types of ground states.
After that, the dynamics for a two component BEC was considered.
The breathing mode was discussed for a two component system without dissipation and it was shown that in 1D these frequencies are dominated by largest interaction, either the interspecies or the intraspecies interaction.
Furthermore, the two-body losses were taken into account. It was found that the behavior for small times depends on the dissipation rate and the form of the ground state. Since scattering processes between both components which lead to two-body losses can only happen in the coexisting region, a BEC with separated components exhibits a higher stability. Due to the existence of a trapping potential the decay curves show an oscillating form for all three different kinds of ground states. Their frequencies seemed identical to the breathing mode frequencies. A closer look on the evolution of the densities revealed that the densities either pulsate for no separation or both components swap their position in the potential while shrinking. That pulsating behavior was previously observed for the breathing mode.
For the case of the separation of both components, the Quantum-Zeno effect was observed. That means for dissipative systems, that the losses of such a system decreases for large values of the coupling parameter. It was observed only in the case of state separation since the region where both components coexist was not refilled as fast as they dissipated. If both components of the BEC overlap completely, the Quantum-Zeno effect does not appear.
In 2D, a two component BEC exhibits a quite similar behavior. However, it was observed

that an asymmetric trap also influences the losses. The components in x- and y-direction of the current which plays an important role oscillate with different frequencies leading to additional oscillations in the decay curves.
Note, that all numerical computations for the 1D and 2D case have been accompanied by these approximations for small times and showed on the one hand the limitation of these approximations but gave also additional evidence for the validation of the program.
Since the model of the Gross-Pitaevskii equation was used which assumes a large number of particles in the condensed state, one has to be careful if this description is still reasonable for a dissipative system when a lot of atoms have already left the condensate. We expect that in 3D, a similar evolution in time of the condensate. The stability of the condensate will be larger if the coexisting region of both components is small. A separation of both species should lower the losses. Also the asymmetry of the trap could lead to different pulsating frequencies along all spatial directions.

Bibliography

[1] K. B. David et al. “Bose-Einstein condensation in a gas of a sodium atoms”. In: *Phys. Rev. Lett.* 75 (1995), pp. 3969–3973.

[2] M. H. Anderson et al. “Observation of Bose-Einstein condensation in a dilute atomic vapor”. In: 269 (1995), pp. 198–201.

[3] C. J. Myatt et al. “Production of Two Overlapping Bose-Einstein Condensates by Sympathetic Cooling”. In: *Phys. Rev. Lett.* 78 (1997), p. 586.

[4] P.S. Julienne et al. “Collisional Stability of Double Bose Condensates”. In: *Phys. Rev. Lett.* 78 (1997), p. 1880.

[5] F. Dalfovo et al. “Theory of Bose-Einstein condensation in trapped gases”. In: *arXiv:9806038* (1998).

[6] C. J. Pethick and H. Smith. *Bose-Einstein Condensation in Dilute Gases*. Cambridge University Press, 2008.

[7] Schwabl. *Statische Mechanik*. Springer, 2006.

[8] J. Rogel-Salazar. “The Gross-Piatevskii Equation and Bose-Einstein condensates”. In: *arXiv:1301.2073* (2013).

[9] J. N. Fuchs, X. Fuchs, and R. Combescot. “Collective Modes of a Trapped Lieb-Liniger Gas”. In: *Laser Physics* 14 (2004), pp. 551–555.

[10] C. Gies et al. “Finite-temperature theory of the trapped two-dimensional Bose gas”. In: *Phys. Rev. Lett.* 69 (2004), p. 023616.

[11] H.-P. Breuer and F. Petruccione. *Theory of open quantum systems*. Oxford University Press, 2002.

[12] G. Barontini et al. “Controlling the dynamics of an open many-body quatnum system with localized dissipation”. In: *Physical Review Letters* 110 (2013), p. 035302.

[13] J. Dziarmaga and K. Sacha. “Condensate Heating by Atomic Losses”. In: *Laser Physics* 14 (2004), pp. 628–630.

[14] J. M. Thijssen. *Computational Physics*. Cambridge University Press, 2007.

[15] H. J. C. Berendsen. *Simulating the Physical World. Hierarchical Modelling from Quantum Mechanics to Fluid Dynamics*. Cambridge University Press, 2007.

[16] Valeriy A. Brazhnyi et al. “Dissipation-Induced Coherent Structures in Bose-Einstein Condensates”. In: *Phys. Rev. Lett.* 102 (2009), p. 144101.

[17] S. B. Papp, J. M. Pino, and Wieman. “Tunable Miscibility in a Dual-Species Bose-Einstein Condensate”. In: *Phys. Rev. Lett.* 101 (2008), p. 040402.

[18] Tin-Lun Ho and V. B. Shenoy. “Binary Mixtures of Bose Condensates”. In: *Phys. Rev. Lett.* 77 (1996), pp. 3276–3279.

[19] R. Navarro, R. Carrertero-Ganzalez, and P. G. Kevrekidis. “Phase Separation and Dynamics of Two-component Bose-Einstein Condensates”. In: *Phys. Rev. Lett.* 80 (2009), p. 023613.

List of Figures

2.1 Condensate fraction $\frac{N_0}{N}$ for the BEC 5
2.2 Thomas-Fermi approximation 10

3.1 Sketch for the physical situation of an open quantum system. 13

4.1 Imaginary time evolution for the harmonic oscillator. 21
4.2 Ground state density for the harmonic oscillator 22
4.3 Ground state density for the Gross-Pitaevskii equation. 23
4.4 Behavior of the density over time after changing the trapping potential by 40% 24
4.5 Breathing mode frequency versus the interaction. 25

5.1 Reproduced plot from the paper 28
5.2 The second plot from the paper 28
5.3 Plot for the program which solves equation 3.33 and 3.34 29
5.4 Plot in order to check the convergence of the program with respect to the time steps 30

6.1 Ground state of a two level system for $\kappa_{11} = \kappa_{22} = 4$ and $\kappa_{12} = 3$. 32
6.2 Ground state of a two level system for $\kappa_{11} = \kappa_{22} = 3$ and $\kappa_{12} = 5$. 32
6.3 Ground state of a two level system for $\kappa_{11} = 8$, $\kappa_{22} = 0$ and $\kappa_{12} = 8$. 33
6.4 State diagram for the state separation 34
6.5 Comparison of the Gauss approximation and the numerical obtained ground state for $\kappa_{11} = \kappa_{22} = 6$ and $\kappa_{12} = 4$ 36
6.6 Density profiles for $\kappa_{11} = \kappa_{22} = 6$ and $\kappa_{12} = 4$ calculated numerically and with a Gauss ansatz 37
6.7 State diagram for the Gauss approximations 37

7.1 Breathing mode frequencies versus the interaction κ_{12} 39
7.2 Logarithmic plot for the decay for one component for different γ, $\kappa_{11} = \kappa_{22} = 4$ and $\kappa_{12} = 2$. 40
7.3 Density plots at different times for $\gamma = 10$, $\kappa_{11} = \kappa_{22} = 4$ and $\kappa_{12} = 2$. . . . 41
7.4 Comparison of the different approximations with the numerical result for $\kappa_{11} = \kappa_{22} = 4$, $\kappa_{12} = 2$ and $\gamma = 10$ 43
7.5 Comparison of the decay curves according to the exact solution (red), formula 7.10 (green) with a numerically calculated ground state and equation 7.11 using a variational ansatz (blue) 44
7.6 Comparison of the analytical and numerical obtained density profile for the case $\gamma = 10$, $\kappa_{11} = \kappa_{22} = 4$ and $\kappa_{12} = 2$ 45
7.7 Current and density plot for $\kappa_{11} = \kappa_{22} = 4$, $\kappa_{12} = 2$ and $\gamma = 10$ 47
7.8 Plot for different values of γ, $\kappa_{11} = \kappa_{22} = 2$ and $\kappa_{12} = 6$ 48
7.9 Density plots at different times for $\gamma = 10$, $\kappa_{11} = \kappa_{22} = 2$ and $\kappa_{12} = 6$. . . . 49
7.10 Comparison of the complete solution of the GPE (red), the analytically obtained solution in equation 7.20 (blue) and the approximation according to equations 7.1 and 7.2 (green) 50

7.11 Comparison of the approximations according to formulas 7.23 and 7.20 using the numerical obtained ground state with the numerical solution of the GPE 51
7.12 Comparison of the decay according to formula 7.20 with Gauss approximation (red curve) and numerical obtained ground state (blue curve) for $\gamma = 10$, $\kappa_{11} = \kappa_{22} = 2$, $\kappa_{12} = 6$ 52
7.13 Current $j_2(x,t)$ (red curve) for the case of the separation of the densities $n_1(x,t)$ (green) and $n_2(x,t)$ (blue) 53
7.14 Zeno effect for $\kappa_{11} = \kappa_{22} = 2$ and $\kappa_{12} = 6$ 54
7.15 Decay curves for different values of γ and for $\kappa_{11} = 2$ and $\kappa_{22} = \kappa_{12} = 6$ . . 55
7.16 Density plots at different times for $\gamma = 10$, $\kappa_{11} = \kappa_{12} = 6$ and $\kappa_{22} = 2$ . . . 55
7.17 Density profiles $n_1(x,t)$ and $n_2(x,t)$ and current $j_1(x,t)$ for different times with $\gamma = 10$, $\kappa_{11} = \kappa_{12} = 6$ and $\kappa_{22} = 2$ 56
7.18 Density profiles $n_1(x,t)$ (blue curve) and $n_2(x,t)$ (red curve) and current $j_1(x,t)$ (violet curve) for different times with $\gamma = 10$, $\kappa_{11} = \kappa_{12} = 6$ and $\kappa_{22} = 2$ 58
7.19 Logarithmic plot of $N(t)/N_0$ for different $\kappa_{11} = \kappa_{22}$ and fixed $\kappa_{12} = 6$ and $\gamma = 10$. 59
7.20 Decay for the case of state separation and conservation of symmetry. 59

8.1 Different ground states for two-dimensional BEC in a harmonic trap. 61
8.2 Densities for the same values as in figure 8.1 but with $a_t = 2$ 62
8.3 State diagram for the two-dimensional case 63
8.4 Comparison of the Gauss approximation with the numerically obtained solution 64
8.5 Gauss approximation, numerical calculated density profile and their difference $\Delta n(x,y)$ for $\kappa_{11} = \kappa_{22} = 4$ and $\kappa_{12} = 10$. 65
8.6 State diagram in two dimensions using equations 8.4 and 8.5 66

9.1 Logarithmic plot for the particle number of one component for different γ, $\kappa_{12} = 2$ and $\kappa_{11} = \kappa_{22} = 4$ in 2D. 68
9.2 Evolution of the densities for $\gamma = 10$, $\kappa_{11} = \kappa_{22} = 4$ and $\kappa_{12} = 2$ 69
9.3 Comparison of the exact decay curve for $\gamma = 10$, $\kappa_{11} = \kappa_{22} = 4$ and $\kappa_{12} = 2$ with the approximations according to the equations 9.1/9.2 (red curve), 9.7 (blue) and the numerical result (red) 70
9.4 Plot of the complete numerical solution, equations 9.7 with a numerical ground state and 9.9 for $\gamma = 10$, $\kappa_{11} = \kappa_{22} = 4$ and $\kappa_{12} = 2$ 71
9.5 Comparison of the Gauss shaped approximation with the numerical solution of the Gross-Pitaevskii equation for $\gamma = 10$, $\kappa_{11} = \kappa_{22} = 4$ and $\kappa_{12} = 2$ . . . 72
9.6 Plot of the numerical solution and the expression 9.9 for $\gamma = 10$, $\kappa_{11} = \kappa_{22} = 4$ and $\kappa_{12} = 2$ for a trap with no asymmetry and a frequency ratio $\frac{\omega_y}{\omega_x} = 2$ . . 72
9.7 Current and density plots for different times with the settings $\gamma = 10$, $\kappa_{11} = \kappa_{22} = 4$ and $\kappa_{12} = 2$ 73
9.8 Decay curves for $\kappa_{11} = \kappa_{22} = 7$, $\kappa_{12} = 2$, $\gamma = 50$ and different a_t 75
9.9 Density and current plots for $\kappa_{11} = \kappa_{22} = 7$, $\kappa_{12} = 2$, $\gamma = 50$ and $a_t = 2$ . . 76
9.10 $N(t)$ for $\kappa_{11} = \kappa_{22} = 0$, $\kappa_{12} = 12$ and various values for γ 77
9.11 Evolution of the density over time for $\kappa_{11} = \kappa_{22} = 0$, $\kappa_{12} = 12$ and $\gamma = 5$ . . 78
9.12 Comparison of equations 9.14/9.15, 9.1/9.2 and the numeric result for $\gamma = 5$, $\kappa_{11} = \kappa_{22} = 0$ and $\kappa_{12} = 12$ 79
9.13 Plot for $\gamma = 5$, $\kappa_{11} = \kappa_{22} = 0$ and $\kappa_{12} = 12$ using equations , 9.14/9.15 and the numeric result 79
9.14 Current of the initially right component and density for $\gamma = 5$, $\kappa_{11} = \kappa_{22} = 0$ and $\kappa_{12} = 12$ 80

9.15 Decay curves for $\gamma = 50$, $\kappa_{11} = \kappa_{22} = 0$, $\kappa_{12} = 12$ and different values for a_t 81
9.16 Density and current plots for $\gamma = 50$, $\kappa_{12} = 12$ and $\kappa_{11} = \kappa_{22} = 0$ and $a_t = 8$ 82
9.17 Plot for $N(t)$ for $\kappa_{11} = \kappa_{12} = 20$,$\kappa_{22} = 0$ and different γ 83
9.18 Plots for $j_1(x, y)$ (red) and $j_2(x, y)$ (blue) for $\kappa_{11} = \kappa_{12} = 20$, $\kappa_{22} = 0$ and $\gamma = 10$ 85

Appendix

1 Gross-Pitaevskii equation with dissipation

1.1 One-body loss

Now, we derive formula 3.25 with the definitions of $\hat{H} = \hat{H}_{kin} + \hat{H}_{pot} + \hat{H}_{int} = \hat{H}_0 + \hat{H}_{int}$ and the Lindblad equation 3.9. We start with the general ansatz for the expectation values of $\hat{\Psi}(\vec{r})$:

$$\begin{aligned} i\hbar Tr\left[\dot{\hat{\rho}}\hat{\Psi}(\vec{r})\right] = i\hbar\langle\dot{\hat{\Psi}}(\vec{r})\rangle &= Tr\left[\hat{\Psi}(\vec{r})([\hat{H},\hat{\rho}] + i\hbar\hat{\mathcal{D}}(\hat{\rho}))\right] \\ &= Tr\left[\hat{\Psi}(\vec{r})\hat{H}\hat{\rho} - \hat{\Psi}(\vec{r})\hat{\rho}\hat{H} + i\hbar\hat{\Psi}(\vec{r})\hat{\mathcal{D}}(\hat{\rho})\right] \\ &= Tr\left[\hat{\rho}\hat{\Psi}(\vec{r})\hat{H} - \hat{\rho}\hat{H}\hat{\Psi}(\vec{r}) + i\hbar\hat{\Psi}(\vec{r})\hat{\mathcal{D}}(\hat{\rho})\right] \end{aligned} \tag{A.1}$$

First, we calculate $Tr\left[\hat{\rho}\hat{\Psi}(\vec{r})\hat{H}_0\right]$:

$$\begin{aligned} Tr\left[\hat{\rho}\hat{\Psi}(\vec{r})\hat{H}_0\right] &= Tr\left[\hat{\rho}\int d\vec{r}'\hat{\Psi}(\vec{r})\hat{\Psi}^\dagger(\vec{r}')\left(-\frac{\hbar^2}{2m}\nabla'^2 + V_{ext}(\vec{r}')\right)\Psi(\vec{r}')\right] \\ &= Tr\left[\hat{\rho}\int d\vec{r}'\left(\delta(\vec{r}-\vec{r}') + \hat{\Psi}^\dagger(\vec{r}')\hat{\Psi}(\vec{r})\right)\left(-\frac{\hbar^2}{2m}\nabla'^2 + V_{ext}(\vec{r}')\right)\Psi(\vec{r}')\right] \\ &= Tr\left[\hat{\rho}\left(-\frac{\hbar^2}{2m}\nabla^2 + V_{ext}(\vec{r})\right)\Psi(\vec{r})\right. \\ &\left.+\hat{\rho}\int d\vec{r}'\hat{\Psi}^\dagger(\vec{r}')\left(-\frac{\hbar^2}{2m}\nabla'^2 + V_{ext}(\vec{r}')\right)\Psi(\vec{r}')\Psi(\vec{r})\right] \\ &= \left\langle\left[-\frac{\hbar^2}{2m}\nabla^2 + V_{ext}(\vec{r})\right]\hat{\Psi}(\vec{r})\right\rangle + Tr\left[\hat{\rho}(\hat{H}_{kin} + \hat{H}_{pot})\hat{\Psi}(\vec{r})\right] \end{aligned} \tag{A.2}$$

For the interaction term, we derive:

$$\begin{aligned} &Tr\left[\hat{\rho}\hat{\Psi}(\vec{r})\hat{H}_{int}\right] = Tr\left[\hat{\rho}\frac{U_0}{2}\int d^3x'\hat{\Psi}(\vec{r})\hat{\Psi}^\dagger(\vec{r}')\hat{\Psi}^\dagger(\vec{r}')\Psi(\vec{r}')\Psi(\vec{r}')\right] \\ &= Tr\left[\hat{\rho}\frac{U_0}{2}\int d\vec{r}'\left(\delta(\vec{r}-\vec{r}') + \hat{\Psi}^\dagger(\vec{r}')\hat{\Psi}(\vec{r})\right)\hat{\Psi}^\dagger(\vec{r}')\Psi(\vec{r}')\Psi(\vec{r}')\right] \\ &= \frac{U_0}{2}\left\langle\hat{\Psi}^\dagger(\vec{r})\hat{\Psi}(\vec{r})\hat{\Psi}(\vec{r})\right\rangle + Tr\left[\hat{\rho}\frac{U_0}{2}\int d\vec{r}'\hat{\Psi}^\dagger(\vec{r}')\hat{\Psi}(\vec{r})\hat{\Psi}^\dagger(\vec{r}')\hat{\Psi}(\vec{r}')\hat{\Psi}(\vec{r}')\right] \\ &= 2\cdot\frac{U_0}{2}\left\langle\hat{\Psi}^\dagger(\vec{r})\hat{\Psi}(\vec{r})\hat{\Psi}(\vec{r})\right\rangle + Tr\left[\hat{\rho}\hat{H}_{int}\hat{\Psi}(\vec{r})\right] \end{aligned} \tag{A.3}$$

Now, the dissipator according to equation 3.22:

$$
\begin{aligned}
&Tr\left[\hat{\mathcal{D}}(\hat{\rho})\hat{\Psi}(\vec{r})\right] \\
&= -Tr\left[\int d\vec{r}'\gamma(\vec{r}')\left(\hat{\Psi}^\dagger(\vec{r}')\hat{\Psi}(\vec{r}')\hat{\rho}\hat{\Psi}(\vec{r}) + \hat{\rho}\hat{\Psi}^\dagger(\vec{r}')\hat{\Psi}(\vec{r}')\hat{\Psi}(\vec{r}) - 2\hat{\Psi}(\vec{r}')\hat{\rho}\hat{\Psi}^\dagger(\vec{r}')\hat{\Psi}(\vec{r})\right)\right] \\
&= -Tr\left[\int d\vec{r}'\gamma(\vec{r}')\left(\hat{\rho}\hat{\Psi}(\vec{r})\hat{\Psi}^\dagger(\vec{r}')\hat{\Psi}(\vec{r}') + \hat{\rho}\hat{\Psi}^\dagger(\vec{r}')\hat{\Psi}(\vec{r}')\hat{\Psi}(\vec{r}) - 2\hat{\rho}\hat{\Psi}^\dagger(\vec{r}')\hat{\Psi}(\vec{r})\hat{\Psi}(\vec{r}')\right)\right] \\
&= -Tr\left[\int d\vec{r}'\gamma(\vec{r}')\left(\hat{\rho}(\hat{\Psi}^\dagger(\vec{r}')\hat{\Psi}(\vec{r}) + \delta(\vec{r}-\vec{r}'))\hat{\Psi}(\vec{r}') + \hat{\rho}\hat{\Psi}^\dagger(\vec{r}')\hat{\Psi}(\vec{r}')\hat{\Psi}(\vec{r})\right.\right. \\
&\quad \left.\left. -2\hat{\rho}\hat{\Psi}^\dagger(\vec{r}')\hat{\Psi}(\vec{r}')\hat{\Psi}(\vec{r})\right)\right] \\
&= -\langle\gamma(\vec{r})\Psi(\vec{r})\rangle
\end{aligned}
\tag{A.4}
$$

Inserting equations A.2, A.3 and A.4 back into formula A.1, one is able to obtain equation 3.25.

1.2 Condensate mixture with two-body loss

We will only consider the dissipative term of equation 3.9 since the calculations for the parts for kinetic energy, the external potential and inter- and intraspecies interactions are equal to the one body-loss case.
The Lindblad operators for a local two-body loss between species i and j read

$$\hat{A}(\vec{r}) = \hat{\Psi}_i(\vec{r})\hat{\Psi}_j(\vec{r}) \tag{A.5}$$

$$\hat{A}^\dagger(\vec{r}) = \hat{\Psi}_j^\dagger(\vec{r})\hat{\Psi}_i^\dagger(\vec{r}) \tag{A.6}$$

Thus, the dissipating part for the expectation value of $\dot{\Psi}(\vec{r})$ for the species i with $i \neq j$ becomes:

$$
\begin{aligned}
&Tr\left[\hat{\mathcal{D}}(\hat{\rho})\hat{\Psi}_i(\vec{r})\right] \\
&= -Tr\left[\int d\vec{r}'\gamma(\vec{r}')\left(\hat{A}^\dagger(\vec{r}')\hat{A}(\vec{r}')\hat{\rho}\hat{\Psi}_i(\vec{r}) + \hat{\rho}\hat{A}^\dagger(\vec{r}')\hat{A}(\vec{r}')\hat{\Psi}_i(\vec{r}) - 2\hat{A}(\vec{r}')\hat{\rho}\hat{A}^\dagger(\vec{r}')\hat{\Psi}_i(\vec{r})\right)\right] \\
&= -Tr\left[\int d\vec{r}'\gamma(\vec{r}')\left(\hat{\rho}\hat{\Psi}_i(\vec{r})\hat{A}^\dagger(\vec{r}')\hat{A}(\vec{r}') + \hat{\rho}\hat{A}^\dagger(\vec{r}')\hat{A}(\vec{r}')\hat{\Psi}_i(\vec{r}) - 2\hat{\rho}\hat{A}^\dagger(\vec{r}')\hat{\Psi}_i(\vec{r})\hat{A}(\vec{r}')\right)\right] \\
&= -Tr\left[\int d\vec{r}'\gamma(\vec{r}')\left(\hat{\rho}\hat{\Psi}_i(\vec{r})\hat{\Psi}_i^\dagger(\vec{r}')\hat{\Psi}_j^\dagger(\vec{r}')\hat{\Psi}_j(\vec{r}')\hat{\Psi}_i(\vec{r}')\right.\right. \\
&+ \left.\left.\hat{\rho}\hat{\Psi}_i^\dagger(\vec{r}')\hat{\Psi}_j^\dagger(\vec{r}')\hat{\Psi}_j(\vec{r}')\hat{\Psi}_i(\vec{r}')\hat{\Psi}_i(\vec{r}) - 2\hat{\rho}\hat{\Psi}_i^\dagger(\vec{r}')\hat{\Psi}_j^\dagger(\vec{r}')\hat{\Psi}_i(\vec{r})\hat{\Psi}_j(\vec{r}')\hat{\Psi}_i(\vec{r}')\right)\right] \\
&= -Tr\left[\int d\vec{r}'\gamma(\vec{r}')\left(\hat{\rho}\hat{\Psi}_j^\dagger(\vec{r}')\hat{\Psi}_j(\vec{r}')\hat{\Psi}_i(\vec{r})\hat{\Psi}_i^\dagger(\vec{r}')\hat{\Psi}_i(\vec{r}')\right.\right. \\
&+ \left.\left.\hat{\rho}\hat{\Psi}_j^\dagger(\vec{r}')\hat{\Psi}_j(\vec{r}')\hat{\Psi}_i^\dagger(\vec{r}')\hat{\Psi}_i(\vec{r}')\hat{\Psi}_i(\vec{r}) - 2\hat{\rho}\hat{\Psi}_j^\dagger(\vec{r}')\hat{\Psi}_j(\vec{r}')\hat{\Psi}_i^\dagger(\vec{r}')\hat{\Psi}_i(\vec{r}')\hat{\Psi}_i(\vec{r})\right)\right] \\
&= -Tr\left[\int d\vec{r}'\gamma(\vec{r}')\left(\hat{\rho}\hat{\Psi}_j^\dagger(\vec{r}')\hat{\Psi}_j(\vec{r}')\hat{\Psi}_i(\vec{r})\hat{\Psi}_i^\dagger(\vec{r}')\hat{\Psi}_i(\vec{r}')\right.\right. \\
&+ \left.\left.\hat{\rho}\hat{\Psi}_j^\dagger(\vec{r}')\hat{\Psi}_j(\vec{r}')\hat{\Psi}_i^\dagger(\vec{r}')\hat{\Psi}_i(\vec{r}')\hat{\Psi}_i(\vec{r}) - 2\hat{\rho}\hat{\Psi}_j^\dagger(\vec{r}')\hat{\Psi}_j(\vec{r}')\hat{\Psi}_i^\dagger(\vec{r}')\hat{\Psi}_i(\vec{r}')\hat{\Psi}_i(\vec{r})\right)\right]
\end{aligned}
$$

$$
\begin{aligned}
&= - Tr \left[\int d\vec{r}' \gamma(\vec{r}') \left(\hat{\rho}\hat{\Psi}_j^\dagger(\vec{r}')\hat{\Psi}_j(\vec{r}')\delta(\vec{r}' - \vec{r})\hat{\Psi}_i(\vec{r}') + \hat{\rho}\hat{\Psi}_j^\dagger(\vec{r}')\hat{\Psi}_j(\vec{r}')\Psi_i^\dagger(\vec{r}')\hat{\Psi}_i(\vec{r}')\hat{\Psi}_i(\vec{r}) \right.\right. \\
&+ \left.\left. \hat{\rho}\hat{\Psi}_j^\dagger(\vec{r}')\hat{\Psi}_j(\vec{r}')\hat{\Psi}_i^\dagger(\vec{r}')\hat{\Psi}_i(\vec{r}')\hat{\Psi}_i(\vec{r}) - 2\hat{\rho}\hat{\Psi}_j^\dagger(\vec{r}')\hat{\Psi}_j(\vec{r}')\hat{\Psi}_i^\dagger(\vec{r}')\hat{\Psi}_i(\vec{r}')\hat{\Psi}_i(\vec{r}) \right) \right] \\
&= - \left\langle \gamma(\vec{r}) |\Psi_j(\vec{r})|^2 \Psi_i(\vec{r}) \right\rangle
\end{aligned} \tag{A.7}
$$

This is the dissipative part of equations 3.33 and 3.34. The other parts of both Gross-Pitaevskii equations can be derived in the same way as shown in the previous section 1.1.

2 Conversion to units according to [16]

To measure the time in units of $\frac{2}{\omega}$ and space in units of the harmonic oscillator length $a = \sqrt{\frac{\hbar}{m\omega}}$, the following parameters change to:

$$
\begin{aligned}
t = \tilde{t}\frac{2}{\omega} &\rightarrow \frac{\partial}{\partial t} = \frac{\omega}{2}\frac{\partial}{\partial \tilde{t}} \\
x = \tilde{x}a &\rightarrow \frac{\partial^2}{\partial x^2} = \frac{1}{a^2}\frac{\partial^2}{\partial \tilde{x}^2} \\
\int |\tilde{\Psi}|^2 d\tilde{x} = \frac{4N_0|a_s|}{a} &\rightarrow \tilde{\Psi} = \sqrt{\frac{4N_0 a_s}{a}}\Psi
\end{aligned}
$$

Inserting these transformation rules gives:

$$
i\hbar\frac{\omega}{2}\partial_{\tilde{t}}\tilde{\Psi} = -\frac{\hbar^2}{2ma^2}\partial_{\tilde{x}}^2\tilde{\Psi} + U\frac{a}{4N_0 a_s}|\tilde{\Psi}|^2\tilde{\Psi} - i\gamma(\tilde{x})\tilde{\Psi}
$$

Using the definition of $a = \sqrt{\frac{\hbar}{m\omega}}$ gives:

$$
i\partial_{\tilde{t}}\tilde{\Psi} = -\partial_{\tilde{x}}^2\tilde{\Psi} + \frac{a}{2N_0 a_s \hbar\omega}U|\tilde{\Psi}|^2\tilde{\Psi} - \frac{2i\gamma(x)}{\hbar\omega}\tilde{\Psi}
$$

For a Gauss shaped dissipation of the form

$$
\gamma(x) = \gamma_0 e^{-\frac{x^2}{2\zeta^2}}
$$

all parameters transform like the following:

$$
\begin{aligned}
\tilde{U} = \sigma &= \frac{a}{2N a_s \hbar\omega}U \\
\tilde{\gamma_0} &= \frac{2\gamma_0}{\hbar\omega} \\
\tilde{\zeta} &= \frac{\zeta}{a}
\end{aligned}
$$

Thus, the new GPE reads:

$$
i\partial_{\tilde{t}}\tilde{\Psi} = -\partial_{\tilde{x}}^2\tilde{\Psi} + \tilde{U}|\tilde{\Psi}|^2\tilde{\Psi} - i\tilde{\gamma}(\tilde{x})\tilde{\Psi}
$$

3 Useful formulas

$$\int_0^\infty x^n \; e^{-ax^m} \; dx = \frac{a^{-\left(\frac{n+1}{m}\right)}}{m} \Gamma\left(\frac{n+1}{m}\right), \tag{A.8}$$

where $\Gamma(x)$ is the Γ-function with the identities $\Gamma(x+1) = \Gamma(x)x$ and $\Gamma\left(\frac{1}{2}\right) = \sqrt{\pi}$. Note, that $a \in \mathbb{R}$, $n > -1$ and $m > 0$.

Statement

I hereby declare that the work presented here was formulated by myself and that no sources or tools other than those cited were used.

Bonn, _____
date

_____
signature